DETECTION TECHNIQUES FOR TENUOUS PLANETARY ATMOSPHERES

Stuart A. Hoenig
Jay Abramowitz

FIFTH SIX-MONTH REPORT

July 1, 1965 - December 30, 1965

NsG-458

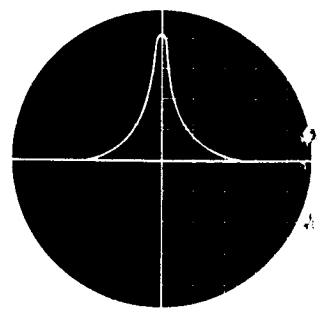

ENGINEERING RESEARCH LABORATORIES

COLLEGE OF ENGINEERING
UNIVERSITY OF ARIZONA
TUCSON, ARIZONA

FIFTH SIX-MONTH REPORT

July 1, 1965 - December 30, 1965

NsG-458

DETECTION TECHNIQUES FOR TENUOUS PLANETARY ATMOSPHERES

TO

Dr. T. L. K. Smull
Grants and Research Contracts Office, Code SC
National Aeronautics and Space Administration
Washington, D. C., 20546

Stuart A. Hoenig, Principal Investigator
Jay Abramowitz, Graduate Associate

Field Emission and Space Systems Laboratory
Department of Aerospace and Mechanical Engineering
The University of Arizona
Tucson, Arizona

I. INTRODUCTION

This report will cover the work performed on contract NsG-458, between The University of Arizona and the National Aeronautics and Space Administration, from the period of July 1, 1965 to December 30, 1965.

The contract was set up for the development of new types of gas detection and analysis apparatus for tenuous planetary atmospheres. A secondary aim has been an effort to gain an improved understanding of the basic phenomena that occur between gases and metals.

II. INFORMAL STATUS REPORT

During this period of the contract the principal investigator spent June 1 - September 5 as a visiting staff member at Bell Telephone Laboratories in Murray Hill, New Jersey. The summer was devoted to a study of the optical properties of thin films of Ta_2O_5. This research was most interesting and proved to be an excellent introduction to thin film technology. Chemical detection devices based on thin films are becoming more common, and thin films will be important in the electronic device technology of the future. For these reasons it was felt most important that we gain a background in this area.

During the summer, work continued in the Field Emission and Space Systems Laboratory (FESS). Mr. Melvin Eisenstadt finished his thesis and received the Ph.D. in Aerospace Engineering. He is now on the faculty of the University of California at Santa Barbara. His thesis involved the use of a molecular beam in a study of chemisorption of H_2 versus H on hot palladium. One paper on this work has appeared in the Review of Scientific Instruments (November, 1965) and another has been submitted to the Journal of Chemical Physics.

This study of the chemisorption of H versus H_2 was done as part of the basic research program supported under NsG-458. The chemical reactions of hydrogen atoms and molecules are the simplest reactions that can be studied in an experimental situation. The wave functions of hydrogen have been determined with great precision and an experiment of this type offers an excellent opportunity to test various theories of metal-gas interactions.

Mr. Eisenstadt's thesis is reprinted in its entirety as an Appendix to this report. The most interesting result was the fact the hydrogen atoms have a lower sticking probability on palladium, than hydrogen molecules. This seems to be due to the poor transfer of energy from the atom to the metal lattice when impact occurs. This result had been to some extent predicted by theory and this is discussed in detail in the Appendix.

In September 1965 Mr. Jay Abramowitz joined the group as a Ph.D. candidate in Mechanical Engineering. His work to date has been on the surface ionization program.

In our previous reports we have discussed the design and construction of a large (18" x 22") U-H-V vacuum system. The construction costs were covered primarily by NsG-458 with assistance from State funds. This system is the largest U-H-V apparatus on the campus and has been the focus of an interdisciplinary program.

At the moment, staff members from the Lunar and Planetary Laboratory are using the system to test a proton gun for radiation bombardment of simulated lunar soil materials. This gun was designed and built in the FESS laboratory under a small subcontract from the Lunar and Planetary Laboratory (LPL). The gun will be tested and refined in the large vacuum systems and then a separate facility will be designed so that the LPL staff can run a long series of tests on many different materials.

When the LPL program is finished, in the large U-H-V system, several other experiments are planned on thin film growth by evaporation and sputtering. This work is a joint venture of the FESS laboratory and the Astronomy and the Electrical Engineering Departments of the University.

In the latter part of 1966 we hope to begin installing an improved hydrogen molecular beam for surface physics studies under the planned program of NsG-458.

This general University use of a NASA supported facility is a good example of the interdisciplinary studies that have developed at The University of Arizona. The design and construction of apparatus for other groups have allowed the FESS laboratory to support a full time technician. This technician, Mr. Ira Clough, has proved to be invaluable in the design and construction of research apparatus. With his able assistance the FESS laboratory has become a general campus facility for coordination and promotion of research by cooperating departments. This would not have been possible without the continuous support of NASA on NsG-458 and the provision of added space from an NSF Research Facilities Grant in 1964.

During this period the major efforts, in research on new detectors, were concentrated on improvements to the field ionization detector for water vapor and the surface ionization detector for hydrogen in air. In a conference with NASA staff members in September 1965 it was indicated that the plans for the Voyager experiment on Mars had been changed and no measurements were planned during re-entry through the Martian atmosphere. This in turn implied that a water detection system was needed which would operate at the pressures existing on the surface of Mars (5 millebars). A careful review was made of other possible methods for measurement of Martian water vapor and it was

decided to try to adapt the field ionization system for high (5mb) pressure operations. The review and a discussion of the new parameters of the detector are given in a later section. Here we shall only note that it may be possible to operate the field ionization brush in the corona discharge mode at pressures up to one atmosphere with adequate sensitivity to water vapor.

In our earlier reports mention was made of the fact that the field ionization system, if operated at higher voltages, could serve as an ion source for a mass spectrometer. The work of several investigators was cited in this connection, particularly H. D. Beckey[1]. A field ionization system designed by Dr. Beckey is now commercially available from the ATLAS GMB of Bremen, Germany.

On November 9 a discussion was held with Dr. Charles Giffen of the Jet Propulsion Laboratory. Dr. Giffen indicated that a great need existed for a field ionization source to be used with a mass spectrometer for the Voyager program. A field ionization source has many advantages; for example, the fragile and power consuming filament is entirely absent. The break-up of complex molecules, that is always observed with electron bombardment ionization, is almost entirely eliminated with field ionization. Furthermore, if the field ionization system is operated at lower voltages it becomes a specific detector for water vapor[2].

In the past a major limitation on field ion sources has been the low ion currents available with the single point field ionizers. For the past year the FESS laboratory has been studying the operating characteristics of multiple point field ionization sources as part of the water vapor detection program. In our talks with Dr. Giffen it appeared that a source of this type might provide large enough ion currents for the Voyager system.

In order to develop this idea plans have been made for JPL to assist the work of the FESS laboratory with the purchase of a mass spectrometer of

the type used at JPL. The FESS laboratory will develop a field ionization source for this instrument.

We feel that this type of activity has many advantages. In the FESS laboratory we have often felt that we were not aware of NASA problems and needs for new types of detectors. It was also apparent that no direct relation existed whereby new detectors developed by the FESS laboratory could be used by NASA field facilities.

This new relation with JPL will bring us much closer to an actual operational facility and allow us to keep up with NASA's problems in the areas of detection of gases. The development of new detectors under NsG-458 will continue; our relation with JPL will provide added support for certain very expensive laboratory apparatus. We feel most strongly that this relation with JPL will strengthen our work under NsG-458 as well as providing an important link between NASA, JPL and the University.

The other major area of work under NsG-458 has been a continuation of studies of the surface ionization of hydrogen on hot palladium. As we mentioned in our earlier reports this reaction takes place in air or nitrogen at one atmosphere and has the potential of being an important safety device for hydrogen fueled rocket facilities. The need for a detector of this type has become more apparent recently because of reports of serious accidents with liquid hydrogen systems.

In our last report we indicated that a surface ionization system could be used as a detector for hydrogen in air. The experimental system and some typical results with directly heated palladium filaments were shown in our last report. This work was used by Major C. W. Carlson (U. S. Army) as part of his M.S. thesis in Mechanical Engineering at The University of Arizona.

Since our last report we have improved the filament design and provided for a better control of the filament temperature. This has resulted in improved operation with less scatter in the experimental data. However, directly heated filaments are always somewhat fragile and to adapt the detector for field operation we have been developing an indirectly heated ionizer. This new system is being tested and the results appear quite encouraging.

Surface ionization is interesting in its own right especially since in the case of hydrogen on palladium the Saha equation predicts that such ionization is very unlikely. We are building a diffusion system to measure the $\frac{e}{m}$ ratio of the positive ions produced by hot palladium. This will allow us to determine whether the ions are H_2^+ or H^+ and may give some clue as to the mechanism which produces them.

Surface ionization may also be effective for detection of other gases. Tests in the FESS laboratory indicate that CO may be detected at CO/air ratios as low as 1%. Ammonia may be detected in air at NH_3/air ratios of parts per million. If it appears that detection of either of these two gases is of interest to NASA more effort will be expended in this area.

The area of surface effects in air at one atmosphere leads naturally to the effects of gases on semiconductors. Discussions at Bell Telephone Laboratories during the summer indicated that it may be possible to detect water vapor at very low partial pressures by the effect of water vapor on the characteristics of silicon pn junctions.

Problems of this type of great interest to electronic engineers concerned with semiconductor passivation and arrangements have been made with the Electrical Engineering Department for a joint study program. This effort will be a small scale one, initially. If the results are favorable the work will be expanded.

This concludes the informal part of the report. In the next sections, detailed and more formal reports will be given of our work in various areas.

III. THE DETECTION OF WATER VAPOR IN GASES (EXISTING TECHNIQUES)

The detection of water vapor in gases is a very old problem in engineering. A great deal of effort has been expended in this area and a number of devices are available for measurement of water vapor under various conditions. However, no one detector has all the proper characteristics needed for space applications.

The most general reference on the entire topic is the set of four volumes edited by Wexler[3]. Volume 1 of Ref. 3 covers most of the methods in use for detection of water vapor but since it is a collection of papers by a variety of authors it is not too easy to use a general reference, or as an introduction to the subject.

The various methods used for detection of moisture may be considered under a series of subsections, most of these descriptions are taken from Ref. 3.

1. Dew Point Devices

This is the oldest and most reliable method at relative humidities (R.H.) of 1% or more. A variety of methods may be used for condensing the water vapor and detecting the condensate. For very low R.H. $< 0.1\%$ the detector acts as a pump since it removes water vapor from the system. Detection of the condensate for R.H. below 0.01% becomes time consuming and difficult. Devices of this type are probably not adapted for space applications such as the exploration of Mars.

2. Optical Absorption Techniques

Devices and methods of this type normally make use of the large absorption of water vapor in the visible or near infrared regions of the spectrum. Sensitivities of as high as 1 part per million are reported, Ref. 3, p. 428, but calibration may be difficult and other gases, i.e. CO_2 may interfere. Optical detectors may be useful in space applications where their complexity does not introduce excessive difficulty.

3. Surface Reaction Techniques

Since the words adsorption, absorption, absorbent, etc. are often used interchangeably it seems worthwhile to introduce the standard definitions at this point. The definitions are those usually given in Chemical Handbocks.

a) Adsorption, the adherence, in a thin layer, of a gas or liquid to a solid surface.

b) Absorption, penetration of a liquid or gas into the interior of a solid.

c) Chemisorption, a strong chemical reaction between a liquid or gas and a solid. Usually the liquid or gas is strongly bonded to the surface by this reaction.

d) Adsorbent, a solid which reacts with a liquid or gas by the methods of a) or c) above.

e) Adsorbate, that material, gas or liquid, which is bonded to the surface by the methods of a) or c) above.

f) Absorbent, a material which allows a liquid or gas to enter into its interior, method b) above, i.e. a sponge.

g) Absorbate, a gas or liquid which enters an absorbent.

Most surface reaction systems depend upon the absorption of ambient water vapor by an organic or inorganic material. This in turn changes some measurable property of the material. This change is related to the ambient water vapor pressure in a more or less empirical or analytical way, generally the former. All processes of absorption involve the passage of water vapor into minute passages in the absorbent. Condensation may or may not occur and the response of the instrument may be more or less dependent upon the time needed for water vapor to diffuse in or out of the absorbent.

Absorption devices act as pumps and may seriously deplete the water vapor from a small sample. The effect of absorbed water may be detected in many different ways some of which are listed below.

a) Change of Length

This is the method used in the familiar "hair hygrometer".

b) Change in Mass

A detector of this type is sometimes used, the almost infinitesimal change in mass being detected as a change in the natural frequency of a quartz crystal oscillator[3]. If problems of response time and apparatus complexity can be overcome, a detector of this type may have a space application (see Ref. 3, Vol. 1, p. 578).

c) Change of Capacitance

Water vapor molecules are highly polar and absorption of water vapor will change both the AC and DC capacitance of the absorbent. There are problems with interference by other polar molecules and with long term changes in calibration when exposed to vacuum in space, but detectors of this type have a great potential for planetary investigations, Ref. 3, Vol. 1, p. 372.

d) Change of Resistance

Devices of this type depend upon the formation of a surface layer of adsorbed water which is detected as an effective surface leakage usually with low voltage AC currents. These devices may have great potential and systems of this type are under study by a number of organizations. As in c) above, other polar molecules may give false readings. The advantages and problems of such systems are discussed in great detail by several investigators in Ref. 3, Vol. 1.

e) Electrolytic Sensors

The P_2O_5 detector is typical of this type of detector. The water is adsorbed by the P_2O_5 and electrolyzed by an applied voltage. Several commercial versions of this device are available but since P_2O_5 has a rather high vapor pressure ($\sim 10^{-5}$ torr at $300^{\circ}K$) it is not suitable for long time exposure to vacuum in space. There may also be problems of interpretation if the water vapor is mixed with a gas of unknown composition as may be the case on a planet.

This completes our review of the various types of detectors commercially available. In the next two sections we would like to consider two new methods for detection of water vapor. These methods offer certain potential advantages and we feel that they are worth investigating for this reason.

IV. NEW DETECTORS FOR WATER VAPOR IN GASES

1. Chemisorption of Water Vapor on Semiconductors

In Ref. 4 Allen and Buck reported on experiments involving the chemisorption of water vapor on semiconductors. This is an attractive technique because of its enormous potential for sensitivity at parts per million levels without the need for complex electrical apparatus. Buck and Allen

consider first a p type (hole conducting) material. If such a material is exposed to an acceptor gas, i.e. O_2, the change in resistance will be quite small since the material is already strongly p type. On the other hand, exposure to a donor gas, i.e. H_2O, will result in the surface becoming n type. This n type surface acts as a low resistance in parallel with the interior p type material and the effective change in resistance is quite large. Since silicon will withstand considerable heating, the effect can be reversed and, therefore, used as a detector for donor type gases. The potential sensitivity of such a detector is very high; Buck et al. indicate that as few as 10^6 atoms might be detectable. This is at least a factor of 10^4 better than comparable systems such as those discussed in Section III.

A more sophisticated system would make use of a pn junction diode. Buck et al. consider a reverse biased junction diode. The p region is a high resistivity material and the n region is a low resistivity material. Chemisorption of a donor material on the pn junction area can result in surface breakdown and this effect may be used as a detector for donor gases.

Buck et al. report some experiments on this effect with various gases. Water vapor, acetone, ammonia and amine vapors are donors; nitrogen, argon, helium and other inert gases are neutral; oxygen, ozone and the halogens are acceptors. The predicted sensitivity to as little as 10^6 atoms of gas was essentially confirmed.

The importance of this work lies in the fact that the common atmospheric gases O_2, N_2, A are either <u>acceptors</u> or <u>neutral</u>. Therefore, it should be possible to construct a detector for water vapor in air by using a pn junction diode.

Since this area is of importance to the electrical engineers concerned with semiconductors Mr. V. Wells of The University of Arizona Electrical Engineering Department has modified several commercial junction diodes for test purposes. These diodes are being tested as part of our water vapor detection program. The results will be reported in a future report.

Since this mutual area of interest exists between the AME and EE Departments we have made plans for certain interdisciplinary activities. The EE Department is developing a thin film circuits laboratory and part of this work will make use of apparatus, skills and techniques developed under NsG-458.

We feel that this is a good example of the useful technological fallout from the Space Program.

2. The Corona Discharge

In our earlier reports we discussed the field ionization of water and reported on our own results, and those of Schmidt[2] which indicated that this method could be used as a specific detector for water vapor. However, operation at field ionization voltages (10-15 KV) is only possible if the total pressure is $5 \cdot 10^{-2}$ torr or less. Above this pressure total gas breakdown and arc formation occurs.

In attempting to make use of the multipoint field ionization source at pressures above $5 \cdot 10^{-2}$ torr it was noted that operation in the corona mode was possible.

Corona discharges have been known for many years and the pertinent work has been reviewed in a recent book by Loeb[5]. It is most important to note that corona discharge is <u>not</u> the phenomena used in the usual cold cathode pressure gauge. In a cold cathode gauge the two electrodes are effectively quite close to one another and ions are generated in the gas phase by electrons which are confined by a magnetic field.

In a corona discharge the primary electrode is a sharp metal point or points and the secondary electrode is at effectively an infinite distance away so that discharge takes place to the surrounding gas. (A good example of this type of discharge is the familiar Tesla coil used for finding leaks in glass apparatus.)

Corona discharges are characterized by the local breakdown of a gas near a sharp point held at a positive potential. This sharp point produces a high local field gradient which in turn is able to accelerate ions and electrons. These charged particles can ionize other neutral species by collision or can generate photons by striking the anode. These photons can ionize neutral species in the gas phase.

These two effects combine to produce enough negatively charged particles (electrons and ions) to maintain a steady corona discharge. The discharge is limited to the area near the point because it is only in that region that the field gradient is high enough to initiate and maintain a discharge.

It is clear that a field ionization system consisting of a multi-point brush will be most advantageous for starting a corona discharge. This is natural when we recall that both field ionization and corona discharge require high local field gradients. This in turn indicates that a multi-point brush might be used as a detector for water vapor in the "field-ion-mode" at total pressures of $5 \cdot 10^{-2}$ torr or less and in the "corona-mode" above $5 \cdot 10^{-2}$ torr. No change in geometry would be needed; simply a reduction in applied voltage as the shift from one mode to another takes place.

It has been known for many years that corona discharges are quite sensitive to the presence of water vapor. Many authors have referred in a

qualitative way to this and in Arizona it is often noted that in winter when the relative humidity is low (4%) the breakdown voltage for open conductors is about 30 KV while in summer (R.H. ~ 60%) the breakdown voltage is about 12 to 15 KV.

This great sensitivity to water vapor is quite understandable if we recall that water vapor has a high normal dipole moment while all the normal atmospheric gases, i.e. O_2, N_2, H_2, CO_2, and A have zero dipole moments. This in turn indicates that water vapor will be drawn to the positively charged point and easily ionized by the combination of a high local field gradient and electron impact.

This method of detection of water vapor, by means of its large dipole moment, is very similar to the field ionization of water that occurs at higher voltages and lower ($< 5 \cdot 10^{-2}$ torr) pressures. The major difference is that in the "corona mode" ionization occurs in the gas phase and we measure the discharge current through the discharging brush. Whereas in the "field ionization mode" ionization occurs on the surface of the brush and the ion current is collected on an ion collector at some distance from the ionization source.

In order to investigate the utility of a corona discharge for detection of water vapor a vacuum system has been modified to provide a controlled environment. A thermostatted source of water vapor has been designed to produce air of known relative humidity at various total pressures. A 0-3 KV stable power supply has been provided to drive the corona discharge. A commercial humidity detector, which operates on the change in resistance of an absorbent as the ambient water vapor pressure changes, has been ordered and will be installed by January 1, 1966.

This system will permit us to test the corona water vapor detector and the semiconductor detector (Sect. IV) as well. It is important to indicate that considerable care is needed in operation of humidity chambers for calibration of humidity detectors. We have noticed that if the chamber is operated at a high relative humidity, i.e. 75%, simply letting in drier air, i.e. 25% R.H., does not immediately lower the actual relative humidity to 25%. If the walls of the chamber are at room temperature, an hour may be needed for the system to equilibriate. At 200°F this time is shortened to some 20 minutes. Al_2O_3 insulators which are very effective under normal conditions become almost useless after exposure to air at 75% R.H.

Several authors, Ref. 2, 3, have mentioned time lags in the response of instruments operating with water vapor. We feel that this may be partially due to a failure to allow for equilibrium between the vapor and the test system itself.

A corona discharge detector has an advantage over absorption systems in that it does not pump water vapor or deplete it from the system. The water molecules are ionized and the ions are discharged into the gas where they are neutralized by collision with other gas particles.

There appears to be a disadvantage to the "corona mode" in that the ions cannot be collected as in the "field ion mode". Therefore, the actual discharge current itself must be monitored. This involves the measurement of microamp currents at high, i.e. KV voltages. This presents certain difficulties in both the laboratory and field operations, but similar problems have been encountered and solved with the usual cold cathode gauge systems.

Another disadvantage of the corona discharge is its strong dependence on the total pressure. However, if a separate measurement of the total pressure

is available the corona current can be used as a measure of the partial pressure of water vapor.

We feel that the corona detector deserves investigation in spite of its obvious problems. The main reason for this feeling is the fact that a system equipped with a field ionization mass spectrometer source can be adapted for operation as a corona detector by simply changing the voltage applied to the ionizer.

For example a planetary landing capsule, equipped with a field ion mass spectrometer, could operate as a corona detector for water vapor without any appreciable added weight.

V. A SURFACE IONIZATION DETECTOR FOR HYDROGEN IN AIR AT ONE ATMOSPHERE

In our last six month report we mentioned the possibility that a surface ionization detector might be suitable for a hydrogen-in-air safety device. A few experiments were performed and a typical response curve was shown. A great deal of work has been done since that time and we will review the entire problem in a general way.

Conventional hydrogen detectors operate by burning the hydrogen to water and either measuring the amount of water produced or the heat output of the reaction. Detectors of this type are quite limited in their response to low hydrogen concentrations and, of course, oxygen is necessary for combustion. This precludes operation in a vacuum or inert, i.e. nitrogen, environment.

Recently a most ingenious detector has been reported by Parametrics Inc. of Waltham, Massachusetts[6]. This device makes use of a special metal-oxide alloy which contains a radioactive gas. In the presence of hydrogen the metal-oxide is reduced and the gas is released. The decay in the radio activity of the source is used as a measure of the ambient hydrogen pressure.

This detector is quite effective and the surface ionization detector studied in the FESS laboratory is not thought of as being competitive with the Parametrics radioactive detector but rather as filling a different need. For example, the radioactive decay device cannot be tested without at least partially destroying its capability as a detector. Furthermore, the radioactive elements decay in activity with time, because of residual hydrogen in the atmosphere and the normal half life of K^{85}, (10.6 years). Because of this loss in sensitivity, Ref. 6 indicates that if the ambient hydrogen concontration is 2 parts per million, the K^{85} detector would require replacement after about 35 days of continuous operation. (In Ref. 6 the authors indicate that the usual range of H_2 concentration in their laboratory is 1 - 20 ppm.)

In comparison, the surface ionization detector mentioned earlier can be cycled from storage to operating condition (for testing) innumerable times without damage to the sensitive element. The storage life on the ionization detector would probably be set by the storage lifetime of the associated electronics since the system itself is entirely of metal and ceramic construction.

For these reasons we feel that the surface ionization detector has a definite place as a special safety device. A typical use might be as a detector that could be stored in a space vehicle on a launching area and activated if hydrogen leakage were suspected.

In this period of the program we have improved on the results reported earlier. The experimental system and a typical early calibration curve are repeated from our last report in Figs. 1, 2. Several things should be noted here; first, the vertical bars represent the maximum scatter over several runs. Second, the scatter is primarily dependent upon the use of directly heated

palladium coils for ionizing the hydrogen. The operating temperature of 850°C was quite difficult to measure with an optical pyrometer and the fragility of the filament precluded the use of thermocouples.

In Fig. 2 we have added some new results obtained by Mr. Abramowitz. The slight nonlinearity evident in the curve from the Fourth Annual Report has been greatly reduced. These results were obtained by more careful control of flow conditions and filament temperature and appear to be quite encouraging. There seems to be no question that this method can be used as a detector for hydrogen. However, the Pd coils are fragile and it is difficult to maintain them at a constant temperature as slight variations in gas flow occur.

In our new system the palladium will be in sheet form heated indirectly by a cartridge heater*. The palladium sheet temperature will be monitored by a Pt - Pt / Rh thermocouple. This system will be more reliable and more resistant to shock and vibration.

VI. MEASUREMENT OF THE ION SPECIES EMITTED FROM HOT PALLADIUM

Emission of positive and negative ions from heated metals has been reported for many years. Richardson[7] indicates that the ions emitted by hot palladium are generally those of sodium and potassium. However, this ion current decays after continued heating and a residual current is measured which is related to the ambient conditions near the heated palladium. Other investigators have reported this effect to be greatest when hydrogen was the ambient gas and this has resulted in a long controversy (Ref. 7, 8, 9) over whether or not hydrogen ions are generated by hot palladium. (It is, of course, this hydrogen ion current which is detected by the system we have been discussing above.)

---

*The Watlow Company of St. Louis, Missouri has been most helpful in this program.

This entire question is naturally a rather important one, and some of the pertinent factors have been discussed in a recent book by Kaminsky[10]. For effective surface ionization the work function of the ionizing surface must be larger or at least equal to the ionization potential of the ambient gas molecules. For example the work function of palladium is about 5 ev, the ionization potential of potassium is 4.32 ev. Experimentally, hot palladium is found to be an excellent ionizer for potassium atoms.

In the case of Pd/H_2 the situation is reversed, the ionization potential of hydrogen is 15.6 ev. and one would not expect hydrogen to be directly ionized by palladium. It is precisely this difficulty which has led certain investigators to question the existence of hydrogen ions from hot palladium.

To estimate numerical values for the expected ionization of H_2 on hot Pd we make use of the Saha equation from Ref. 10,

$$\alpha_{\epsilon=o} = \frac{g+}{go} \exp \left| \frac{(\phi - I)}{kT} \right| .$$

Here the subscript $\epsilon = 0$ indicates that no applied electric field is present, the symbol α represents the ratio of the positive ions emitted per second to the total number of neutral atoms or molecules emitted per second. g_+ , g_o are the statistical weights of the ionized and neutral species, ϕ and I are the work function of the surface and the ionization potential of the reacting gas respectively.

For the hydrogen-palladium system ϕ = 5 ev, I = 15.6 ev and the applied field is too small to introduce any error into the assumption that $\epsilon = 0$. Choosing T = 1150°K permits a calculation of α if g+/go is known. We shall <u>assume</u> that if the neutral species are molecules, then the ions

are molecular ions and vice versa. Then g+/go ~ 1/2 and we may solve for α (the actual choice of $\frac{g+}{go}$ will not effect our final result). Under these conditions we find

$$\alpha \sim 10^{-50} \quad .$$

This indicates that the probability of positive ion emission is vanishingly small. It is precisely this result which led certain investigators, i.e. Ref. 9 to predict that no hydrogen ions could be generated by hot palladium.

In the next section we will derive an experimental value of α from our data and indicate that it has a value of about

$$\alpha \sim 2 \cdot 10^{-10} \quad .$$

We feel that the discrepancy between these two values may be explicable in terms of the knowledge that hydrogen is very soluble in palladium and solution occurs in the form of ions (H^+). (See Mr. Eisenstadt's thesis in the appendix, p. 32, for a discussion of this point.)

We suggest that as the ambient H_2 pressure increases near the filament the concentration of H^+ ions inside the metal lattice increases proportionately. The excape of some fraction of these ions from the lattice produces the measured current. To date we have no proof of this mechanism; it is hoped that proof will emerge from the diffusion experiment discussed elsewhere in this report.

To estimate the flux of H_2 molecules to and from the surface we make the following assumptions

1. the gross motion of the gas may be neglected by comparison with the high mean velocity of the H_2 molecules.

2. the flux of H_2 molecules to the surface is controlled by kinetic rather than flow considerations. This in turn implies that

no viscous or concentration boundary layer exists near the hot filament.

The total pressure is 760 torr, the average gas temperature near the filament is somewhere between the filament temperature of 850°C and room temperature 23°C. The gas consists of a mixture of H_2 and N_2 in thermal equilibrium. The number density of H_2 molecules is 1% of the density of N_2 molecules.

The flux of H_2 molecules to the surface is given by the usual kinetic relation

$$N_{H_2} = \frac{1}{4} M_{H_2} \bar{v}_H^2 \left(\frac{1}{cm^2\ sec}\right)$$

Assuming an average temperature for the gas we can obtain a mean velocity

$$\bar{v}_{H_2} = 1.7 \cdot 10^5 \frac{cm}{sec}$$

The number density M_{H_2} is 1% of the nitrogen molecule number density and therefore

$$M_{H_2} = 3 \cdot 10^{17} \frac{1}{cm^3} \quad .$$

Assuming that the Pd filament is a wire 3 cm in length and $2.54 \cdot 10^{-2}$ cm in diameter we obtain the total surface area and then the actual flux of H_2 molecules to the wire surface,

$$N_{H_2}A = 2.8 \cdot 10^{21}\ sec^{-1} \quad .$$

If each molecule were singly ionized and the ions collected, the current would be about 45 amps. Since the actual currents under the above conditions are about 10^{-8} amps the ionization efficiency (the factor α from our earlier

calculation using the Saha equation) must be about

$$\alpha = 2 \cdot 10^{-10} \quad .$$

Earlier we calculated a value of

$$\alpha = 10^{-50}$$

from the Saha equation. This difference of a factor of 10^{40} is one of the largest discrepancies between theory and experiment that the authors have ever observed.

For this reason we feel that another mechanism is at work and suggest the solution of hydrogen in palladium with the evaporation of ions from the metal.

Our belief in the existence of an ion current from Pd in H_2 is based upon our experiments. These experiments repeated dozens of times by three different investigators, indicate that positive ions are definitely emitted by hot palladium in a hydrogen ambient. The nature of these ions is unknown; they may be H_2^+, H^+ or a Pd/H ion. To settle this question we are building a system to measure the $\frac{e}{m}$ ratio of the ions by diffusion techniques. In the absence of a mass spectrometer the diffusion system discussed by Loeb[11] seems most effective. The $\frac{e}{m}$ ratio of hydrogen ions is so different from that of sodium or potassium that we should have no difficulty in separating ions by their $\frac{e}{m}$ ratio.

A drawing of the system itself is shown in Fig. 3. A nitrogen-hydrogen gas mixture moves through a rectangular duct. Ions are generated by a hot filament and are carried along by the gas while diffusing in the applied electric field. The different ions may be separated in $\frac{e}{m}$ ratio because of their

different rates of diffusion. The method is quite sensitive but it gives only the number of ions of each $\frac{e}{m}$ value relative to one another. However, particular $\frac{e}{m}$ values can be established because a new Pd wire always emits great numbers of N_a^+ and K^+ ions when heated. The problem is analogous to calibrating a mass spectrometer. The results of this study will be given in our next report.

REFERENCES

1. Beckey, H.,
Field Ionization Mass Spectroscopy
Advances in Mass Spectroscopy
ed. Elliot, R., Pergammon Press, N. Y. p. 1, 1964.

2. Schmidt, Von W.
Masspectrometric Investigations of the Field-Ionization of Water Vapor on Tips of Tungsten, Platinum and Iridium. (In German)
Zeit. Fur. Nature.,
Band 19, Heft 3, pp. 318 (1964).

3. A. Wexler editor
Humidity and Moisture, Vol. I, II, III, IV
Reinhold Pub. Co., New York, 1963.

4. T. Buck, F. Allen and J. Dalton
Surface Effects in Detection
p. 147, Spartan Books Inc., Washington, D.C., 1965.

5. L. Loeb
Electrical Coronas
University of California Press, Berkeley, 1965.

6. O. Cucchiara et al.
Detection of Hydrogen Aboard Aerospace Flight Vehicles
April 1964
Defense Documentation Center AD 600153

7. O. Richarson
The Emission of Electricity from Hot Bodies
Longmans Green and Company, New York, 2 ed. 1921, Chap. VI, VII.

8. C. Bachman, P. Silverberg
Thermionic Ions from Hydrogen-Palladium
J. Appl. Phys.
29, No. 8, 1266-1267 (1958)

9. Yu. I. Belyzkov, N. I. Ionov
Pulsed Mass-Spectrograph Investigation of Desorption of Hydrogen and Deuterium from Palladium
Zh. Tekh. Fiz. (In Russian)
30, No. 2, 216-222 (1960).

10. M. Kaminsky
Atomic and Ionic Impact Phenomena On Metal Surfaces
Academic Press, N. Y. 1965

11. L. Loeb
Fundamental Processes of Electrical Discharge in Gases
p. 5, J. Wiley and Sons, N. Y., 1939.

FIGURES

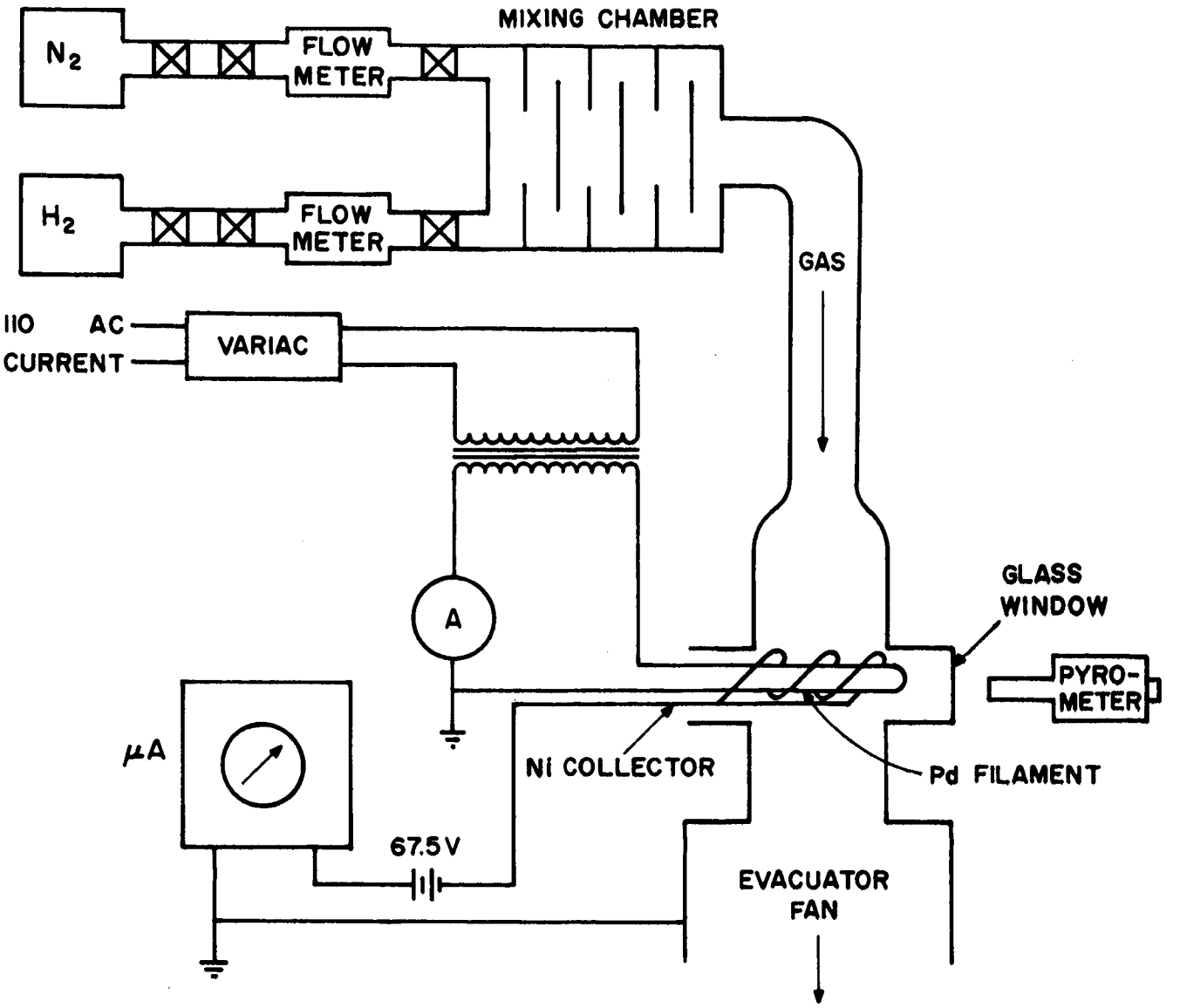

FIG. 1

HYDROGEN DETECTOR SYSTEM

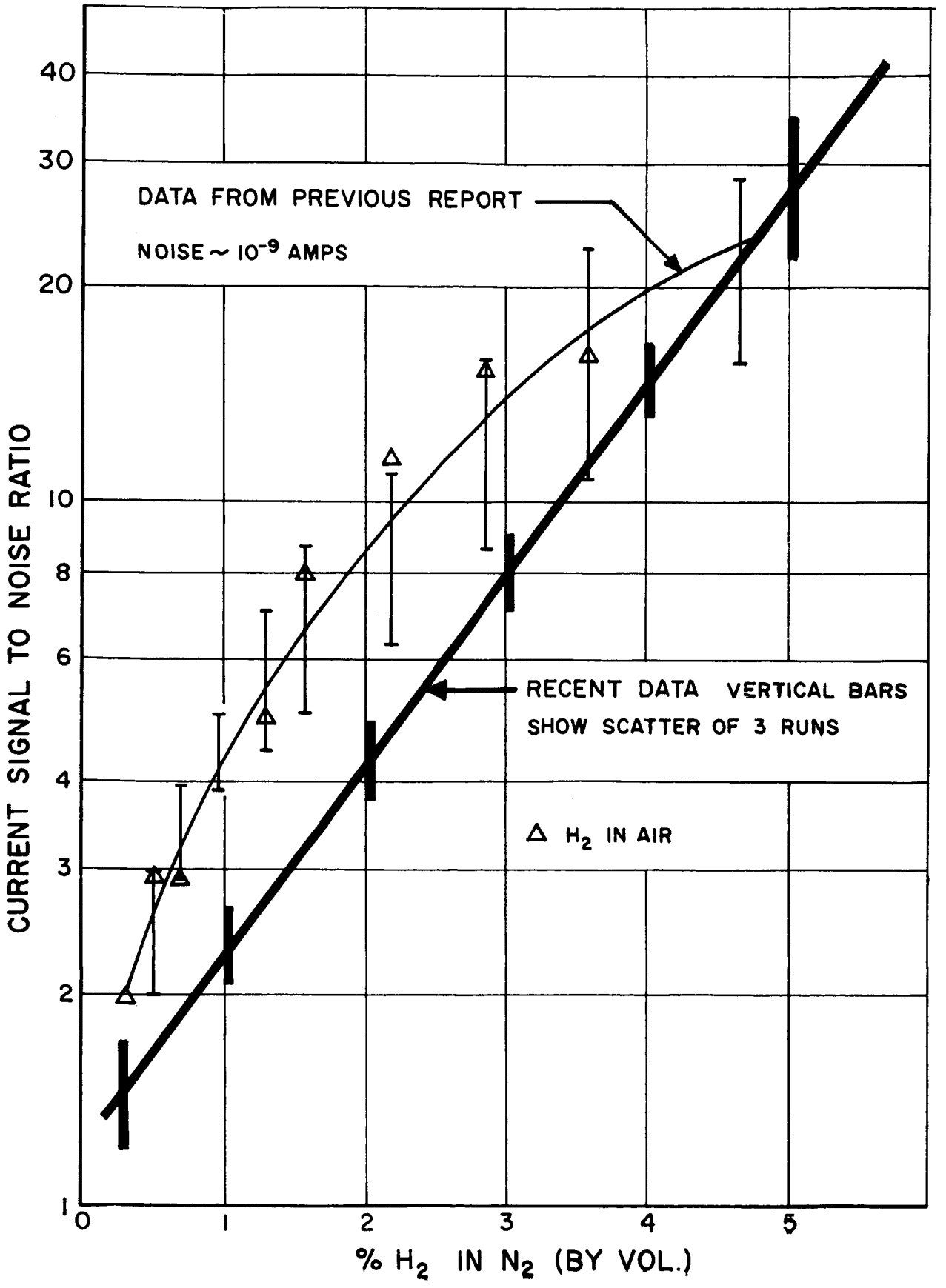

FIG. 2 RESPONCE OF THE SURFACE IONIZATION DETECTOR

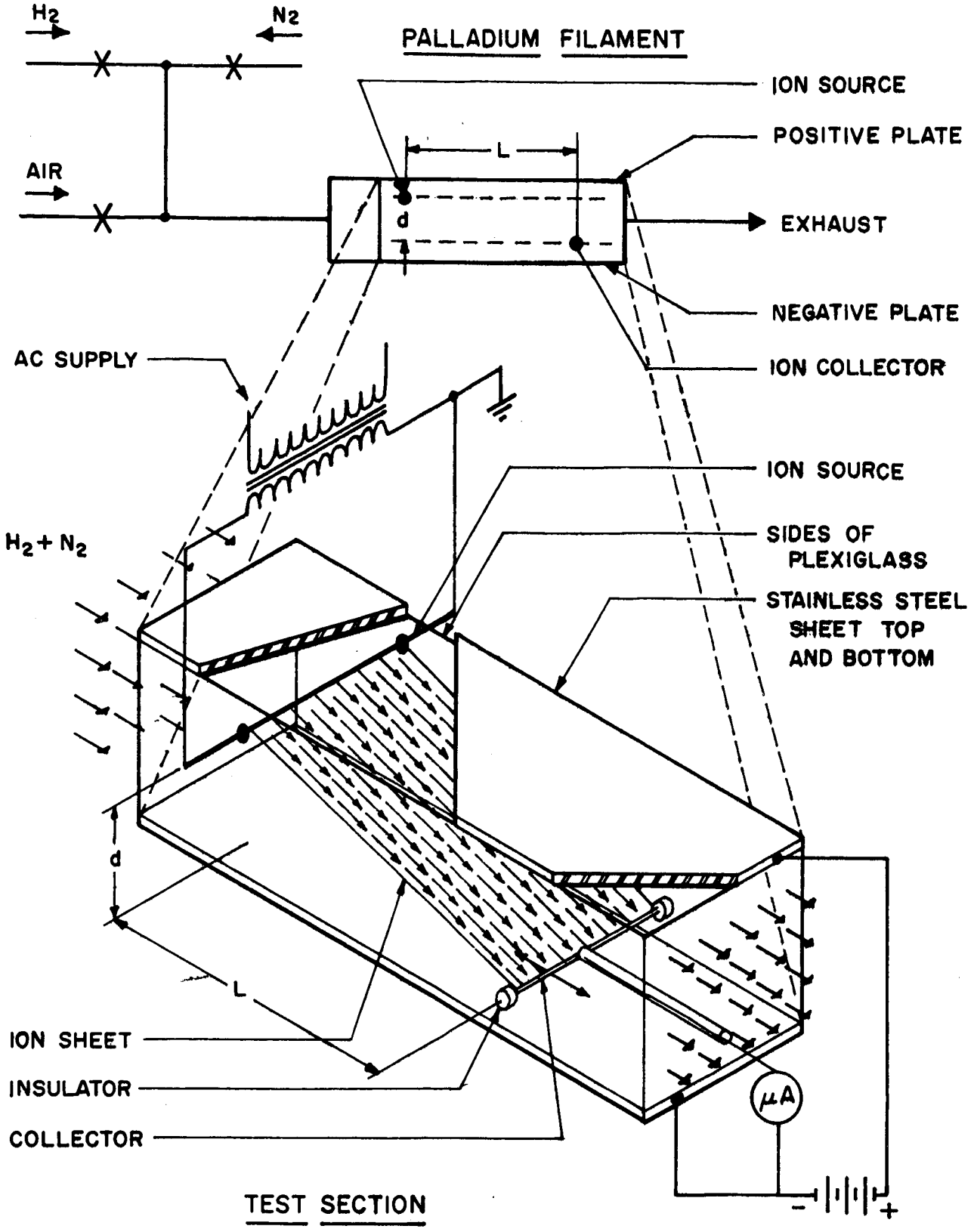

FIGURE 3. DIFFUSION SYSTEM FOR MEASUREMENT OF e/m OF IONS FROM HOT PALLADIUM.

APPENDIX

In this appendix Dr. Eisenstadt's Ph.D. Dissertation is reproduced in its entirety. The figures and graphs are in the order that they appeared in the dissertation. The appendix forms a separate section of this report which is complete in itself.

CHANGE IN THE THERMIONIC EMISSION CURRENT OF PALLADIUM DUE TO CHEMISORPTION OF ATOMIC AND MOLECULAR HYDROGEN

by

Melvin M. Eisenstadt

A Dissertation Submitted to the Faculty of the

DEPARTMENT OF AEROSPACE AND MECHANICAL ENGINEERING

In Partial Fulfillment of the Requirements
For the Degree of

DOCTOR OF PHILOSOPHY

In the Graduate College

THE UNIVERSITY OF ARIZONA

1 9 6 5

STATEMENT BY AUTHOR

This dissertation has been submitted in partial fulfillment of requirements for an advanced degree at The University of Arizona and is deposited in the University Library to be made available to borrowers under rules of the Library.

Brief quotations from this dissertation are allowable without special permission, provided that accurate acknowledgment of source is made. Requests for permission for extended quotation from or reproduction of this manuscript in whole or in part may be granted by the head of the major department or the Dean of the Graduate College when in his judgment the proposed use of the material is in the interests of scholarship. In all other instances, however, permission must be obtained from the author.

SIGNED: Melvin Eisenstadt

ACKNOWLEDGMENT

The author takes this opportunity to express his gratitude to Dr. Stuart A. Hoenig. It was Dr. Hoenig who initially suggested this research program and who provided guidance and encouragement throughout the course of the investigation. The writer's appreciation also goes to Dr. Myron Corrin of the Chemistry Department, who provided several stimulating discussions.

For aid in the fabrication of the vacuum apparatus, the author thanks Mr. Gerald Fields and Mr. Ira Clough for the metal work, and Mr. Harry Nunnamaker for the glass blowing.

The writer also thanks his wife, Pauline, for showing a great deal of patience and for providing a home environment conducive to completing this work.

Finally, the author wishes to express his appreciation to the National Aeronautics and Space Administration for providing the financial assistance required by this project.

TABLE OF CONTENTS

Table of Contents (Continued)

Table of Contents (Continued)

Table of Contents (Continued)

LIST OF FIGURES

List of Figures (Continued)

LIST OF TABLES

ABSTRACT

The thermionic emission current from a palladium filament at 1,000°C was measured while the filament was exposed first to a molecular hydrogen beam and then to a beam of atomic hydrogen.

The beam source was a tungsten-26% rhenium tube. The molecular beam effused from the source at room temperature; the atomic beam was obtained by heating the beam source to 2,400°K, thereby thermally dissociating the molecular hydrogen. The experiments were performed in an ultra-high vacuum system, with background pressures in the 10^{-9} torr range.

The results indicate that the thermionic emission increases as the beam intensity increases, for both H and H_2. This indicates that hydrogen chemisorbed on palladium at 1,000°C forms a dipole layer with the positive side away from the surface, thus decreasing the work function. The decrease in work function was greater during molecular beam operation than during operation of the atomic beam, indicating that H_2 chemisorbed more readily than H. This is attributed to a difference in the sticking coefficients of H and H_2 on palladium.

The sticking coefficient of atomic hydrogen was found to be lower than that of molecular hydrogen by a factor of about 1/2. This difference is attributed to the mechanism by which energy is exchanged between the gas and the metal lattice during a collision. Most of the slow moving molecules (300°K) transfer enough kinetic energy to the palladium

lattice during a collision so that they can be adsorbed. The more energetic atoms (2,400°K) are not so successful in this energy transfer, consequently a considerable fraction of them will strike the surface and rebound back to the gaseous state.

When gaseous molecular or atomic hydrogen chemisorbs on palladium, the chemisorbed species is atomic hydrogen for both cases. Thus, molecular hydrogen must dissociate before chemisorbing. A question then arises as to whether or not this dissociation is the rate determining step for the chemisorption of H_2 on palladium. It was found that dissociation is not rate determining.

Chapter 1

INTRODUCTION

1.1 History

The chemisorption of gases on surfaces is a well-known phenomenon and is responsible for many significant surface effects. These effects are important in such diverse fields as corrosion and catalysis.

The early period of chemisorption research activity can be considered as extending from about 1915 to the middle 1920's. The first systematic study of the chemisorption of gases on metals was initiated by Langmuir[1], who investigated the interaction between hot tungsten filaments and various gases at low pressures. Interest in chemisorption grew quickly, and Langmuir was followed by Roberts and other workers. As the number of workers grew, so did the number of theories which attempted to explain experimental data. These theories stressed such properties as crystal structure, electronic configuration of the solid and gas, or the previous history of the metal, such as heating or cold working. The problem was further complicated by the fact that many of the data were contradictory and were often not reproducible.

During the one or two decades prior to World War II, much evidence was given in favor of the crystal structure being the most dominant factor in chemisorption. The group which postulated electronic configuration was active, but data presented by Beeck and others[2] indicated that the chemisorption process could be explained in terms of crystal

structure. This explanation was supported by theoretical analyses, such as that of Sherman and Eyring[3].

The postwar period saw a renaissance of the electronic configuration theory. The work of Schwab, Dowden, and others left little doubt that chemisorption could be explained qualitatively in terms of the electron configuration of the adsorbent and adsorbate[4,5]. However, the previous results which showed the definite effects of crystal structure were still valid, since the structure of the surface determined the locations of the chemisorption bonds. The bonding forces themselves were attributed to electronic interaction.

The most recent general review of chemisorption is that of Hayward and Trapnell[6], and it seems clear from their discussion that chemisorption processes can be understood, at least qualitatively, in terms of the present electronic configuration theory.

1.2 Recent Developments

Techniques and equipment for scientific research have developed at an extraordinary rate in the past one or two decades. Chemisorption workers have taken full advantage of these developments. The spectrum of techniques includes such things as infra-red studies for determining chemisorption bond strengths and magnetic studies to find the effect of chemisorption on the paramagnetic susceptibilities of adsorbents.

The recent progress of ultra-high vacuum technology has had great significance for chemisorption researchers. In the previous section, the problem of contradictory data appearing in the literature was mentioned. This was partially resolved when Langmuir[7] showed that certain

surface reactions depended upon surface contamination by extraneous materials. The necessity of using clean systems and non-contaminated surfaces is now generally recognized, and comprises one of the major difficulties for present workers in the field.

It is now possible to generate clean surfaces in vacuum by means of evaporated film techniques[8] or to clean surfaces by means of ion or electron bombardment[9]. While these techniques are very useful, they introduce other uncertainties into the problem. The surface condition of a thin film depends upon the annealing procedure used. These films are usually porous when first formed, and it is difficult to generate two almost identical films unless sintering is very carefully controlled.

Bombardment of a surface by ions or electrons can result in surface roughening, with the degree of roughness depending upon the energy of the ions or electrons used[9]. If surfaces are annealed after bombardment, there is still some question about the final condition of the surface.

Once a clean surface has been obtained, it must be kept free from contamination during the course of an experiment. Using the kinetic theory of gases, it can be shown that a surface can accumulate a monolayer of contaminants in a matter of seconds at a pressure of 10^{-6} torr[10]. This suggests that much of the information given in the literature was obtained on surfaces containing an unknown amount of unknown contaminants, and such data may or may not be typical of the gas-metal system investigated. Even results derived from work performed under good vacuum conditions must be carefully scrutinized.

Pressures in the neighborhood of 10^{-9} torr will yield reasonable working times with little contamination[10]; experiments made under these conditions are usually repeatable and correlate well with other data taken under these conditions. Modern equipment and techniques can produce vacuum conditions in this range.

At present, there is a need for reliable chemisorption data obtained under clean experimental conditions. Such data should prove to be a great aid in formulating a comprehensive theory of chemisorption.

1.3 Purpose of the Present Experiment

It is generally accepted that any metal which catalyzes the hydrogen-deuterium exchange reaction will chemisorb hydrogen as atoms rather than molecules[6]. The group of metals which catalyze this reaction includes most of the transition metals in Group VIII of the periodic table, and several of the other transition metals as well[11]. The atomic mode of adsorption indicates that the H_2 dissociates during the chemisorption process.

Consider two chemisorption processes. In the first, a surface of one of the above mentioned metals is exposed to molecular hydrogen, resulting in chemisorbed atoms on the metal surface. In the second, the surface is exposed to atomic hydrogen, again resulting in chemisorbed atoms. Although the chemisorbed species is the same in both cases, the adsorption processes are different. The first case includes a dissociation; the second does not. The sticking coefficients may also be different for the two cases (the sticking coefficient is defined as the ratio

of the number of particles which are adsorbed to the number of particles which strike the surface, i.e., it is the probability that an impinging particle will adsorb).

This discussion raises two interesting questions concerning differences between chemisorption of atomic and molecular hydrogen. These are:

1. Is the dissociation of molecular hydrogen the rate determining step in the chemisorption of H_2?

2. Is there a significant difference between the sticking coefficients of atomic and molecular hydrogen on these metals?

The present experiment is designed to answer these questions for the specific case of the hydrogen-palladium system. This will be done by comparing the chemisorption of molecular and atomic hydrogen on palladium. The details of the chemical mechanisms involved are discussed in Chapter 3.

1.4 Experimental Techniques

In order to investigate this problem, it is necessary to expose a palladium surface to both a molecular and an atomic hydrogen environment. Consideration of the various methods of generating these environments leads to the selection of a molecular beam system.

It is known that a hot tungsten filament will dissociate a fraction of the H_2 that comes into contact with it[12]. This reaction can be used to provide a source of atomic hydrogen. The atoms resulting from the dissociation reaction can recombine on the system walls and desorb as molecules. The resulting environment would thus be a mixture of

atomic and molecular hydrogen, and it is difficult to define this environment accurately.

An electric discharge could also be used to produce atomic hydrogen[13], which could then be introduced into the vacuum system to strike the palladium surface. Since an electric discharge is very energetic, there would be a strong possibility of forming species such as H^+, H_2^+, or excited H_2 states. Again, the environment would not be well defined.

A molecular beam consists essentially of two chambers separated by an orifice, through which a beam of molecules (or atoms) effuses. The pressure in the source chamber is such that free molecular flow exists. Therefore, a wire placed in the path of the effusing molecules will intercept a known fraction of the beam. If an atomic beam is desired, it is necessary merely to heat the source and thermal dissociation will occur. For hydrogen, temperatures in the neighborhood of 2400°K are required. These temperatures can be obtained by using a tungsten tube for the beam source and electrically heating the tube. The beam system described above will provide a well-defined source of either atomic or molecular hydrogen and will permit a valid comparison of the data taken in both environments[13].

In the present experiments, the change in thermionic emission current from a hot palladium filament was used as a measure of the amount of hydrogen chemisorbed. Filament temperatures in the neighborhood of 1,000°C were utilized. This technique permits acquisition of data in the high temperature range, which is not otherwise available

for the hydrogen-palladium system. In addition, the components required for this technique are compatible with a molecular beam system.

1.5 Selection of Palladium

There were several reasons for the selection of palladium as the metal for the present experiments. Palladium is known to chemisorb hydrogen strongly[6], and to catalyze hydrogenation reactions[14]. These properties are not unique to palladium; they are exhibited by several other transition metals as well.

The literature contains some information concerning molecular hydrogen chemisorption on several metals[6]. Tungsten has been well investigated since tungsten surfaces can be cleaned by electrically heating them to a high temperature (flash filament technique). Molybdenum also possesses this advantage. Nickel is well represented in the literature, as are some of the other ferromagnetic elements. A reasonable amount of work has been done with hydrogen on platinum. However, data for the chemisorption of hydrogen on palladium are scanty.

It was considered most useful to study a metal which had not been highly investigated. Palladium was chosen since it possesses the properties required for this investigation and has not been extensively studied.

Chemisorption of atomic hydrogen on metals has been investigated to a very small extent, and the atomic hydrogen source used in these investigations has usually been a heated tungsten filament[15]. It is difficult to obtain quantitatively meaningful results from such a source

and no information on the questions of Section 1.3 has been obtained in the experiments of Ref. 15.

The molecular and atomic beam experiments performed in the present investigation have not previously been done on any metals, to the author's knowledge.

1.6 High Temperature Chemisorption Information

There are both basic and practical reasons for acquiring high temperature chemisorption data. If a general theory of chemisorption is to be formulated, data should be available throughout a wide temperature range to aid in the formulation. Also, space technology currently needs information concerning reactions on hot surfaces in connection with exit and reentry heating problems. In addition, high temperature chemisorption effects which are measured by thermionic emission techniques provide a method for measuring partial pressures of various gases under vacuum conditions[16,17]. The device which accomplishes this is small, light, and reliable; it is well suited for space missions.

In the past, thermionic emission measurements have been limited to refractory metals. High temperatures were needed to produce the required emission currents. The sensitivity of modern instruments has reduced the temperature requirement, and thermionic emission techniques can now be used to obtain chemisorption information from many non-refractory materials.

The problem at hand is an interdisciplinary one, using specialized techniques. Because of this, the next chapter will be devoted to a brief outline of the various topics that are pertinent to understanding and interpreting the problem. Then the ideas which are derived from chemistry, physics, and vacuum engineering should proceed in a unified manner.

Chapter 2

THEORETICAL CONSIDERATIONS

2.1 Adsorption

Adsorption occurs when two immiscible phases are brought into contact, and the concentration of one component is greater at the interface than in the bulk. We will be concerned with a gas phase and a solid (metal) phase. Adsorption is generally attributed to interaction between the gas and the metal surface. A molecule (or atom) striking a metal surface is attracted to the surface by bonding forces. These forces are often strong enough to retain some of the molecules at the surface, where they will remain until they acquire sufficient energy to break the surface bond. When this energy is acquired, the molecules desorb. Considering this mechanism on a macroscopic scale, we have a dynamic situation in which adsorption and desorption occur simultaneously. Equilibrium occurs when the adsorption and desorption rates are equal.

Two types of adsorption are generally recognized: physical and chemical. By convention, the distinction between the two is the order of magnitude of the heat of adsorption as described below.

2.1.A Physical Adsorption

Physical adsorption is attributed to van der Waal's type forces. The interaction between a pair of non-polar molecules is often described by the Lennard-Jones 6-12 potential. For this potential, the attractive forces are of short range and vary as the inverse seventh power

of the separation[18]. The situation is altered when interaction occurs between a gas molecule and a metal surface. For this arrangement, one can take the sum of the forces between the gas molecule and the surface molecules (or atoms), again using the 6-12 potential. This procedure shows an attractive force which varies as the inverse fourth power of the perpendicular distance between the surface and molecule[19].

Since the van der Waal's forces are relatively weak, physical adsorption is weakly exothermic. The heat of physical adsorption is of the same order of magnitude as the heat of condensation of the gas. This might be expected since the forces between molecules in a liquid are considered to be of the van der Waal's type.

2.1.B Chemisorption

Chemisorption is attributed to the same type of valence forces that control chemical reactions. The heat of adsorption is generally used as the criterion for distinguishing between physical and chemical adsorption. Processes in which the heat of adsorption is of the same order of magnitude as the heat of condensation are classified as physical adsorption; those with higher heats of adsorption are classified as chemisorption. The heat of adsorption criterion for distinguishing physical adsorption from chemisorption is ambiguous since it is possible to have chemisorption bonds whose strength is comparable to van der Waal's bonds.

A good definition of chemisorption has been suggested by Leftin and Hobson[20]. They define chemisorption as an "adsorption which

produces a new chemical species by fragmentation of the molecule or of its electron complement".

The term "chemisorption" implies that the process is specific, i.e., particular metals will chemisorb particular gases. This has been generally found to be the case. A good example is tungsten, which shows a large affinity for oxygen. Tungsten will preferentially chemisorb oxygen from a mixture of seven parts of N_2 to one part of O_2[16]. The same is true of a thirty to one mixture of CO_2 and O_2[21]. This situation would be expected since the heat of chemisorption of O_2 is about twice that of N_2 or CO_2[6]. Both N_2 and CO_2 will chemisorb on tungsten in the absence of O_2.

Consideration of the microstructure of a crystal surface leads to the concept of adsorption sites. A homogeneous metal surface can be visualized as an ordered array of atoms in a plane, with constant interatomic spacing. The potential energy of a gas atom interacting with the surface will vary from point to point due to the geometric arrangement. The surface can be schematically represented as a plane over which the potential energy of the adatom varies periodically (an adatom is an atom which has been adsorbed). A one dimensional analog is shown in Fig. 1. Adatoms tend to chemisorb in the troughs between surface atoms, hence these are called adsorption sites. This type of adsorption is said to be localized. If the potential variations are so small that the troughs effectively vanish, the adsorption is termed non-localized. These concepts were first proposed by Langmuir[22]. Since the surface of a crystal is composed of atoms or molecules with definite spacings, potential variations will be present.

The role of the solid in bonding with adsorbates can be described in terms of the band theory of solids. In this theory the allowed energy levels of the electrons in the solid are grouped into bands, and the electron energies within the bands are considered to be quasi-continuous, that is, the allowed bands may be separated by a forbidden energy zone or they may overlap. In the case of metals, the highest energy band containing electrons is not completely filled[23]. The electrons in this partially filled band have a large number of unfilled energy states available to them and can readily transfer to these states by gaining a small amount of energy. When an electric field is applied to the metal, the electrons in the partially filled energy band acquire a drift velocity in the direction opposite to that of the applied field, resulting in an electric current. The electrons in the filled bands are unable to acquire a drift velocity since they cannot readily change their energy state. Thus, electrical conductivity can be attributed to the presence of electrons in a partially filled (conduction) band.

The conduction electrons can participate in chemical bonding. In the case of ionic bonds, electrons which are given up by the adsorbate enter this conduction band and vice versa. Conduction band electrons are also available for covalent or partial ionic bonding. Since chemisorption can either contribute or remove electrons from the conduction band, it is capable of changing the electrical conductivity of a metal. It should be noted that this process also changes the Fermi level of the solid (the Fermi level is that energy level at which the probability of being filled is 1/2).

If a metal surface is homogeneous, the electron density (or electron cloud) will not terminate abruptly at the surface but will decay asymptotically[24]. The spill-over of electrons at the surface will form a double charge layer with the negative side outermost, as shown in Fig. 2.

Chemisorption will alter this double layer. The adatoms will be held to the surface by a bond having some degree of ionic character. If the adatoms tend to contribute an electron to the conduction band, the outermost layer will be positive, and vice versa. Thus, chemisorption will produce a dipole layer on the surface. A positive outer layer will decrease the work function of a metal; a negative layer will increase it[25].

It has been found that the heat of chemisorption decreases as the degree of surface coverage increases. Thus, gas atoms are chemisorbed more strongly on a clean metal surface than on one which has a partial monolayer of adatoms. One of the major causes of this phenomenon is the fact that metal surfaces are usually heterogeneous rather than homogeneous. Because of this, the bond between the adsorbent and adsorbate is stronger at certain adsorption sites than it is at others[6]. Those sites which exhibit stronger bonding will acquire chemisorbed atoms quickly. The sites with weaker bonding will acquire adatoms only after the stronger sites have been filled. Chemisorption at a site which exhibits strong bonding will release more heat than chemisorption at a site having weaker bonds. Therefore, the heat of chemisorption will decrease as the surface coverage increases.

Lateral interaction between adatoms can also cause the heat of adsorption to decrease as surface coverage increases. Since the adatoms have a net electric charge, interactions between them become significant as the surface becomes crowded. This situation can lead to weaker bonds and mutual depolarization of the ad-layer[24].

Not only does the heat of adsorption change with surface coverage, but there is evidence that the polarity of the dipole layer also changes in some cases. This apparently occurs with hydrogen on several transition metals[26,27] and may be indicative of a change in bond type as chemisorption progresses. This will be discussed further in Section 2.4.

2.1.C Mobility of Chemisorbed Atoms

Figure 1 was previously used in explaining the concept of localized adsorption. Referring to the figure, one of three things can happen as an adatom gains energy. If it gains a small amount of energy, it will remain in the vicinity of the chemisorption site. Energy gains in excess of the heat of desorption will, of course, cause desorption. If an adatom acquires an energy which is sufficient to bring it out of the trough but not enough to permit it to desorb, it will migrate over the surface and adsorb on another site. The energy required for these site-to-site migrations is called the activation energy for surface migration.

The rate of migration depends primarily upon the temperature and surface, with parameters such as degree of coverage possibly exerting a secondary influence. Migration rate increases with temperature

and decreases with the number and strength of the bonds which hold the adatom to the surface.

The migration of hydrogen on tungsten and nickel has been observed by Gomer, Wortman, and Lundy in the field emission microscope[28,29]. They found that a hydrogen layer migrates on tungsten at 180°K, and that a temperature of 240°K will initiate migration on nickel.

It is of interest to determine whether or not hydrogen chemisorbed on palladium is mobile under the conditions of the present experiment (1,000°C). The behavior of hydrogen on palladium should be similar to that of nickel since these metals are similar in electronic configuration (Group VIII of the periodic table), have the same lattice structure (body centered cubic), and have approximately the same heat of chemisorption for hydrogen.

Beeck[14] experimented with the hydrogenation of acetylene using several transition metals as catalysts. Experiments were made at 23°C, and palladium was found to be more active than nickel. This would not be the case if chemisorbed hydrogen was immobile on palladium. Thus, it can be reasonably assumed that hydrogen migrates freely on palladium at room temperature.

Since the present experiments were performed at about 1,000°C, the chemisorbed hydrogen should be highly mobile. If the density of the ad-layer is not too high and the adatoms are highly mobile, the adsorbate can be considered as a two-dimensional gas. The equations describing the behavior of such a gas are analagous to the three

dimensional case. The concept of a two dimensional gas has been discussed by de Boer[30].

2.2 Thermionic Emission and Work Function

The phenomenon of thermionic emission and the various quantities which are related to it will be discussed in this section.

2.2.A The Richardson-Dushman Equation

The electron flow emitted from the surface of a heated metal is called the thermionic emission current, and is described by the Richardson-Dushman equation. This equation can be derived from the free electron theory of metals, as is done by Kittel[23]. In this theory, conduction electrons in the metal have a velocity distribution in accord with Fermi-Dirac statistics. An electron approaching the metal surface, with sufficient momentum in a direction perpendicular to the surface, can overcome the surface potential barrier and escape from the metal. This is shown schematically in Fig. 3. The height of the surface potential barrier is the energy difference between an electron at rest an infinite distance from the surface and an electron at the Fermi level ($\bar{\mu}$ in Fig. 3). The zero energy level is taken as an electron at rest at infinity, while E_L is a reference which denotes the lowest electron energy level in the metal.

The Richardson-Dushman equation is

$$j = AT^2 \exp(-\phi/kT)$$

where j is the current density in amperes/cm^2, A is a constant whose

theoretical value is 120 amps/cm^2-deg^2, and ϕ is the work function[23].

The values of ϕ and A can be determined experimentally by plotting ln j/T^2 vs $1/kT$ (Richardson-Dushman plot). The slope of the resulting straight line is the work function ϕ, while the intercept gives the value of A. The fact that such plots are usually straight lines indicates that the functional form of the equation is correct. The value of the constant A, however, often deviates from its theoretical value. Kittel[23] lists values of A for seven transition metals, and they vary from 30 to 160 amps/cm^2-deg^2.

This variation is not surprising when one considers the assumptions used in the derivation, and the difficulty of reproducing these conditions experimentally. It is assumed that no space charge exists about the emitter. This condition can be approximated experimentally by placing a high potential anode near the emitter. However, the apparent work function decreases with increasing external field strength (Schottky effect). The derivation also assumes that the emitter surface is smooth. The effects of surface roughness and crystallographic orientation of the emitter are discussed in Section 2.2.D and are shown to be significant. Part of the discrepancy between the theoretical and experimental values of A can be attributed to the temperature dependence of ϕ. If ϕ is expressed as $\phi = \phi_o + \alpha T$, where ϕ_o is temperature independent, it can be shown that

$$A_{experimental} = A_{theoretical} \exp(-\alpha/k)$$

Dekker[25] states that $d\phi/dT$ is approximately 10^{-4} electron volts per ^oC. A good discussion of the assumptions involved in deriving the Richardson-Dushman equation has been given by Herring and Nichols[31].

2.2.B Work Function

Two non-equivalent definitions can be found for the work function ϕ; one is simpler and the other more accurate. The simpler one[23] considers the surface potential barrier to be a step function, in which case the work function becomes equal to the quantity $\bar{\mu}$ in Fig. 3.

Wigner and Bardeen[32] define the work function as "the difference in energy between a lattice with an equal number of ions and electrons, and a lattice with the same number of ions but one electron removed". In this definition, the electron need not be removed to infinity, but only far enough so that the image forces become negligible. This occurs at a point "just outside" the surface. The difference between the two definitions may appear to be hair splitting; however, the latter definition permits the explicit expression of the surface potential, which will be used in Section 2.2.C.

The situation can be illuminated by the following quote from Adam[33]:

> "The term 'just outside' leaves something to be desired as a definition. Although our knowledge of the forces on an electron or ion being removed from a neutral phase, possessing no net electric charge of either sign, is incomplete, it is probably true that they (the forces) are partially due to the electrical double layer in the surface, and partly to an 'image force', ... This image force is of longer range than the other (bonding) forces; its value is $e^2/4r^2$, where e is the charge on a particle, and r its distance from the surface; and it falls to a negligibly small value at about 10^{-3} cm. from the surface. The Volta potential is the potential at a distance of about 10^{-3} cm. from the surface. There is no appreciable indefiniteness in this, provided that there is no other charged conductor within a distance of the first, comparable with 10^{-3} cm., since the potential alters but slowly in free space, in the absence of other charged conductors close at hand."

The above definition of the Volta potential is valid. However, one usually considers the Volta potential difference between two metals rather than the Volta potential of a single one. It is known that two different metals placed in contact with each other assume slightly different potentials. The difference of potential is called the Volta potential difference, and is simply $V_a - V_b$, where V_a and V_b are the Volta potentials of metals a and b. It has become customary to refer to $V_a - V_b$ as the contact potential difference rather than the Volta potential difference. The following section will elaborate on this topic.

2.2.C Relationship Between Work Function, Surface Potential, and Contact Potential Difference

A number of symbols will be used to represent various physical quantities in this section. For the convenience of the reader, these symbols are listed below:

$\bar{\mu}$ = electrochemical potential of an electron

μ = chemical potential of an electron

n = number of electrons in a thermodynamic system

ϕ_{outer} = Volta potential of a metal

ϕ_{inner} = electrostatic potential of a metal

ϕ = work function

e = electric charge of an electron

A = Helmholtz free energy

Subscripts a and b denote metals a and b.

The electrochemical potential ($\bar{\mu}$) of an electron is defined in the usual thermodynamic manner

$$\bar{\mu} = \left(\frac{\partial A}{\partial n}\right)_{T,V}$$

Thus, $\bar{\mu}$ is the work done in bringing an electron from infinity and adding it to the metal at the Fermi level (see Fig. 3). If the electrostatic potential of the metal (ϕ_{inner}) is changed, the value of $\bar{\mu}$ will change by an amount $-e\Delta\phi_{inner}$. The value of ϕ_{inner} can be varied by moving external charges, hence $\bar{\mu}$ depends upon conditions external to the metal as well as internal. This quantity is cumbersome to work with, therefore we define

$$\mu = \bar{\mu} + e\,\phi_{inner}$$

where μ is the chemical potential and depends only upon the internal state of the metal. It is independent of the electrostatic potential.

In accord with Wigner and Bardeen's definition, the work function can be written in terms of the difference in electrochemical potential of an electron inside the metal and "just outside" the surface (10^{-3}cm.). Doing this,

$$e\phi = \bar{\mu}_{outer} - \bar{\mu}_{inner}$$

and $\bar{\mu}_{inner}$ is the same as the quantity $\bar{\mu}$ described in the previous paragraph. Thus,

$$\phi = \frac{\bar{\mu}_{outer}}{e} - \frac{\bar{\mu}_{inner}}{e} = -\phi_{outer} - \frac{\bar{\mu}_{inner}}{e} = \phi_{inner} - \phi_{outer} - \frac{\mu}{e}$$

where ϕ_{outer} is the Volta potential of the metal. The quantity $\phi_{outer} - \phi_{inner}$ is called the surface potential, and is attributed to the double layer of electric charge at the surface.

If two metals, a and b, at the same temperature, are brought into electrical contact, the condition for thermodynamic equilibrium is

$$\bar{\mu}_a = \bar{\mu}_b$$

Using the above equation for ϕ, this condition becomes

$$\phi_a - \phi_b = (\phi_b - \phi_a)_{outer} = V_{ab}$$

where V_{ab} is the Volta potential between the metals, or the contact potential difference. This effect is illustrated schematically in Fig. 4.

2.2.D Effect of Surface Condition on Work Function

The value of the work function depends, to some extent, upon surface conditions. This would be expected since the position of positive ions in the metal crystal relative to the position of an escaping electron will affect the interaction forces. In an attempt to evaluate the effect of surface roughness, Lewis[34] calculated the effect of an oblate spheroid projecting above a smooth surface. He found that the image force was reduced by about 25% in the neighborhood of the projection, causing a lower value of the work function.

Crystal surfaces usually include a number of crystallographic planes, and these planes have different geometries. This, too, will cause variations in work function. An example of this effect was illustrated by Müller[35], who determined the work function for nine of the crystal planes of tungsten. The work function varied by as much as 30% over these planes.

2.3 Chemisorption Bonds of Atoms to Transition Metals

Present theory explains chemisorption bonding in terms of the electronic configuration of the metal and adsorbate. This section will discuss types of chemisorption bonds and will present evidence which confirms the electronic configuration theory.

2.3.A The Ionic Bond

Early measurements of the work function of metals indicated that chemisorption of certain chemical species was accompanied by a large change in work function. The magnitude of the change indicated the formation of an ionic bond between the adsorbent and adsorbate. Typical cases of ionic bonds are the chemisorption of cesium or thorium on tungsten. Here the adsorbate donates an electron to the Fermi level of the tungsten, and the resulting Cs^+ or Th^+ ions cause a positive charge layer near the surface. This layer decreases the work function significantly.

A simplified illustration of the energies involved in the electron transfer is shown in Fig. 5. As long as the ionization potential of the adsorbate is less than the work function of the metal, electron transfer from the adsorbate to the adsorbent tends to occur. For the opposite situation ($I > \phi$), the tendency is for an electron to leave the adsorbent and join the adsorbate, resulting in a negative surface charge layer. A detailed discussion of the conditions leading to positive and negative surface charge layers has been given by Dowden[36].

2.3.B The Covalent Bond

Before discussing the covalent bond, it is convenient to consider Pauling's theory of the structure of metals[37]. Pauling considers each quantum state associated with an individual atom as an "orbital". Each orbital can contain two electrons with opposite spins, or one electron, or none. When atoms are formed into solid transition metals, three types of orbitals arise, namely:

i. bonding orbitals, which are responsible for the cohesion of the solid. These orbitals are usually dsp hybrids*.

ii. atomic orbitals, which are associated with individual atoms, but are not used in bonding the solid together. Paramagnetic properties of transition metals are attributed to the existence of atomic d orbitals.

iii. metallic orbitals, which participate in electrical conduction.

As an example of bonding and atomic orbitals, consider the first transition period. When calcium is reached, the 4s orbitals are full. After this, the d orbitals begin filling. According to Pauling[38], the d orbitals form bonding orbitals until chromium is reached, after which atomic d orbitals begin to appear. As the end of the transition period is reached, no further d orbitals are available.

*The term dsp hybrids implies a system where the s, p, and d energy levels overlap and interact to form a composite bond which has a character somewhat different from a normal s, p, or d type of bond.

Dowden[36] and Dilke, Eley, and Maxted[39] proposed that chemisorption involved the formation of a covalent bond between the adsorbate and an unfilled or partially filled atomic d orbital. This implied that transition metals would be active in chemisorption.

This hypothesis has been validated experimentally. Reynolds[4] performed experiments on the hydrogenation of benzene using a copper-nickel alloy as catalyst. Catalytic activity decreased as copper content increased; the catalyst being completely inactive at 40 atomic percent copper. This was attributed to the d orbitals of nickel being filled by s electrons from the copper. Couper and Eley[40] performed similar experiments on the ortho-para hydrogen conversion, using a palladium-gold catalyst. Their results were similar.

Dilke, Eley, and Maxted[39] have provided a strong validation of the electronic chemisorption theory. They reasoned that since the paramagnetic susceptibility of a transition metal is due to singly occupied d orbitals, chemisorption should decrease paramagnetism. They were able to verify this experimentally.

While the electronic configuration theory has been successful in explaining chemisorption on transition metals, it is not all inclusive at the present. For example, oxygen is known to chemisorb on several non-transition metals[6], and this cannot be explained in terms of vacant d atomic orbitals.

2.3.C Partial Ionic Character of Covalent Bonds

The literature contains a large amount of information about the surface potential changes for various chemisorption reactions. Much

of this has been brought together by Culver and Tompkins[24]. If one considers the chemisorption of a single gas on several metals, the values of the surface potential change will cover a rather large range. This may indicate that bonding is neither ionic nor covalent, but something in between.

Pauling[38] has considered this type of bond and calls it a "covalent bond with partial ionic character". He considers two bonding structures, one covalent and one ionic. If the two structures involve the same number of unpaired electrons, the bond can resonate between the two structures and a covalent bond with partial ionic character can be formed. This condition is generally met in the chemisorption of diatomic molecules.

The "amount of ionic character" is the ratio of the observed dipole moment of the molecule to the dipole moment associated with the ionic bond. Pauling gives an empirical relationship for this quantity.

$$\text{Amount of ionic character} = 1 - \exp\left[-1/4(X_a - X_b)^2\right]$$

where X_a and X_b are the electronegativities of the elements involved. The electronegativity is a measure of the ability of an atom (or molecule) to attract an electron to itself and is related to the ionization energy and the electron affinity. The atom with the highest electronegativity is the negative end of the dipole. These concepts will be used in the discussion of surface charge layers caused by chemisorption.

2.4 Effect of Hydrogen Chemisorption on Work Function

It was previously noted (Section 2.1.B) that chemisorption will alter the double layer residing near a metal surface. This alteration, which is due to the ionic character of chemisorption bonds, will change the work function. A double layer of charge with the positive side outermost will aid an electron escaping from the metal, thus lowering the work function; the reverse is true of a layer with the negative side outermost.

The magnitude of the change in work function can be calculated by considering the double charge layer as a capacitor in free space. The resulting equation is

$$\Delta\phi = 4\pi n_s \theta \sigma$$

where n_s is the number of adsorption sites per cm^2, θ is the fraction of the surface covered with adsorbent, and σ is the dipole moment of the adsorbate-adsorbent bond, expressed in statcoulomb-cm. This equation is valid only for small values of θ since mutual depolarization can occur at higher coverages.

2.4.A Prediction of the Polarity of the Dipole Layer

One can attempt to predict the dipole layer polarity using the presently available theories. Baker and Jenkins[41] discuss the conditions leading to positive and negative dipole layers. They conclude that a large adsorbent work function is conducive to a positive outward dipole layer, and vice versa. This can be seen clearly in Fig. 5. They also discuss the effect of the density of states function in the

neighborhood of the Fermi level. If an electron is added to the metal the Fermi level rises, consequently the work function falls. Since a large work function is conducive to positive ion formation, a density of states function which can accommodate a large number of electrons with a small rise in Fermi level will aid in the formation of positive adsorbate ions. The reverse is true for negative ion formation.

Shifting of the Fermi level due to chemisorption may be significant in thin films, where the surface to volume ratio is high. The effect decreases as the surface to volume ratio diminishes, and is probably negligible for adsorbents in the shape of thick filaments. This difference can cause difficulties in comparing data derived from thin films and from filaments.

A second method for predicting polarity is also available. According to Pauling, when a bond is formed between two atoms, the more electronegative one will be the negative side of the resulting dipole. Thus, we may use both work function and electronegativity as criteria for dipole polarity. Values of these quantities for several metals are shown in Table I[38,42].

The table shows that hydrogen chemisorption on these metals will cause negative diople layers in the order

Negative W Co Fe (Ni Cu) Ag Pd (Pt Au) Positive

with tungsten being the most negative and platinum or gold most positive. The accumulated data given by Culver and Tompkins[24] shows that this order is generally followed, with only cobalt deviating

considerably. The experimentally determined order is

Negative W Fe Cu Ag Ni Co Au Pt Positive

with values for Ag, Ni, and Cu being very close to each other. Surface potentials ranged from -0.48 to -0.14 volts. Most of the data come from experiments at room temperature. This comparison shows that the present theory can predict the relative effect of hydrogen chemisorption on the dipole polarity of several transition metals. By "relative" it is meant that the polarity change of one metal is compared to the polarity change of other metals. The theory is unsuccessful, however, in predicting whether the ad-layer is positive or negative.

Consider the hydrogen-palladium system. If the electronegativity is used to determine the polarity of the surface charge layer, one would expect the adsorbed hydrogen to form a positive layer since hydrogen is slightly less electronegative than palladium (Table I). On the other hand, one could use the ionization potential of hydrogen and the work function of palladium to determine the polarity of the surface charge layer. This approach would predict a negative surface layer since the ionization potential is greater than the work function.

The behavior of hydrogen absorbed in bulk palladium, however, favors the positive layer. Experiments on the paramagnetic susceptibility of palladium[23] indicate that the hydrogen electron is contributed to the 4d band of the palladium, resulting in a positive hydrogen ion. If this process occurred on the surface, the adsorbate would be positively charged.

The problem is further complicated by the fact that the electrical charge of the ad-layer is temperature dependent in some cases. This effect is discussed in the two following sections. Thus, it can be stated that the present theory cannot be used to determine the polarity of the ad-layer. One must resort to empirical data.

It is of interest to determine whether the chemisorption bonds between hydrogen and the metals discussed above are covalent, ionic, or something in between. The fact that the surface potentials of the metals change when hydrogen is chemisorbed indicates that the surface dipole layers change, hence the bonds must have some ionic character. Couper and Eley[40], however, calculated the energy involved in forming ionic bonds when hydrogen is chemisorbed. They found that ionic bond formation would be highly endothermic. Hydrogen chemisorption on transition metals has been shown to be exothermic in a large number of experiments[6]. Therefore, these chemisorption bonds must be covalent with partial ionic character.

2.4.B Experimental Investigations of Work Function Change Due to Hydrogen Chemisorption (Ni and Pt)

Only the nickel-hydrogen and platinum-hydrogen systems will be discussed in this section. These two were selected because of the similarities between their electron configurations and that of palladium. Table I indicates that the change in work function of palladium due to hydrogen chemisorption should fall somewhere between the changes

experienced by nickel and platinum and should lie closer to platinum than to nickel. The palladium-hydrogen system will be discussed in the next section. However, it should be noted that experimental data are scanty.

Changes in work function due to chemisorption can be measured directly by photoelectric experiments. Surface potential changes can be determined by saturated diode or capacitor techniques. The vibrating capacitor arrangement described by Zissman[43] has proven to be very effective in work function measurements.

As long ago as 1929, Suhrmann[44] investigated the change in work function of platinum due to hydrogen chemisorption, using the photoelectric method. He worked at hydrogen pressures ranging from .01 to .001 torr and observed that the work function decreased as hydrogen pressure increased.

Sachtler[45] was apparently suspicious of the surface conditions in these experiments and ran similar ones for nickel. However, he deposited nickel films under two different sets of conditions: "clean" and "dirty". His "dirty" film was formed in a vacuum of 10^{-6} torr and reacted in a manner similar to the platinum described above. His "clean" film, which was deposited at a pressure of less than 10^{-7} torr, showed an opposite effect; the work function increased upon hydrogen exposure. As could be expected, surface contamination was a strong influence. The "clean" results were confirmed by Culver, Pritchard, and Tompkins[46].

Mignolet[26,47,48] has done extensive work in determining surface potentials. For the nickel-hydrogen system he found that the surface

potential goes negative as hydrogen contacts nickel, indicating dipoles with the negative side outward (increase in work function). As the coverage increases, however, the dipole polarity changes. The same effect was found for hydrogen on platinum. He attributed this to the formation of a physisorbed hydrogen layer over the chemisorbed layer, with the physisorption providing the positive outward layers. This work was done with background pressures in the 10^{-6} torr region.

The reversal of the dipole polarity has been confirmed by two recent experiments. Rootsaert, van Reijen, and Sachtler[27] investigated the hydrogen-platinum chemisorption. They evacuated a field emission system to a background of about 10^{-10} torr. Hydrogen was then admitted until a pressure of 10^{-7} torr prevailed. Using a platinum field emission tip, they determined the surface potential as a function of temperature over the range of 80°K to about 300°K. Their results are shown in Fig. 6 and can be interpreted as follows. Hydrogen chemisorbs on platinum in two ways. The weaker chemisorption causes a positive surface potential, and vice versa. As the platinum is heated, the weakly bonded hydrogen is desorbed and the surface potential goes more negative. At about 250°K, the strongly bonded atoms begin to desorb, and the negativity of the surface potential diminishes.

A similar effect was found for the hydrogen-nickel system by Crossland and Pritchard[49]. They found that the change in surface potential due to hydrogen chemisorption was negative until the coverage was about half a monolayer. Adsorption beyond this point caused a decrease in the negativity.

The work of Pliskin and Eischens[50] helped to clarify the situation. They investigated the infra-red absorption spectrum of platinum supported on both alumina and silica. This work was done first in hydrogen and then in deuterium. Bonds were found at two different frequencies in each case, with the support material having no effect. The absorbed frequencies were not the same for hydrogen and deuterium. In order to determine whether or not any of these bonds corresponded to molecular adsorption, the experiment was then run with a hydrogen-deuterium mixture. If H_2 and D_2 had been adsorbed in the previous cases, then HD would be adsorbed from the mixture and a new absorbed frequency would result. This was not observed. Thus Mignolet's hypothesis of physisorbed molecules was disproved. From these results, it can be concluded that both hydrogen and deuterium chemisorb atomically on platinum. Although some adsorbed molecular hydrogen must be in equilibrium with the atomic species, its concentration is too small to be observed by infra-red spectroscopic techniques.

2.5 The Hydrogen-Palladium System

It is well known that hydrogen diffuses into bulk palladium, and that the combination will form palladium-hydrogen alloys. A wealth of information is available on this topic. In contrast, very little is available concerning the surface reactions of these elements.

2.5.A Hydrogen and Palladium in Bulk

The present investigation is concerned with the hydrogen-palladium interface. If hydrogen permeates the palladium filament to any

great extent during the experiments, surface conditions will be affected since diffusion into and out of the metal will change the hydrogen concentration on the surface. The temperature-pressure-concentration relationships of the hydrogen-palladium system have been extensively investigated[51] and show that the quantity of hydrogen occluded by palladium diminishes with increasing temperature and decreasing pressure. These relationships indicate that hydrogen occlusion by the palladium filament should be negligible for the experimental conditions used in this investigation.

The extent to which hydrogen is occluded can be determined by electrical resistance measurements. This topic has been discussed by Smith[52]. As hydrogen enters the palladium, the resistance increases until the atomic ratio of H/Pd is about 0.8, at which point the resistance has approximately doubled. Further hydrogen occlusion reduces resistance. This phenomenon was used to check for hydrogen occlusion in the palladium filament utilized in the present experiment. The resistance of the filament did not change when it was exposed to the hydrogen beam, indicating that hydrogen occlusion was either absent or occurred to a very small extent. This is discussed further in Section 5.3.B.

2.5.B Hydrogen-Palladium Chemisorption

As previously stated, information about hydrogen-palladium chemisorption is scarce. Two papers will be discussed in this section.

The first is a paramagnetic susceptibility experiment done by Reyerson and Solbakken[53]. They deposited palladium on silica gel

and measured susceptibility as a function of the quantity of hydrogen adsorbed and the weight of the palladium film. This was an attempt to gain information on the surface states of palladium atoms. Their results show that paramagnetic susceptibility depends upon surface to volume ratio and indicate that there are about 2 unpaired d band electrons per atom at the surface, compared to 0.6 in the bulk material.

Adsorption isotherms at $0^{o}C$ are also presented and are of interest. The isotherms are shown in Fig. 7, with the numbers indicating the percent palladium (by weight) in the silica gel-palladium specimens. The following quote, taken from the paper, explains the behavior.

> "The shape of the isotherms shows that two kinds of sorption exist and the first is essentially complete before the second begins. At very low pressures the hydrogen is rapidly and strongly sorbed, giving a Langmuir type of isotherm. This sorption is essentially complete by the time the hydrogen pressure reaches 1 mm. No doubt this part of the isotherm represents monolayer adsorption on the available palladium surface. The isotherm remains horizontal for all of the samples until the hydrogen pressure exceeds 2 mm. At a pressure between 2 and 3 mm. the amounts sorbed increase, reaching a final value at about 30 mm. pressure of hydrogen. The pressure at which the second abrupt increase begins is in excellent agreement with that found by Gillespie and coworkers(51) for bulk palladium at $0^{o}C$. ..... There is little doubt that the second rise in the isotherms shows the amount of hydrogen that penetrates into the aggregates or crystallites of palladium on the gel surface."

The hypothesis of two types of bonds is quite tenable, considering the previously discussed data for nickel and platinum. The assumption of a Langmuir type isotherm existing during complete monolayer coverage is very doubtful since the Langmuir isotherm assumes that the adatoms do not interact. This condition is probably not met when the coverage approaches a full monolayer. Background pressures were in the 10^{-6} torr range.

The low pressure end of the isotherms shows that the quantity of hydrogen adsorbed increases with increasing palladium mass. This would indicate that some hydrogen is diffusing into the bulk. The possibility of absorption for both the hydrogen-tungsten and hydrogen-nickel systems was suggested by Trapnell[54] and has been confirmed for the tungsten case by Moore and Unterwald[55]. Considering the bulk behavior of palladium, some hydrogen absorption near the surface would not be surprising.

Suhrmann and coworkers[56] investigated the electrical resistance of a thin palladium film (90 Angstroms) during hydrogen chemisorption. The results show that the resistance increases with hydrogen pressure initially, reaches a maximum, and then decreases. Suhrmann postulates that the first hydrogen molecules dissociate into atoms, and then chemisorb on the sites of low work function as negative ions by removing electrons from the metal. This causes an increase in resistance (and work function). Following this, atoms are dissociated into protons and electrons on the remaining sites. These then diffuse into the film and reduce the resistance. According to Suhrmann, the second mechanism does not affect the work function since the surface coverage does not change during the process.

In the discussion following this paper, the diffusion of hydrogen into the palladium film was not disputed. The proposed mechanism was questioned rather strongly by Selwood, however.

There are many difficulties involved in making resistance measurements on thin films. Without delving into details, it can be

stated that this type of work is still in its early stages and in many cases the conclusions are still not clear.

2.6 Reaction Rates

The rate of a chemical reaction can be expressed in terms of rate constants. Consider the reaction

$$A + B + C + \ldots\ldots \longrightarrow P + Q + \ldots\ldots$$

If C_a is the concentration of reactant A, the rate of change of C_a can be represented by

$$\frac{dC_a}{dt} = k\, C_a^{\alpha}\, C_b^{\beta}\, C_c^{\gamma} \ldots\ldots$$

The quantity k is called the rate constant, while the sum of the exponents $(\alpha + \beta + \gamma + \ldots)$ is known as the order of the reaction. These exponents are usually determined experimentally.

2.6.A The Arrhenius Equation and the Activated Complex

The rates of chemical reactions are strongly temperature dependent, consequently the rate constants must be functions of temperature. This function is given by the Arrhenius equation, which states that

$$k = A \exp\,(-E^*/RT)$$

where A is a constant, E^* is the activation energy for the reaction, and R is the gas constant.

The presence of an activation energy indicates that an energy barrier exists between the reactants and products. The reactants must

possess sufficient energy to overcome this barrier if the reaction is to occur. The situation is shown schematically in Fig. 8 for the reaction $A + BC \rightleftharpoons AB + C$. In the diagram, E^* represents the activation energy and ΔH is the heat of reaction. The reaction can go in either direction. However, a higher activation energy is required for the reverse direction.

The existence of an energy barrier leads to the concept of the "activated complex". The state of the reactants at the top of the energy barrier is called the activated complex. This theory has been treated in detail by Glasstone, Laidler, and Eyring[57]. They consider the activated complex to be a distinct state, consequently a simple chemical reaction can be represented as

$$A + BC \underset{k_2}{\overset{k_1}{\rightleftharpoons}} A^* + B^* + C^* \underset{k_4}{\overset{k_3}{\rightleftharpoons}} AB + C$$

where the asterisk superscript denotes the activated complex state. The equation shows that the reaction occurs in two steps, with appropriate rate constants for each step.

2.6.B Energy and Free Energy

The Arrhenius equation has been successfully used in many cases. However, accurate experiments have shown that it is really an approximation. A more accurate expression would involve activation free energy rather than activation energy, since the driving force of a chemical reaction is the difference in free energy between reactants and products. The Gibbs free energy is

$$F = H - TS$$

where H is the enthalpy, T is the temperature, and S is the entropy.

Since the activation free energy (F^*) is the difference in free energy between the initial and activated states,

$$F^* = \Delta H - T\Delta S - S\Delta T$$

where ΔH is the enthalpy of activation (heat of activation) and ΔS is the entropy of activation. The constants in the Arrhenius equation can be evaluated from experiments run under isothermal conditions. For this situation, $\Delta T = 0$ and

$$F^* = \Delta H - T\Delta S \qquad \text{isothermal process}$$

Substituting F^* for E^* in the Arrhenius equation,

$$k = B \exp(\Delta S/R) \exp(-\Delta H/RT)$$

where B is a constant.

The fact that the Arrhenius equation, without the entropy term, yields good results in many cases indicates that the temperature variation of ΔS is small compared to the temperature variation of ΔH for these cases.

2.6.C Rate Determining Step of a Reaction

There are some reactions in which several intermediate steps can appear between the reactants and the products. This occurs frequently in heterogeneous catalysis. An example would be a reaction in which the reactants first form bonds with the catalyst surface, then form bonds

with each other, and finally break the surface bonds to be desorbed as the reaction products. This process can be represented by the equation

$$\underset{\text{reactants}}{A + B + 2M} \rightleftharpoons \underset{\text{adsorbed reactants}}{A{\cdot}M + B{\cdot}M} \rightleftharpoons \underset{\text{adsorbed product}}{A{\cdot}B{\cdot}2M} \rightleftharpoons \underset{\text{desorbed product}}{AB + 2M}$$

where M represents an active catalyst site.

These consecutive reactions lead to the concept of the rate determining step. Quoting Benson[58], "In systems of consecutive reactions it sometimes may occur that there is one step which is very much slower than all the subsequent steps leading to the product. The rate of production of product may depend on the rates of all the steps preceding the last slow step but will not depend on any of the subsequent steps, all of which are rapid compared to the last slow step". The last slow step is called the rate determining step of the reaction.

Chapter 3

ANALYSIS OF THE PRESENT EXPERIMENT

3.1 General

The present experiment was described in general terms in Chapter 1. Essentially, a hot palladium filament was bombarded with a beam of molecular hydrogen, and the thermionic emission current was measured as a function of beam intensity. This procedure was then repeated with atomic hydrogen. Comparison of the two sets of data should yield information about the differences between the two chemisorption mechanisms. This chapter will discuss the mechanisms involved and will indicate the significance of such comparisons.

3.2 Adsorption-Desorption Mechanisms of H and H_2 on Palladium

The reaction mechanisms of the adsorption-desorption of H and H_2 will now be postulated. These are shown below in schematic form, followed by an explanation.

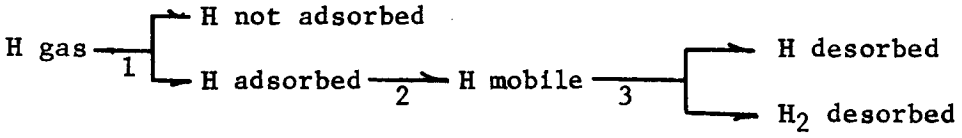

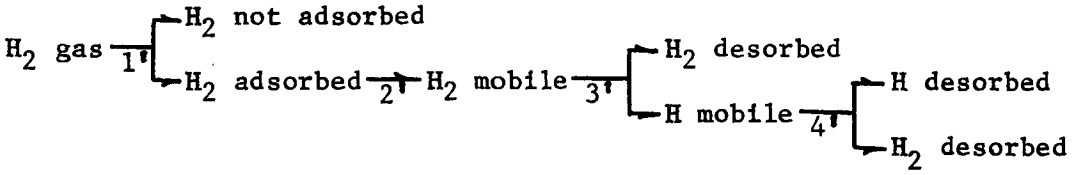

For the case of atom hydrogen, step 1 shows that an impinging atom either sticks to the surface or does not. This step is governed by the sticking coefficient. The adsorbed H then becomes mobile (step 2). From the mobile state, it can either desorb or recombine with another atom (step 3). Since the recombination is highly exothermic (103 kcal/mole), the molecule formed by this reaction will be highly energetic and will desorb. This desorption should be almost instantaneous.

The H_2 mechanism shows the same first step as the H, although the sticking coefficients are not necessarily the same for the two cases. The adsorbed H_2 will pass into a mobile layer (step 2') from which it will either desorb as a molecule or dissociate into mobile atoms (step 3'). Step 4' is the same as step 3 in the H mechanism.

The times required to go from the adsorbed state to the mobile state (steps 2 and 2') are short compared with the times required for other parts of the reactions. For this reason, steps 2 and 2' can be neglected, and the hydrogen can be considered as adsorbing in the mobile state.

The differences between the two postulated reactions can now be attributed either to a difference in sticking coefficients (steps 1 and 1') or to the desorption of H_2 at step 3'. These differences will be discussed further in Section 3.4.

3.3 Composition of the Adsorbed Layer

Experimentally, the thermionic emission currents will be measured as a function of beam intensity. In order to make a valid

comparison between data acquired from the molecular and atomic beams, it is necessary that the adsorbate be the same in both cases. For the sake of discussion, assume that atomic hydrogen chemisorption increases the emission current (work function decreases). Suppose a molecular beam of given intensity impinges on the hot filament, and this results in a particular emission current. The experiment is then run again with an atomic beam of the same intensity, and the thermionic current is higher in the atomic case. One would then be tempted to say that more hydrogen was chemisorbed in the atomic beam experiment. This statement is true only if the adsorbate is atomic hydrogen in both cases. If a significant amount of H_2 exists on the surface, such comparisons are difficult.

The mechanisms described in Section 3.2 indicate that only atomic hydrogen will exist on the surface during atomic beam experiments. However, some adsorbed H_2 will be present during molecular beam operation. The fraction of H_2 in the ad-layer must be estimated.

This is done in Appendix A. The results show that the fraction of H_2 in the ad-layer is very small. Comparison of the data taken during atomic and molecular beam experiments will therefore be valid.

3.4 Residence Times

It was shown in Section 3.2 that the differences between adsorption of atomic and molecular hydrogen on palladium could be attributed either to a difference in sticking coefficients for the two cases or to the desorption of H_2 at step 3' of the reaction equations. Sticking coefficients will be discussed in Chapter 7. If only certain palladium

sites are capable of dissociating H_2, then the amount of H_2 desorbed at step 3' should depend upon the number of surface sites visited by a hydrogen molecule during its lifetime on the surface. The number of sites visited will be calculated in this section.

The residence time equation is discussed in Appendix A. As given by de Boer[30], this equation is

$$\tau = \tau_o \exp (\Delta H/RT)$$

where τ is the length of time which an adsorbed particle spends on the surface (residence time), τ_o is the time required for one oscillation of an adsorbent surface atom, and ΔH is the heat of adsorption. As discussed in Appendix A and Section 2.6.B, the free energy of adsorption should be used in place of the heat of adsorption. Since we are presently concerned with order of magnitude calculations only, the heat of adsorption will be used.

The value of τ_o can be estimated from the Debye theory of solids.

$$\nu = \frac{k\theta_D}{h} = \frac{1}{\tau_o}$$

where ν is the oscillation frequency and θ_D is the Debye temperature. The value of θ_D for palladium is 270^oK[23]. Substituting numerical values,

$$\tau_o = 1.75 \times 10^{-13} \text{ seconds}$$

The H_2 residence time can be found by substituting the value of the heat of adsorption in the residence time equation. Since H_2

physisorbs on palladium, the heat of adsorption of H_2 can be taken as the heat of vaporization. This value is 0.215 kcal/mole[59].

$$\tau_{H_2} = 1.94 \times 10^{-13} \text{ seconds}$$

To find the time spent at each site, the activation energy for mobility is substituted for ΔH. This quantity can be estimated as about 20% of the heat of adsorption[6]. Then,

$$\tau'_{H_2} = 1.79 \times 10^{-13} \text{ seconds}$$

These figures show that an H_2 molecule will visit slightly more than one site during its residence time. Recalling that this is an order of magnitude calculation, the molecule may visit somewhere in the neighborhood of ten sites. However, the calculation shows that the number of sites visited will be small. If only certain palladium sites are capable of H_2 dissociation, desorption of H_2 at step 3' may be significant.

3.5 Summary

This chapter has yielded some interesting and useful results. It has been found that the concentration of H_2 adsorbed on the surface during molecular beam operation will be small, and the ad-layer can be considered as atomic hydrogen. Since the adsorbed species is atomic hydrogen when either the atomic or molecular beam is operating, the results obtained from these two modes of operation can be compared and we can find which operational mode yields a greater amount of chemisorbed hydrogen.

The results of such a comparison can then be used to gain knowledge about the reaction mechanisms shown in Section 3.2. There are two possibilities; either the atomic beam or the molecular beam will result in more hydrogen chemisorption.

If a greater amount of hydrogen is chemisorbed from the atomic beam, it will indicate either that H_2 is desorbed at step 3' of the reaction equations, or that the sticking coefficient of H is greater than that of H_2, or both.

If the opposite is true, the conclusion would be that the sticking coefficient of H_2 is larger than that of H. This turns out to be the actual case, as discussed in Chapters 7 and 8.

Chapter 4

DESIGN OF THE EXPERIMENTAL SYSTEM

4.1 Previous Experimental Work

The change in the thermionic emission current of palladium due to the chemisorption of molecular hydrogen has been investigated by Eisenstadt and Hoenig[17]. They enveloped a hot palladium filament in a molecular hydrogen environment and measured the thermionic emission current from the filament to a collector as a function of hydrogen pressure. These experiments were made under equilibrium conditions, in the sense that the adsorbed hydrogen was in equilibrium with the gaseous hydrogen.

The results of Ref. 17 were needed in order to design the beam system used in the present experiments. First, Ref. 17 showed that the thermionic emission current from a palladium filament changed by a measurable amount when hydrogen was chemisorbed. Hence the present beam experiments were feasible. Second, Ref. 17 defined the hydrogen pressure range over which the change in thermionic emission current was detectable. This information was essential for the beam system design, as will become evident in Section 4.3.B.

The remainder of this chapter will discuss the design and instrumentation of the beam system, as well as several of the operating parameters. The details of the operating procedure will be discussed in the next chapter.

4.2 Vacuum Pumping Equipment

The importance of clean surfaces was discussed in Chapter 1 where it was stated that background pressures in the neighborhood of 10^{-9} torr were required for conditions of reasonable cleanliness. The pumping arrangement used in the present experiments achieved backgrounds in this range. A detailed description of how this was accomplished will be given in Section 5.2. For the present, it will suffice to say that the system was first evacuated with a 1-1/2 hp. mechanical vacuum pump and a two inch diameter oil diffusion pump which was equipped with a chevron type water cooled baffle to prevent oil from back-streaming into the system. This combination yielded a vacuum of about 10^{-5} torr. Lower pressure was then obtained in the vacuum chamber by means of a 50 liter/second Vac-Ion pump (Varian Associates, Palo Alto, Califo., model 912-6000). The beam source was evacuated with an 8 liter/second Vac-Ion pump (Varian, model 911-5000). During operation, the hydrogen introduced into the vacuum chamber by the beam was pumped away by the 50 liter/second Vac-Ion pump. This pump is rated at 50 liters/second for air; however, it pumps hydrogen at 135 liters/second.

The physical arrangement of these pumps is shown in Fig. 9.

4.3 The Beam Source

The beam source is considered as the part of the apparatus used to deliver the molecular and atomic beams to the vacuum chamber. Figure 10 is a schematic drawing of the beam source, while Fig. 11 is a photograph of its components which are external to the vacuum chamber.

The three pieces of tungsten-26% rhenium tubing shown in Fig. 10 were heated electrically to produce the atomic beam. These three pieces will be referred to as the "oven". Figure 12 is a photograph of the oven, mounted in the vacuum chamber.

The beam was produced by admitting hydrogen into the beam source by means of the hydrogen leak as shown in Fig. 10. The control and measurement of the hydrogen pressure in the beam source will be discussed in Section 4.3.D. From the beam source, the hydrogen effused (as a beam) through the radial hole in the oven wall. The next five sections will discuss the beam source design.

4.3.A Thermal Dissociation of Molecular Hydrogen

The beam source delivered a beam of either atomic or molecular hydrogen. In Section 1.4, it was stated that almost all of the hydrogen would be dissociated at a temperature of 2400°K. This information comes from the values of the equilibrium constant for the hydrogen dissociation reaction given by Huff, Gordon, and Morrell[60]. The results (Appendix C and Fig. 28) show that about 95% of the hydrogen will be dissociated at 2400°K, provided the source pressure is below 100 microns. Lower pressures yield greater dissociation and vice versa. The experimental work of Lockwood, Helbig, and Everhart[61] approximately confirms the calculations of Appendix C. They measured the degree of dissociation of hydrogen flowing from a hot tungsten tube, using a proton beam scattering technique. Their results show that over 87.5% of the hydrogen was dissociated at a tube temperature of 2380°K and a pressure of 10 microns.

4.3.B Operating Pressures and Orifice Diameter

The results of Ref. 17 show that the thermionic emission current from palladium increases as the ambient hydrogen pressure increases. This effect is significant over a hydrogen pressure range extending from 10^{-8} to 10^{-5} torr. It is therefore necessary for the beam to produce equivalent pressures in this range. By "equivalent" it is meant that the number of gas particles impinging on the filament per cm^2 per second from the beam is the same as the impingement rate per cm^2 when the filament is enveloped in a gaseous environment at a pressure P_e (subscript e denoting "equivalent").

In order to calculate the beam source pressure and the diameter of the beam source orifice required to produce P_e, it is necessary to know the geometric arrangement of the filament and oven. This is shown in Fig. 13. A polished stainless steel plate was inserted between the oven and the filament. This served as an electrical shield and a heat shield and will be discussed in Section 4.4.E. The plate had a 0.24 cm hole through which the beam passed. The distance from the oven to the filament was fixed at 1.27 cm . A smaller dimension would result in a greater beam intensity at the filament. However, Fig. 13 shows that a distance less than 1.27 cm would be unreasonable since both the shield and collector had to fit into this space.

The calculations which determine the equivalent pressure (P_e) as a function of beam source pressure (P_o) and orifice diameter are shown in Appendix D. The results shown in Fig. 29 indicate that an orifice diameter of .015 cm is about the smallest size which will

yield the required equivalent pressures. The beam source pressure is limited by the requirement that free molecular flow exist in the region of the orifice.

It was desirable to select as small an orifice diameter as was practical since the hydrogen coming out of the orifice entered the vacuum chamber and had to be pumped out during beam operation. A small orifice size was therefore conducive to maintaining low pressures in the vacuum chamber. For this reason, an orifice diameter of .015 cm. was selected.

4.3.C Fabrication of the Oven

The oven dimensions are shown in Fig. 10. A tungsten-26% rhenium alloy was used since this material has satisfactory strength at high temperature (2400°K) but is not as brittle as unalloyed tungsten. Unfortunately, it possesses the same poor machining characteristics as tungsten.

The .015 cm. orifice was drilled by an electric arc discharge machine (Elox Corp), using a number 93 steel twist drill as the electrode. The Elox machine was also used to cut the tubing to the proper size and to drill the larger tubing when necessary.

As shown in Fig. 10, the three pieces of tubing are brazed together. Because of the high temperatures which prevailed at the brazed joints when the oven was heated, platinum was used as the filler material. It was necessary to braze the joints quickly since the tubing will oxidize rapidly in air at the melting point of platinum. An oxygen-hydrogen torch was used for the brazing.

It was necessary to bring both hydrogen and electrical power through the vacuum chamber wall to the oven. This was accomplished with two Varian medium current feedthroughs (model 954-5019) as shown in Fig. 10. The brazed joints between the oven and the feedthroughs used a nickel-gold alloy (Nioro) as the filler material.

The electrical power for heating the oven was supplied by passing 110 volt AC through a Variac and then through a step-down transformer. The current vs. temperature characteristics of the oven are shown in Fig. 14. Temperatures were measured at the center of the small tube (orifice location) with an optical pyrometer and were corrected for the emissivity of tungsten at the operating wavelength of the pyrometer.

4.3.D Control and Measurement of Hydrogen Pressure

Pure hydrogen was admitted to the beam source by means of a heatable palladium tube. The palladium tube hydrogen leak (K and B Glass Apparatus Co., Schenectady, N. Y.) was heated to about 200°C while commercial grade hydrogen was passed through a surrounding jacket. The palladium then selectively diffused hydrogen into the beam source. The purity of the incoming hydrogen was checked with a residual gas analyzer (Consolidated Electrodynamics Corp., Pasadena, Calif., model 21-612). No gas other than hydrogen was found. The sensitivity of the instrument was such that a partial pressure of 10^{-9} torr of a gas such as nitrogen could be detected.

The hydrogen flow rate was controlled by a bakeable variable leak valve (Granville-Phillips Corp., Boulder, Colo.). This valve was very sensitive and provided excellent control of the hydrogen pressure in the

beam source. It should be noted that the 8 liter/second Vac-Ion pump shown in Fig. 10 was turned off when the beam was operating. It was used only during pumpdown.

Three different gauges were used to measure the beam source pressure. This was necessary since no single gauge would accurately cover the large range of beam source pressures. Pressures from 10^{-9} torr to 1 micron were measured with an ionization gauge (Vacuum Electronics Corp., Plainview, N. Y., model TG 75). A Pirani gauge (Consolidated Vacuum Corp., Rochester, N.Y., model GP-140) measured pressures from 10 microns to 200 microns, while a cold cathode gauge (Vactek Inc., Bedford, Mass., model 700) bridged the gap from 1 to 10 microns.

4.3.E Flow-Pressure Relations in the Beam Source

The calculations in Appendix D are based upon the pressure at the beam source orifice. The pressure gauges were located somewhat upstream of the orifice, however. This situation requires that the pressure at the orifice be calculated from the measured pressure. At first glance this may appear to be a straightforward pressure drop calculation. For the case in which the oven is not heated this is true. When the oven is hot however, the computation must include the effects of dissociation and thermomolecular flow.

The calculations are shown in Appendix E. The results are:

$P_g/P_o = 1.96$ when the oven is at room temperature

$P_g/P_o = 0.771$ when the oven is at 2400^oK

where P_g is the measured pressure and P_o is the pressure at the beam source orifice. These ratios will be used in the data reduction procedures.

4.4 Thermionic Emission from the Filament to the Collector

Measurement of the thermionic emission current from a hot filament to a collector is usually straightforward. It generally involves heating the filament, biasing the collector at an appropriate positive voltage, and measuring the current flow from the collector to ground.

The physical arrangement of the equipment used in the present experiments introduced complications. The tungsten oven acted as an electron emitter when heated to 2400°K. The 50 liter/sec Vac-Ion pump operated in the vicinity of the collector and presented another possible source of charged particles which could be attracted by the collector. These problems were minimized by introducing a stainless steel shield between the oven and collector, and by the appropriate biasing of the various components, as discussed below.

4.4.A Physical Arrangement of the Components

The physical arrangement of the filament, collector, shield, and oven are shown in Fig. 13. The filament was a 0.025 cm. diameter palladium wire, five cm. long and was heated electrically. The cylindrical collector was fabricated from 60 mesh stainless steel screen. A 0.48 cm. diameter hole was punched through the collector and was aligned optically with the beam source orifice and the hole in the shield. This

permitted the hydrogen beam to impinge upon the center portion of the filament without interference from the screen.

The shield was made from 24 gauge, type 304 stainless steel and completely shielded the filament and collector from the oven except in the region of the hole. The portion of the beam which passed through the hole either struck the filament or flowed into the mouth of the Vac-Ion pump. The remainder of the beam was deflected into the upstream region of the vacuum chamber and was eventually removed by the Vac-Ion pump. The shield can be considered as a flow constriction from the point of view of pumping. The area of the shield was 20.7 cm^2, compared to an area of 82.3 cm^2 for the cross section of the vacuum chamber. Thus, the shield blocked 25.2% of the flow area. As discussed in Chapter 6, the effect of this blocking was not significant.

A grid, fabricated from 0.050 cm. diameter nickel wire, was placed at the mouth of the Vac-Ion pump to prevent charged particles from leaving the pump. It was biased as described in Section 4.4.D.

Figure 15 is a schematic drawing of the entire system and shows the arrangement of the power supplies used to bias the various components. Values used for these bias voltages are discussed in the remainder of this chapter.

4.4.B Collector Bias and Emission Current Measurement

It has been found that the thermionic emission current from a hot filament increases as the collector voltage increases. This is as expected since a higher collector bias (positive voltage) will reduce the negative space charge in the region of the filament. The space

charge is caused by the presence of electrons which have been emitted by the filament and are traveling toward the collector. If the collector voltage is raised to too high a level (kilovolt range) the thermionic emission current may be enhanced by a field emission current, which is not desirable. A collector bias of +190 volts was found to yield emission currents which could be measured with relative ease (10^{-11} ampere range). Consequently this bias potential was used. A stable power supply (John Fluke Co., Seattle, Wash., model 407)* provided the bias voltage. This power supply allowed a maximum variation of $\pm$ 0.1 volts at 190 volts.

Measurement of very low currents becomes difficult if the circuit components pick up extraneous currents which are of the same order of magnitude as the currents being measured. It is then necessary to use very good shielding techniques and to find methods of eliminating low levels of noise. In the present experiments these problems were eliminated by shielding and by using the +190 volt collector bias.

An electron which leaves the filament and travels to the collector will arrive with an energy of at least 190 electron volts. This is well above the ionization potential of either H or H_2[42]. Consequently the possibility of gaseous hydrogen being ionized by electron collisions must be considered. When hydrogen is ionized, electrons are freed from the atoms or molecules. These electrons are attracted by the collector and will impinge upon it. Thus, the electron flow to the collector will be due to both the thermionic emission current and the electrons released by the ionization of hydrogen. The magnitude of the electron flow due

*Courtesy of Dr. M. Davis, Nuclear Engineering Dept., Univ. of Arizona

to ionization has been calculated in Appendix F and was found to be negligible.

The circuit used to measure the emission current is shown in Fig. 15. The collector was spot welded to a stainless steel rod, which was attached to a high voltage vacuum feedthrough (Varian, model 954-0006). Electrons which traveled to the collector flowed to ground by passing through the bias power supply and the microammeter (Hewlett Packard Co., Palo Alto, Calif., model 425A). Coaxial cable was used for all wiring in the measuring circuit.

4.4.C Filament Temperature

The thermionic emission current from a hot metal surface is strongly dependent upon the surface temperature. Thus, it was necessary to control the filament temperature accurately. The arrangement for accomplishing this is shown in Fig. 15.

Electrical power to heat the filament came from a 4 volt, 240 ampere hour storage battery which was charged before each set of data runs was made. The power was brought into the vacuum chamber by means of an 8 pin electrical feedthrough (Varian, model 954-5014). Filament temperature was controlled by means of a nichrome slide wire resistor, and the temperatures were measured at the filament center (hottest point) with an optical pyrometer (Pyrometer Instrument Co., Bergenfeld, N. J., model 95). These temperature measurements were corrected to account for the palladium emissivity at the operating wavelength of the pyrometer. A 1-1/2 inch viewing port (Varian, model 954-5041)

was located in such a manner that both the filament and the oven temperature could be optically measured through it.

A voltage drop of 1.34 volts across the filament was required to maintain a temperature of 1,000°C. As shown in Fig. 15, the positive side of the battery was grounded. The DC potential on the filament therefore varied from zero at one end to -1.34 volts at the other. This potential did not vary during data runs, within the accuracy of the voltmeter (± 0.02 volts).

4.4.D Oven Bias and Vac-Ion Pump Grid Bias

As previously mentioned, the oven acted as a thermionic emitter when it was heated (2400°K). In order to inhibit electron emission from the oven, it was biased at +180 volts with dry cell batteries. An AC potential of about 1-1/2 volts was superimposed upon the DC bias since the oven was heated with alternating current. The DC potential was so much higher than the AC, however, that the effect of the small AC ripple could not be detected in the data.

A nickel grid was placed at the entrance of the Vac-Ion pump and was biased at -125 volts by means of a DC power supply (Heath Corp., Benton Harbor, Mich., model IP-32). The negative bias repelled electrons, and thus prevented them from leaving the pump and entering the vacuum chamber. Positive particles either impinged upon the grid or were accelerated by it. These particles could enter the chamber with an energy in the neighborhood of 125 electron volts (assuming singly charged particles). Since the collector was biased at +190 volts, the particles were repelled before they could strike the collector.

The grid bias was brought into the vacuum chamber via the same 8 pin feedthrough that supplied the filament power.

4.4.E Function of the Shield

The shield acted as both a thermal and an electrical barrier between the oven and the filament. The thermal effect will be discussed first.

For the sake of discussion, assume that the shield is not present. As described in Section 4.4.C, the filament temperature was measured with an optical pyrometer. This could be done quite accurately as long as the oven was not heated. When the oven was hot, however, the visible spectrum which it radiated masked the spectrum radiated by the filament and the filament temperature could not be measured.

An attempt was made to determine the change in the electrical resistance of the filament due to radiant heating by the oven. This was done by observing the current flow through the filament from the constant voltage battery with an ammeter (see Fig. 15). The resistance could then be calculated from Ohm's Law. The ammeter was capable of detecting a 2% current change. The current remained the same with the oven either hot or cold. The lack of a current change must be attributed to the sensitivity of the ammeter since the presence of the hot oven undoubtably increased the filament temperature somewhat.

The problem was minimized by introducing a radiation shield between the oven and the filament. Radiant energy could be transmitted through the 0.24 cm hole in the shield, but this was the only passage available. By using the shield arrangement, the filament temperature

could be set while the oven was cold, after which the oven could be heated.

The filament temperature would be expected to rise slightly when the oven was heated, even with the shield installed. Indications are that this did occur. However, the temperature rise was small and did not affect the data significantly. This will be discussed further in Section 6.5.

The possibility of gas particles ionizing on the hot oven surface had to be considered. Although the degree of ionization of hydrogen is negligible at 2400°K[62], it is possible that some of the background gases would ionize at this temperature. Thus, the shield was biased at +150 volts in order to attract any electrons released by the ionization process. Positive ions were repelled. The positive bias also inhibited any thermionic emission from the shield.

4.5 The Vacuum Chamber

The vacuum chamber consisted of a single piece of 4 inch diameter, 11 gauge, type 304 stainless steel tubing which was 12-3/4 inches long. Ten radial access ports were provided for the mounting of electrical feedthroughs, a viewing port, an ion gauge, and other equipment required for the experiments. The access ports were fabricated from 1-1/2 inch diameter, 16 gauge, type 304 stainless steel tubing. Varian ConFlat flanges were welded to the ends of both the vacuum chamber and the access ports.

The various vacuum feedthroughs were bolted to the access ports; all of the bolted joints utilized Varian ConFlat flanges. This flange

design consists essentially of a circular knife edge on each flange. The knife edges of two mating flanges are separated by a copper gasket. When the flanges are tightened, the knife edges deform the gasket and a vacuum seal is formed. These joints are bakeable and very reliable.

The vacuum system was leak checked with a helium leak detector (Consolidated Electrodynamics Corp., model 24-120) when necessary.

Photographs of the vacuum system and associated equipment are shown in Figs. 16 and 17.

Chapter 5

EXPERIMENTAL PROCEDURES

5.1 General

The experimental procedures will be discussed in four parts. First, the techniques used for achieving ultra-high vacuum conditions will be described. The second part will deal with the procedure used for determining thermionic emission current as a function of hydrogen beam intensity. Part three will describe the method used for determining the pressure in the vacuum chamber during beam operation. Finally, the data reduction procedures will be described.

5.2 Obtaining Vacuum Conditions

The arrangement of the various vacuum pumps and valves is shown in Fig. 9. The system was first evacuated to about 25 microns with the mechanical pump. When this pressure was obtained, the oil diffusion pump was turned on and chilled water ($50^{\circ}F$) was passed through the baffle. This pumping combination reduced the system pressure to about 10^{-5} torr.

Bakeout commenced when the pressure was in the 10^{-5} torr range. Insulating walls were placed around the system, and three 1,000 watt electrical resistance heaters were actuated. The temperature was raised to $250^{\circ}C$ over a period of about 6 hours. When the bakeout temperature ($250^{\circ}C$) was reached, both Vac-Ion pumps were turned on. The pressure then fell to the 10^{-6} torr range in about 12 hours.

At this point, the ionization gauges, hydrogen leak, and cold cathode gauge were outgassed. It should be noted that these components were outgassed while the system was baking.

After outgassing, the valves leading from the vacuum chamber and the leak system to the diffusion pump were closed. All pumping was done by the Vac-Ion pumps from this point on. After baking the system for another 24 hours, the pressure in the vacuum chamber and the leak system were both in the 10^{-7} torr range. The hydrogen oven was then outgassed by slowly heating it to 2,000°K and maintaining this temperature for about two hours.

Bakeout was then continued for an additional 24 hours, after which the system was slowly cooled (about 6 hours for cooling). Thus, the pumpdown and bakeout procedure required about 3 days.

The background pressure after cooling varied somewhat from bakeout to bakeout. The minimum pressure attained in the vacuum chamber after bakeout was 8×10^{-10} torr, while the maximum was 3×10^{-9} torr. Background pressure in the leak system was about double that in the vacuum chamber.

The filament and the collector were the only metal parts which were outgassed after bakeout. This was done to minimize the possibility of filament burnout. The filament was outgassed by electrical heating. The collector was cleaned by electron bombardment, utilizing the electrons emitted by the hot filament. Outgassing of these two components did not raise the background pressure significantly. Pressures remained in the 10^{-9} torr region.

5.3 Obtaining Thermionic Emission Current Data

The thermionic emission current from the palladium filament was measured under four sets of conditions, with similar procedures being used for all four. These conditions were:

1. Filament at 1,000°C, oven at room temp. (molecular beam)
2. Filament at 1,000°C, oven at 2,400°K (atomic beam)
3. Filament at 1,100°C, oven at room temp.
4. Filament at 1,100°C, oven at 2,400°K

5.3.A Filament and Oven Operation

Filament temperature was controlled by a slide wire resistor, as described in Section 4.4.C. The first step was to determine the slide wire settings which yielded temperatures of 1,000°C and 1,100°C. This was done by varying the slide wire position while monitoring the filament temperature with an optical pyrometer. The settings which gave the desired temperatures were recorded so that these temperatures could be reproduced when the filament could not be observed optically. An ammeter was used to measure the filament heating current (Fig. 15). The ammeter readings corresponding to the two filament temperatures of interest were also noted.

The filament was then cooled and bias voltages were applied to the various components as discussed in the previous chapter. The ionization gauge used to measure the vacuum chamber pressure was turned off since it was a source of unwanted charged particles.

The microammeter was then turned on. It indicated small currents when the filament was cold. This was attributed to electrical pickup

by the circuit components and wiring. These currents were negated by the null box (Gyra Electronics Corp., La Grange, Ill., model CS-57) shown in Fig. 15. The null box was a stable battery supply, capable of supplying small currents. The output of the null box was placed across the microammeter and was then adjusted so that the meter indicated zero.

The next paragraph applies only to operation with the oven hot (atomic beam). The procedure for molecular beam operation (oven at room temp.) will then be continued.

The oven was brought up to temperature after the microammeter was zeroed. Heating the oven caused the vacuum chamber pressure to increase. The oven was kept at 2,400°K and the vacuum chamber was pumped down for about an hour before any hydrogen was admitted. This procedure resulted in a background pressure of about 6×10^{-9} torr in the neighborhood of the filament. Since the microammeter was zeroed before the oven was heated, any current flow indicated by the meter could be attributed to heating the oven and the shield. The magnitude of this current was about 10^{-12} amperes. This was negated by adjusting the null box output so that the microammeter again indicated zero.

The filament was then heated to either 1,000°C or 1,100°C, depending upon the data run. The current indicated by the microammeter was the thermionic emission current from the filament to the collector at the initial experimental conditions (hydrogen beam not operating, vacuum chamber at background pressure). This will be referred to as I_o.

5.3.B Beam Operation

The control and measurement of the hydrogen pressure in the beam source was discussed in Section 4.3.D. The operating procedure consisted of maintaining a given pressure in the beam source and recording the thermionic emission current corresponding to that pressure. The source pressure was then increased and the emission current was again recorded, etc. Beam source pressure was varied from 3×10^{-9} torr to 150 microns during the course of a data run. The pressure at each data point was held constant until the emission current remained stable for at least 15 seconds.

Data were taken as the beam source pressure increased and also as it decreased. If these two sets of data did not agree, it might be indicative of the palladium absorbing hydrogen. Agreement between the two data sets was good, as discussed in Sections 6.2 and 6.3.

Experiments were made using two different filaments. Both filaments came from the same roll of wire, which had a purity of 99.999% (Leytess Metal and Chemical Corp., New York).

5.4 Vacuum Chamber Pressure During Beam Operation

During operation, hydrogen flowed from the oven into the vacuum chamber in the form of a molecular or an atomic beam. This flow caused an increase in the vacuum chamber pressure. Since the magnitude of this increase might bear upon the validity of the experimental data, runs were made in which vacuum chamber pressures were recorded. The pressure increase had a small effect on the data, as will be discussed subsequently.

The procedure followed for determining vacuum chamber pressure during beam operation was straightforward. Hydrogen was admitted to the leak system and the beam was operated in its normal manner, both hot and cold. Vacuum chamber pressures were measured at two positions, as described below.

Section 4.4.A discussed the fact that the shield acted as a flow constriction to hydrogen being pumped out of the vacuum chamber. For this reason it was necessary to measure the pressure both upstream and downstream of the shield. Upstream pressure was measured by a nude ion gauge (Fig. 15). The downstream pressure was determined by measuring the current flow to the 50 liter/sec Vac-Ion pump. The current is proportional to the pressure inside the pump. Calibration curves of current vs. pressure are provided by the manufacturer.

The downstream pressure was lower than the upstream pressure, as expected. The upstream pressure did not affect the data while the downstream pressure had a small effect since the filament was located in the downstream region. The magnitude of this effect will be discussed in Section 6.4.

Thermionic emission data was not taken during these pressure runs since the nude ion gauge was operating.

5.5 Data Reduction

The raw data was in the form of emission current as a function of the pressure indicated by the leak system gauges. Both of these parameters were multiplied by appropriate constants in order to present the data in its final form.

The thermionic emission current (I_o), which was measured with the beam not operating and the vacuum chamber at background pressure, varied somewhat from run to run. To negate the effect of this small variation, all of the emission currents (I) were divided by I_o. This resulted in a "normalized" current (I/I_o). The quantity I/I_o was plotted rather than the thermionic emission current (I).

It was desirable to plot I/I_o vs. $P_{equivalent}$ since this appeared to be the clearest manner of presenting the data. $P_{equivalent}$ was defined in Section 4.3.B. It is the condition for which the number of gas particles impinging on the filament per cm^2 per second from the beam is the same as the impingement rate per cm^2 when the filament is enveloped in a gaseous environment at a pressure $P_{equivalent}$. In order to present the data in this form, the gauge pressures (raw data) were multiplied by the conversion factors calculated in Appendices C and D.

Chapter 6

EXPERIMENTAL RESULTS

6.1 General

Experiments were performed under the four sets of conditions listed in Section 5.3, using two different palladium filaments. The results obtained from the first filament are shown in Fig. 18, while Fig. 19 presents the data acquired with the second filament.

6.2 Molecular Beam Results

Curve 1 in Fig. 18 and curve 5 in Fig. 19 show the results of the molecular beam runs with the filament at 1,000°C. Curve 1 was constructed from data taken during two runs; all of the data points fell within the envelope shown.

The two sets of data which constitute curve 1 appear to be in good agreement and the spread is within the limits of experimental error, as discussed in Section 6.5. Curve 1 compares favorably with the results of Ref. 17. The maximum value of I/I_o was about 3-1/2 at a pressure of 5×10^{-6} in Ref. 17; curve 1 shows a value of about 4-1/4 at this equivalent pressure. The general shape of curve 1 also compares well with the results of Ref. 17.

The data presented in curve 5 of Fig. 19 were obtained in the same manner as those shown in curve 1. However, a different palladium filament was used. The two curves agree well, with the maximum value of I/I_o being 3.8 for curve 5.

As stated in the previous chapter, data were taken as the beam source pressure was increased and also as it decreased. There was some spread in the data acquired under these two conditions. However, this was no greater than the spread which appeared between different runs. It should be noted that the emission currents measured while the beam source pressure was decreasing were generally slightly higher than those observed during increasing pressure operation. This may or may not be indicative of an absorption hysteresis effect. The present experimental equipment was not designed to measure this effect with any degree of accuracy. It can be measured with an arrangement such as that used by Moore and Unterwald[55].

The data show that the thermionic emission current increases as the beam intensity increases, indicating that the chemisorbed hydrogen forms a surface dipole layer with the positive side outermost. This will be discussed in the next chapter.

The limits of free molecular flow from the beam source are shown in Figs. 18 and 19 for both a hot and a cold source. This limit was taken as the beam source pressure at which the mean free path of a gas particle in the source was ten times the diameter of the beam source orifice (see Appendix D). Molecular beam data are plotted somewhat beyond this limit. The end points of curves 1 and 5 correspond to the mean free path being seven times the orifice diameter.

The data which were taken with the molecular beam operating while the filament was held at 1,100°C are plotted as curve 3. These results are from a single run. The curve has higher emission current values

than curves 1 and 5, but has lower values of I/I_o. This result is as expected; higher filament temperatures increase the emission current but reduce the coverage of chemisorbed hydrogen.

6.3 Atomic Beam Results

The results obtained by operating the atomic beam while the filament was at 1,000°C are shown in curve 2 of Fig. 18 and curve 6 of Fig. 19. Curve 2 contains data taken during three runs, while curve 6 is constructed from two runs. As in the case of molecular beam operation, data were taken both as the beam source pressure increased and as it decreased. Once again, the spread in the data taken under these two conditions was not greater than the spread between different runs. All of the data points fell within the envelopes shown in the figures. Curves 2 and 6 represent data from two different filaments. They are in good agreement, with the maximum values of I/I_o being 3.2 for curve 2 and 2.9 for curve 6.

Curve 4 presents the data from an atomic beam run with the filament at 1,100°C. It is very similar to the molecular beam data at this filament temperature, for the same reasons.

The values of I/I_o are consistently lower for the atomic beam experiments than for molecular beam operation. This fact is the most significant piece of information derived from the data. It indicates that when a palladium filament at 1,000°C is exposed to atomic and molecular beams of equal intensity, more hydrogen is chemisorbed on the filament from the molecular beam than from the atomic beam. The reasons for this will be discussed in detail in the next chapter.

6.4 Effect of Vacuum Chamber Pressure

Vacuum chamber pressure was measured as a function of equivalent beam pressure, with the beam source hot and cold. Chamber pressures were measured both upstream and downstream of the shield, as described in Section 5.4.

These data were acquired in order to determine whether or not the vacuum chamber pressure had an effect on the validity of the data discussed in Sections 6.2 and 6.3. Since the vacuum chamber pressure after bakeout was in the 10^{-9} torr range and rose only during beam operation, it can be assumed that chamber pressures greater than about 10^{-9} were due to the presence of hydrogen.

The ambient hydrogen pressure in the region of the filament can be taken as the pressure measured in the downstream portion of the vacuum chamber since the filament was located downstream of the shield. Figures 20 and 21 show that this pressure remained below 10^{-7} torr throughout the experiments. This chamber pressure was present when the equivalent beam pressure was in the 10^{-4} torr range and the corresponding value of I/I_o was in the neighborhood of 3 to 4. Now, Ref. 17 shows that an ambient hydrogen pressure of 10^{-7} torr corresponds to a value of I/I_o of about 1.2. Thus, the error introduced by the ambient hydrogen can be estimated as 0.2/3.0, or about 6.7%. This is slightly greater than the spread in the data shown in Figs. 18 and 19. This error was not significant as will be shown in the next section.

The upstream pressures were somewhat greater, reaching a maximum of 1.5×10^{-7} for the hot beam source conditions. Upstream pressures

were measured so that their effect on beam scattering could be determined. The pressures are low enough so that beam scattering is negligible. The mean free path of a hydrogen molecule at a pressure of 10^{-7} torr is about 10^5 cm (see Appendix D) while the distance from the beam orifice to the filament is only 1.25 cm.

The above discussion indicates that the vacuum chamber pressures were low enough so that the difference between the H and H_2 data shown in Figs. 18 and 19 was not significantly affected.

6.5 Error Analysis

There are two general forms that an error analysis can take. The first form is more mathematical in nature and involves the use of statistical methods to minimize random errors and to maximize the reliability of the data[63]. The second method is less sophisticated and depends more upon the judgement of the investigator to evaluate the significance of various error sources[64]. The quantity of data taken in the present experiments is not large enough for the application of statistical methods. Therefore, the following discussion will attempt to estimate the magnitudes of the various errors which are present.

6.5.A Sources of Errors and Their Magnitudes

Several of the error sources have been described in earlier sections. They will be included here for the sake of completeness.

1. Measurement of the filament temperature

The filament temperature was measured with an optical pyrometer. A value of 0.3 was used for the emissivity of palladium. The error

involved in this measurement was determined by first finding the slide wire resistor setting and the current which corresponded to 1,000°C. The resistor was placed at the predetermined setting and the temperature was measured. This procedure was repeated several times. All temperatures were within ±10°C of the first temperature measurement. Thus, the error due to the uncertainty of the filament temperature can be estimated as ±10°C. The ±10°C spread represents operator error, not instrument error. Any error in the calibration of the instrument would be a source of constant error and would not contribute to the data spread. The pyrometer was factory calibrated in July, 1964. Calibration standards were supplied by the National Bureau of Standards.

The significance of the 10°C error in the filament temperature can be estimated by using the Richardson-Dushman equation. The result shows that a 10°C error at 1000°C will result in an emission current error of about 8%.

Four of the curves shown in Figs. 18 and 19 were plotted from data taken during two or more runs (curves 1,2,5, and 6). The spread in each of these curves is of the order of 6%, and this spread is attributed to the 10°C uncertainty in the filament temperature. Figures 18 and 19 indicated that the spread is not excessive in the sense that it will not interfere with interpretation of the data.

2. Filament temperature increase due to heating the oven

The problem of radiant heat transfer from the hot oven to the filament was discussed in Section 4.4.E. The shield helped to minimize

this transfer, but did not eliminate it. Thus, an error exists due to the fact that the filament temperature was slightly higher during atomic beam operation than it was during the molecular beam experiments.

The magnitude of this temperature increase can be estimated by considering the values of I_o with the oven hot and with it cold. By averaging the I_o values given in Figs. 18 and 19, the ratio $I_{o_{\text{hot oven}}}/I_{o_{\text{cold oven}}} = 1.19$ is obtained. Again using the Richardson-Dushman equation, this corresponds to a temperature difference of about 15°C. This error applies only to data taken with the oven hot.

Since a higher filament temperature results in lower hydrogen coverage, it is possible that the values of I/I_o shown in curves 2 and 6 of Figs. 18 and 19 may be somewhat low. The magnitude of this error can be estimated as follows. The maximum value of I/I_o shown by curve 2 is about 3.0. This point corresponds to atomic beam operation with P_e equal to 1.7×10^{-5} torr and the filament at 1000°C. Curve 4 shows a maximum I/I_o value of 1.3. This point corresponds to the conditions just given, except that the filament temperature is at 1100°C. The change in I/I_o which results from a change in filament temperature can be expressed as

$$\frac{\Delta I/I_o}{\Delta T} = \frac{3.0-1.3}{100} = 0.017 \text{ per } ^oC$$

at the stated pressure and temperature range. A temperature error of 15°C will thus cause an error in I/I_o of

$$(I/I_o)_{\text{error}} = (0.017)(15) = 0.255$$

Expressed as a percentage, the error is 0.25/3.0 or 8.5%.

Even if curves 2 and 6 were increased by 8.5%, they would still fall below curves 1 and 5, and the atomic beam would still yield lower values of I/I_o than the molecular beam. It should also be noted that the 15°C error was estimated by attributing the entire difference between the values of I_o to filament temperature differences. Part of the discrepancy is probably due to that nebulous catchall called "operator error", and the 15°C estimate is certainly a maximum value.

3. Emission current increase due to heating the oven

Section 5.3.A discusses the fact that small currents were noted when the oven was heated while the filament was cold. These currents were attributed to either thermionic emission from the oven and shield, or to the ionization of background gases by the oven surface.

This error was compensated for, as discussed in Section 5.3.A, and is therefore considered as being negligible.

4. Error due to hydrogen in the vacuum chamber

The error caused by the small hydrogen pressure in the vacuum chamber (see Section 6.4) varied from 0% at low beam intensities to about 7% at the maximum beam intensity. Thus, the net effect of this error was to slightly increase all values of I/I_o at the higher values of P_e. This error (about 7% at higher values of P_e) was about the same for either atomic or molecular beam operation. Therefore, it would tend to raise all of the curves by about the same amount. Thus, there would be an error in the absolute magnitude of I/I_o, but this would have practically no effect when comparing one curve to another.

5. Electronic equipment

The caliber of the electronic equipment is always a consideration when errors are discussed. The three electronic components (power supply, microammeter, and null box) used in the circuit which measured the thermionic emission current were all precision components. The power supply used to bias the collector was capable of maintaining 190 volts within ± 0.1 volts. No drift was detected when the null box was used to zero the microammeter. The power supplies used to bias the shield and the Vac-Ion pump grid were of lower quality. These were capable of maintaining the bias voltages within $\pm$ 1.0 volts. However, small instabilities could be tolerated at the shield and at the Vac-Ion pump grid.

No significant error is attributed to the electronic equipment.

6. Discrepancies between data taken with different filaments

The largest discrepancy which appears in Figs. 18 and 19 is the spread between data taken from the two different filaments. This amounts to about 14%, compared to about a 6% spread for different runs with the same filament. The 14% discrepancy can be attributed to differences in the geometric arrangement of the filament and collector for the two sets of data.

Filaments were changed by removing the old one and spot welding a new one to the filament power input leads. The new filament was then aligned in the collector by eye. Under these conditions, exact reproduction of the geometry was not possible.

6.6 Effect of Errors on the Validity of the Data

When considering the effect of errors on data validity, there is one question which must be considered. What is the data going to be used for? In the present experiments we are attempting to gain some knowledge about the reactions described in Section 3.2 and we want to know whether more hydrogen is chemisorbed on a palladium surface from an atomic or a molecular beam.

From the preceding discussion, it can be firmly concluded that the values of I/I_o are higher for molecular beam operation than for atomic beam operation for the conditions used in the present experiments. It is this piece of information that will shed some light on the mechanism of hydrogen chemisorbing on palladium.

Chapter 7

DISCUSSION OF THE RESULTS

7.1 Polarity of the Dipole Layer

The curves of Figs. 18 and 19 show that the thermionic emission current from the filament increases as the equivalent hydrogen pressure increases. Thus, hydrogen chemisorption decreases the work function. The work function decrease is caused by chemisorbed hydrogen forming a positively charged layer on the palladium surface.

The problem of predicting the polarity of the dipole layer formed by chemisorbed hydrogen was discussed in Section 2.4.A. It was found that this quantity could not be predicted from the currently available theory.

Reference 17 contains data showing the change in the thermionic emission current of palladium at 1,000°C due to the chemisorption of molecular hydrogen. The emission current increased as the ambient hydrogen pressure increased. The results of the present beam experiments are in accord with this.

7.2 The Reaction Equations and the Data

The data presented in Figs. 18 and 19 show that the values of I/I_o are higher for molecular beam operation than for the atomic beam experiments. Since chemisorbed hydrogen reduces the work function of palladium, the higher emission currents observed during molecular beam

operation indicate that more hydrogen is chemisorbed from the molecular beam than from the atomic beam.

The reaction mechanisms were discussed in Chapter 3. It was concluded that if more hydrogen was chemisorbed from the molecular beam than from the atomic beam, it would indicate that the sticking coefficient of molecular hydrogen on palladium is greater than that of atomic hydrogen on palladium for the conditions of the present experiments. This is the case.

The theory of sticking coefficients is not well understood at present. Numerical values of the sticking coefficient are not generally calculated from first principles; they come from experimental data.

The next four sections will attempt to explain why the sticking coefficient of H is lower than that of H_2 in the present experiments. It will be seen that arguments based upon the heats of adsorption fail to explain the data. Consideration of the energy transfer mechanism between an impinging gas particle and a surface, however, provides a reasonable explanation.

7.3 Heats of Adsorption

The heat of adsorption is a measure of the bond strength between the adsorbate and adsorbent. Generally, a higher heat of adsorption indicates a higher probability that a gas particle impinging on a metal surface will be adsorbed.

The adsorption of molecular hydrogen can be visualized as follows:

1. A molecule impinges on the surface and is physically adsorbed, with a heat of adsorption of about 0.2 kcal/mole (see Section 3.4).

2. The physisorbed molecule takes energy from the crystal lattice and dissociates. The dissociation energy of H_2 is 103 kcal/mole[65]. It should be noted that the metal is cooled locally in the region in which the dissociation occurs since energy is removed from the lattice in this vicinity.

3. The resulting atoms are chemisorbed with a heat of adsorption of 65 kcal/mole of atoms[66].

The chemisorption of gaseous atomic hydrogen involves only the third step.

The molecular physisorption (Step 1) has a weak bond. Hence, the probability of a molecule desorbing after it has been adsorbed is high. The calculations in Section 3.4 show that the residence time of an H_2 molecule on a palladium surface is of the same order of magnitude as the period of oscillation of a surface palladium atom. Consequently a physisorbed hydrogen molecule must dissociate quickly or it risks desorption. Atoms chemisorbing from the gas phase do not go through this process.

Based upon heat of adsorption considerations, it would appear that more hydrogen should be adsorbed from an atomic beam than from a molecular beam. Since the data shows the opposite, another effect must be present which affects chemisorption more strongly than the heats of adsorption, for the conditions of the present experiments.

7.4 Energy Transfer from a Gas to a Metal Lattice

A gas particle which is adsorbed on a metal surface can be visualized as oscillating in a potential well near the surface. This

is shown schematically in Fig. 22. The depth of the potential well (D) corresponds to the heat of adsorption (or bond energy).

A particle approaching the surface possesses kinetic energy. When it collides with a surface atom (or atoms) part of this kinetic energy is transferred to the lattice. The particle will then rebound from the surface. If the energy exchange during the collision was inefficient, the particle may still possess enough energy to escape from the potential well and adsorption will not occur. If sufficient energy was transferred to the lattice, the particle will be trapped in the well. This constitutes adsorption.

The data of Figs. 18 and 19 may be understood in terms of the energy transfer between the atom or molecule and the adsorbent lattice.

7.5 Analytical Studies of the Energy Transfer from a Gas Particle to a Lattice

The problem of the energy transfer between a gas particle and a crystal lattice has been attempted analytically, and a limited amount of information is available in the literature. The analytical procedures used involve several assumptions, and the authors usually state that while the results are not quantitatively accurate, the trends which are indicated are probably valid. The general methods and assumptions used will be discussed below.

Zwanzig[67] considered the problem in one dimension. He represented the crystal as a semi-infinite chain of harmonic oscillators each having a lattice force constant k, as shown in Fig. 23. The interaction potentials which were chosen to represent the forces between the gas

atom and the lattice had to be amenable to analytic treatment. One of these (truncated harmonic oscillator potential) is shown in Fig. 23. The potential well has the parabolic shape representative of a harmonic oscillator. However, the interaction between the gas particle and the surface ends abruptly when the separation between these particles is greater than a predetermined distance R. The interaction potentials used in the calculations were not realistic, but they were amenable to analytical treatment.

Zwanzig solved the equations of motion for two cases, $\mu = 1/2$ and $\mu = 1$, using the truncated harmonic oscillator potential. μ is the ratio of the mass of the gas particle to the mass of a lattice atom (M/m in Fig. 23).

For these cases, he found the following results:

At $\mu = 1/2$ $\quad E_c/D = 2.394$

$\mu = 1$ $\quad E_c/D = 24.54$

E_c is defined as the critical kinetic energy of the incoming gas particle. If it possesses kinetic energy in excess of E_c, it will not adsorb. D is the potential well depth.

These results show that as μ decreases, E_c/D decreases and the efficiency of the energy exchange due to the collision is diminished. The values of μ in the present experiments are small:

$$\mu_{\text{molecular beam}} = 0.0189$$

$$\mu_{\text{atomic beam}} = 0.0094$$

The weaknesses of this analysis have been summarized by Zwanzig[67].

> "Three major approximations have been made in the formulation of the preceding models. Classical mechanics is used, the models are one dimensional, and the interactions are not realistic. Because of these approximations the results cannot be quantitatively correct; but the qualitative features which appear ought to be reliable.
>
> The error introduced into these calculations by using classical mechanics is difficult to estimate. However, we feel that it should not be serious except perhaps for very light molecules."

In addition to the above assumptions, the lattice was considered at rest initially. This corresponds to a lattice at absolute zero of temperature.

Goodman[68] extended the analysis to the three dimensional case. Other than this, his assumptions were the same as Zwanzig's. He found that the energy transferred in a gas-surface collision was less for the 3D lattice than for the 1D case. The difference between the two diminished as μ decreased.

Using the 3D results, Goodman then calculated the accommodation coefficients of five noble gases on clean tungsten, using the Lennard-Jones 6-12 potential as the interaction potential. The accommodation coefficient is defined as

$$\alpha = \frac{T_1 - T_2}{T_3 - T_2}$$

where α = accommodation coefficient

T_1 = temperature of the gas leaving the surface

T_2 = temperature of the gas impinging on the surface

T_3 = temperature of the metal surface

Thus, the accommodation coefficient can be used as a measure of the efficiency of the energy transfer between the gas and the lattice.

A value of $\alpha = 1$ would result if the gas leaving the surface was at the surface temperature.

The calculated results show that the accommodation coefficient decreases as the mass of the gas particle diminishes. The highest value of α was found for xenon and the lowest for helium. These calculated results were compared with the experimental results of Thomas and Schofield[69]. While the magnitudes of the values of α did not agree, the trends were in the same direction. Lighter atoms had lower values of α.

McCarroll and Ehrlich[70] extended the one dimensional case considerably. They used the same model and interaction potential as shown in Fig. 23. However, their investigation covered a large spectrum of values of the various parameters. They were able to do this by programming the equations for a digital computer.

Their results are shown in Fig. 24. The parameters which are plotted are somewhat different than those used by Zwanzig[67]. In these calculations, the width of the potential well (truncated harmonic oscillator, Fig. 23) was kept constant. The potential well depth was then varied by changing the value of k_o, where k_o is the harmonic force constant between the gas particle and the lattice surface atom. The quantity β, which is plotted as the abcissa, is the ratio k_o/k. Thus, the depth of the potential well (D) is implicitly included in the quantity β of Fig. 24.

The quantity E_c/Q_L is plotted as the ordinate. E_c is again the maximum kinetic energy which a gas particle can possess if it is to be adsorbed. Q_L is the binding energy of an atom in a homogeneous lattice.

The trends shown in Fig. 24 agree with those of Refs. 67 and 68.

7.6 Energy Transfer in the Present Experiments

The values of μ plotted in Fig. 24 are not low enough for the present experiments. μ for atomic hydrogen and palladium can be taken as the ratio of the atomic weights, which is 0.0094. For molecular hydrogen, it is twice this value. The lowest value of μ plotted is 0.25. Figure 24 does give the trends for the energy transfer, however, and the results of the present experiments can be qualitatively analyzed by these trends.

Figure 24 shows that the value of E_c decreases as μ decreases, assuming Q_L is held constant. Since Q_L is the lattice binding energy, it is a constant in the present experiments. These curves also show that the effect of β diminishes as μ is reduced. This would indicate that the depth of the adsorption potential well becomes less important as μ decreases. The values of E_c/Q_L become very small for low values of μ, at all of the plotted values of β.

The values of E/Q_L (E is the kinetic energy of an incoming particle) in the present experiments can be estimated. Kittel[23] gives the cohesive energy of palladium as 93 kcal/mole at room temperature. This can be used as Q_L. The kinetic energy of the beam particles can be taken as 3/2 kT, where k is Boltzmann's constant. Doing this

$$\left(\frac{E}{Q_L}\right)_{\text{molecular beam}} = 0.0153$$

$$\left(\frac{E}{Q_L}\right)_{\text{atomic beam}} = 0.122$$

The value of β for the atomic case can be estimated as the ratio of the heat of chemisorption to the lattice binding energy. This quantity is 65/93 or 0.7. The curves for low values of μ are fairly flat in this region of β.

Figure 24 indicates that a value of E/Q_L of 0.122 may very well be above the critical kinetic energy for adsorption. The fact that less hydrogen is chemisorbed on palladium from an atomic beam than from a molecular beam is thus attributed to the energy exchange mechanism. The slower moving molecules ($300^{\circ}K$) transfer sufficient energy to the lattice to cause their adsorption. The faster moving atoms ($2400^{\circ}K$) are less successful in surrendering their kinetic energy through collision with the surface.

It is unfortunate that the data of Figs. 18 and 19 must be explained by trends rather than by the numerical values of the curves in Fig. 24. However, this is the case. Figure 24 respresents the best currently available data on the subject of energy transfer from a gas particle to a solid lattice.

7.7 Dissociation of H_2 as the Rate Determining Step

Two questions were posed in Section 1.3. These are restated below.

1. Is the dissociation of molecular hydrogen the rate determining step in the chemisorption of H_2?

2. Is there a significant difference between the sticking coefficients of atomic and molecular hydrogen on palladium?

The second question has been answered. For the conditions of the experiments, the sticking coefficient of molecular hydrogen is greater than that of atomic hydrogen. This appears to be largely due to kinetic energy considerations.

The first question cannot be answered completely at this time. However, the fraction of adsorbed H_2 which dissociates before being desorbed can be estimated. The estimate involves several assumptions. Consequently, the answer will be an order of magnitude answer only. The procedure will be as follows.

1. The ratio $\theta_{atomic}/\theta_{molecular}$ will be calculated. θ_{atomic} is the fraction of the surface covered with atomic hydrogen during atomic beam operation; $\theta_{molecular}$ is the same quantity for molecular beam operation. Note that the subscript refers to the mode of operation; the adsorbed species is atomic hydrogen for both cases.

2. The kinetic energy distribution in both beams will be calculated.

3. It will be assumed that the kinetic energy of most of the hydrogen molecules is small enough so that energy transfer during a surface collision does not determine whether or not the molecule is adsorbed. A reasonable value will be assumed for the sticking coefficient of H_2. This sticking coefficient will account for factors such as the surface geometry requirements for atomic adsorption of a diatomic molecule[72]. For the atomic beam, however, it will be assumed that energy transfer is the only effect which prevents gaseous atoms which strike the surface from chemisorbing. It will be further assumed that the values of E_c are the same for both cases. By using the above assumptions and the value

of $\theta_{atomic}/\theta_{molecular}$, the kinetic energy distributions can be compared in such a way that the fraction of adsorbed H_2 which dissociates before desorbing can be estimated. This procedure will be followed in the next three sections.

7.7.A Degree of Surface Coverage

The first step is to estimate the ratio of the amount of hydrogen adsorbed from the molecular beam to the amount adsorbed from the atomic beam. A formula for calculating the degree of surface coverage from the change in work function due to chemisorption was given in Section 2.4.

$$\Delta\phi = 4\pi\ n_s\theta\sigma$$

where $\Delta\phi$ is the work function change due to chemisorption, n_s is the number of adsorption sites per cm^2, θ is the fraction of the surface covered with adsorbent, and σ is the dipole moment of the adsorbate-adsorbent bond.

The quantity σ is difficult to evaluate. However, it is not needed for a ratio since it is the same for either atomic or molecular beam operation (chemisorption occurs as atoms for both cases).

$$\frac{\Delta\phi_{molecular}}{\Delta\phi_{atomic}} = \frac{\theta_{molecular}}{\theta_{atomic}}$$

The values of $\Delta\phi$ can be estimated from the Richardson-Dushman equation.

$$\left[\frac{I}{I_o}\right]_{atomic} = \exp\left[\frac{1}{kT}(\phi_o-\phi)_{atomic}\right] = \exp\frac{\Delta\phi}{kT}\ atomic$$

The same procedure can be used to find $\Delta\phi_{molecular}$. Substituting the expressions for the $\Delta\phi$'s into the last equation on pg. 88,

$$\frac{\theta_{atomic}}{\theta_{molecular}} = \frac{\ln\,(I/I_o)_{atomic}}{\ln\,(I/I_o)_{molecular}}$$

Figure 18 shows that $(I/I_o)_{molecular}$ equals 4 at an equivalent hydrogen pressure of 3×10^{-6} torr. The values of θ will be compared for the condition that the number of atoms impinging on the filament is the same from both beams. Since there are two atoms per molecule, the value of $(I/I_o)_{atomic}$ will be taken at a pressure of 6×10^{-6} torr, which gives $(I/I_o)_{atomic}$ equal to 2.2. Substituting values,

$$\theta_{atomic}/\theta_{molecular} = 0.56 \qquad (1)$$

It should be recalled that θ is the surface fraction covered with atomic hydrogen, for both cases.

The above ratio also has a second meaning. If the rate of desorption is first order in θ, then $\theta_{atomic}/\theta_{molecular}$ can be taken as the ratio of the number of incoming hydrogen atoms which are chemisorbed atomically under the two operating conditions. This statement will be proven below.

All of the data were taken during steady state conditions, i.e., the rate at which atoms were chemisorbed was equal to the atomic desorption rate. Assuming that the desorption rate was first order in θ,

adsorption rate = desorption rate = $C\theta$

where C is a constant. The value of C is the same for either atomic or molecular beam operation since we are considering only the desorption of atoms in both cases. The adsorption rate can also be expressed as the rate at which atoms (from either beam) impinge upon the surface multiplied by the probability of chemisorption.

adsorption rate = (atomic impingement rate) x S

According to the nomenclature being used, S_{atomic} is the probability that an atom in the atomic beam will chemisorb when striking the surface, and $S_{molecular}$ is the probability that an atom in the molecular beam will chemisorb. Note that the definition of $S_{molecular}$ is not that of an ordinary sticking coefficient.

Combining the above relations,

$C\theta_{atomic}$ = (atomic impingement rate from the atomic beam) x S_{atomic}

$C\theta_{molec.}$ = (atomic impingement rate from the molec. beam) x $S_{molec.}$

Thus,

$$\frac{C\theta_{atomic}}{C\theta_{molec.}} = \frac{\text{(atomic impingement rate from the atomic beam)} \times S_{atomic}}{\text{(atomic impingement rate from the molec. beam)} \times S_{molec.}} \qquad (2)$$

Now let the two impingement rates be equal. For this situation, Eqs. 1 and 2 can be combined.

$$\frac{S_{atomic}}{S_{molecular}} = \frac{\theta_{atomic}}{\theta_{molecular}} = 0.56 \qquad (3)$$

7.7.B Kinetic Energy Distributions in the Beams

The kinetic energy distributions in the atomic and molecular beams were derived from the speed distributions and are shown in Figs.

25 and 26. The speed distribution in a beam is not Maxwellian; the proportion of faster particles is somewhat greater in the beam distribution than in the Maxwell distribution. The percentages shown in the figures indicate the percent of the beam particles having kinetic energies lower than the indicated values. For example, the 4.5% line shown in Fig. 25 corresponds to a kinetic energy of 2.8 kcal/mole. Thus, 4.5% of the area under the curve lies to the left of 2.8 kcal/mole, or 4.5% of the particles have kinetic energies below this value. Similarly, Fig. 26 shows that 90% of the particles in the molecular beam have kinetic energies below 2.8 kcal/mole.

7.7.C Estimate of the Dissociation of H_2

Assume that the kinetic energies of most of the particles in the molecular beam (say 90%) are below E_c. Thus, the energy exchange mechanism during collision will not prevent most of the molecules from chemisorbing. Figure 26 shows that 90% of the molecules have kinetic energies below E_c if E_c is taken as 2.8 kcal/mole. This value is therefore chosen.

Now assume that the value of E_c is the same for both the atomic and molecular beams. Figure 25 shows that 4.5% of the atomic beam particles have kinetic energies below E_c. It is assumed that all of the atoms which strike the Pd surface with kinetic energies below E_c will chemisorb. Thus, the sticking coefficient for the atomic beam (S_{atomic}) is 0.045. Substituting this value into Eq. 3 of the previous section,

$$S_{molecular} = 0.045/0.56 = 0.08$$

It is found that 8% of the atoms in the molecular beam which strike the surface will chemisorb atomically.

The sticking coefficient of molecular hydrogen (probability that a molecule which strikes the surface will adsorb, physically or chemically) on a hot Pd surface should be about the same as that for H_2 on hot tungsten. This quantity can be taken as 0.3[73].

The situation can now be described a little more clearly. Thirty percent of the molecules which impinge upon the surface are adsorbed, but only 8% of the molecules which impinge are chemisorbed atomically. The remaining 22% are desorbed before they dissociate. Consequently, the fraction of the molecules which dissociate before desorbing is 8/30 or 26.7%.

The assumptions which have been made render this an order of magnitude calculation. Since the calculated value is 26.7%, it would be reasonable to say that at least 5% of the hydrogen molecules which physisorb on the palladium surface will chemisorb. The remainder will desorb before dissociating. The fraction which dissociates is significant, not miniscule. It appears that the desorption/dissociation step shown in Section 3.2 will slow down the H_2 chemisorption reaction somewhat, but it would be difficult to justify calling it the rate determining step of the reaction. The sticking coefficient influences the chemisorption rate more strongly than the desorption/dissociation step, as discussed in Section 8.1.B.

Chapter 8

CONCLUSIONS AND SUGGESTIONS FOR FUTURE RESEARCH

8.1 General Conclusions

In view of the discussion of the previous chapter, it seems reasonable to conclude that the molecular and atomic beam techniques used are satisfactory for studying differences between atomic and molecular chemisorption, at least for the case of hydrogen. The heatable beam source provides a method of obtaining a well-defined atomic hydrogen beam with a minimum of equipment. While it is difficult to fabricate, it is easy to operate.

8.1.A Sticking Coefficients

The sticking coefficient of molecular hydrogen at 300°K on palladium is greater than that of atomic hydrogen at 2400°K on palladium, despite the fact that the heat of chemisorption of the atomic hydrogen is considerably higher than that of the molecular hydrogen. The difference is attributed to the energy exchange mechanism between the gas particle and the metal lattice. A slow moving molecule surrenders enough kinetic energy during a surface collision so that it is trapped in the adsorption potential well. The more energetic atoms must transfer more kinetic energy than the molecules, during the collision, if they are to be adsorbed. Many of the atoms are not successful in doing this.

8.1.B Dissociation of H_2 on a Palladium Surface

A significant fraction of the H_2 adsorbed on a palladium surface will dissociate before it desorbs. An order of magnitude estimate shows that at least 5 to 10% of the physisorbed molecules will dissociate. It is difficult to ascertain whether or not this is the rate determining step in the adsorption-desorption mechanism of H_2 on palladium since the dissociation may be considerably greater than the 10% figure just given. The indications are that while dissociation may slow the reaction down somewhat, it does not act as a serious bottle-neck to the progress of the reaction. If all of the H_2 which strikes the filament is considered as being available for the chemisorption reaction, then it can be stated that more available H_2 is lost to the reaction due to the low sticking coefficient than is lost because of H_2 desorbing before dissociating.

8.2 Suggestions for Future Research

The results obtained from the present experiments have indicated a need for additional experimental and theoretical work. Some of this experimental work can be done with the present beam system, while some will require new equipment and techniques.

8.2.A Analytical Energy Transfer Studies

The sticking coefficient results have significance to analysts working with the energy transfer problem. These results are quite interesting since they indicate that, under certain conditions, the probability of a gas particle being adsorbed is more strongly dependent upon the kinetic energy of the particle than upon the strength of the

adsorption bond. This is in general accord with the analytical results of Refs. 67, 68, and 70.

A first step would be to see if McCarroll could run his analytical procedure[70] for the conditions used herein, and compare results.

8.2.B Experiments with the Existing Beam System

It would be of interest to repeat the present experiments using nickel and platinum in place of palladium. Referring to Fig. 24, such experiments would yield data at different values of μ, while the values of Q_L would vary by only about 20%[23]. In addition, the heats of chemisorption of hydrogen on nickel, platinum, and palladium are close to each other[6]. Consequently, the values of k_o would be similar. The data obtained from all three metals could be compared with the trends predicted in Refs. 67, 68, and 70.

It would also be of interest to obtain data at a number of oven temperatures above 2400°K. The fraction of the atomic beam chemisorbed on a metal surface should decrease as the beam temperature rises, if energy transfer to the lattice is the mechanism governing chemisorption.

8.2.C Sticking Coefficient and Accommodation Coefficient Experiments

The present experiments show that good information concerning sticking and accommodation coefficients is needed. Some clever methods have been devised for obtaining such information, but they have limitations.

McFee and Marcus[74] bombarded several surfaces with a beam of potassium atoms and were able to determine the velocity distribution

of the potassium atoms coming from the surface. The temperature of the potassium atoms could then be found from the velocity distribution. Consequently, the accommodation coefficient could be calculated.

The rotating velocity selector which they used is described in their paper, and will not not be discussed here. The number of potassium atoms in a given velocity range was found by passing the atoms through the velocity selector and then having them impinge on a hot filament. The atoms were ionized, and the ion current was measured.

Surface ionization detectors appear to work well with the alkali metals. However, a mass spectrometer would have to be used as the detector for the common gases such as oxygen, nitrogen, and hydrogen.

The above procedure could be used to measure sticking coefficients by using a pulsed beam and velocity selector. Here, a group of atoms or molecules of a given velocity would impinge upon a surface. The rate at which these particles were reflected or desorbed by the surface could be determined by recording the mass spectrometer output as a function of time. This method would require a very sensitive mass spectrometer since the number of particles in a pulsed beam would probably be very small.

The concept of using some sort of detector to determine how much adsorbate is being given off by the surface is really a method of sidestepping the problems involved in a more direct approach, at least for the sticking coefficient experiments. The more direct approach would be to measure θ as a function of time for the pulsed beam experiments, or measure θ as a function of beam intensity for continuous beam

experiments. Unfortunately, accurate methods are not currently available for making this measurement at low θ values.

The use of infra-red absorption spectroscopy[50] might provide a way of doing this. For example, a given adsorbate-adsorbent combination will absorb electromagnetic radiation of a given frequency. The quantity absorbed is proportional to the number of chemisorption bonds per unit surface area (or to θ). Thus, if the technique is sensitive enough, it could be used to give values of θ directly. This is an area that appears to warrant investigation.

Appendix A

COMPOSITION OF THE ADSORBED LAYER

A convenient way of estimating the fraction of H_2 in the adsorbed layer is by means of residence times. The residence time is the length of time that an average particle spends on the surface before being desorbed. For a steady state situation,

number of H_2 molecules existing on the surface = $n\gamma\tau_{H_2}$

where n is the beam intensity (molecules/cm^2/sec), γ is the sticking coefficient for H_2, and τ_{H_2} is the residence time of an H_2 molecule. If, for the moment, the desorption of H_2 at step 3' of the reaction equations is neglected, then each adsorbed molecule will dissociate into two adsorbed atoms. Then,

number of H atoms existing on the surface = $2\ n\gamma\tau_H$

$$\text{Fraction of } H_2 \text{ on the surface} = \frac{n\gamma\tau_{H_2}}{n\gamma\tau H_2 + 2\ n\gamma\tau_H}$$

$$= \frac{1}{1 + 2\frac{\tau_H}{\tau_{H_2}}}$$

Methods for calculating the residence times of adsorbed species on surfaces are given in Chapter 3 of de Boer[30]. The residence time equation can be derived by considering the probability that an adsorbed particle has sufficient energy to break the adsorption bond. Energy to break this bond is transmitted to the adatom through the vibrations

of the adsorbent surface atoms. Thus, an adatom has a finite probability of acquiring the desorption energy during each oscillation of the adsorbate surface atom (or atoms) to which it is bonded. de Boer[30] suggests the approximate residence time equation:

$$\tau = \tau_o \exp (\Delta H/RT) .$$

where τ is the residence time, τ_o is the time required for one oscillation of an adsorbent surface atom, and ΔH is the heat of adsorption. As discussed in Section 2.6.B, the free energy of adsorption should be used instead of the heat of adsorption. Thus,

$$\tau = \tau_o \exp (\Delta F/RT)$$

In order to solve for the fraction of H_2 on the surface, the quantity τ_H/τ_{H_2} is required.

$$\frac{\tau_H}{\tau_{H_2}} = \frac{\exp (\Delta F_1/RT)}{\exp (\Delta F_2/RT)} = \exp\left[\frac{1}{RT} (\Delta F_1 - \Delta F_2)\right]$$

The quantity to be calculated is

$$\Delta F_1 - \Delta F_2 = \Delta H_1 - \Delta H_2 - T(\Delta S_1 - \Delta S_2) - S(\Delta T_1 - \Delta T_2) \qquad (1)$$

The physical meaning of the symbols used in the above equation and in the remainder of this section are given below.

ΔF_1 = molar free energy change when gaseous H_2 at temperature T is chemisorbed atomically at temperature T'

ΔF_2 = molar free energy change when gaseous H_2 at temperature T is chemisorbed molecularly at temperature T'

ΔH_1 = molar heat of adsorption when gaseous H_2 at temperature T is chemisorbed atomically at temperature T'

ΔH_2 = molar heat of adsorption when gaseous H_2 at temperature T is chemisorbed molecularly at temperature T'

ΔS_1 = molar entropy change when gaseous H_2 at temperature T is chemisorbed atomically at temperature T'

ΔS_2 = molar entropy change when gaseous H_2 at temperature T is chemisorbed molecularly at temperature T'

S_{1a} = entropy of a mole of chemisorbed atoms at temperature T'

S_{2a} = entropy of a mole of chemisorbed molecules at temperature T'

S_g = entropy of a mole of gaseous H_2 at temperature T' and pressure P

$\Delta T_1 = T' - T = \Delta T_2$

The quantities $\Delta H_1'$, $\Delta H_2'$, $\Delta S_1'$, $\Delta S_2'$ are the same as the quantities ΔH_1, ... ΔS_2, except that the changes denoted by the primed quantities occur at constant temperature (T').

Returning to Eq. 1, since $\Delta T_1 = \Delta T_2$, the last term drops out. All of the quantities involved are thermodynamic properties. Therefore, we can require that the chemisorption process follow any path which we choose. The following path will be used. The H_2 is initially at room temperature and a predetermined pressure. It is heated at constant volume to the chemisorption temperature, and then chemisorbs isothermally.

The constant volume heating process is the same regardless of whether the gas adsorbs as molecules or atoms. Therefore, the entropy and enthalpy changes are the same in both cases (molecular or atomic chemisorption) for the heating process. Equation 1 thus becomes

$$\Delta F_1 - \Delta F_2 = \Delta H_1' - \Delta H_2' - T'(\Delta S_1' - \Delta S_2')$$

and the process being considered is an isothermal adsorption at temperature T'. The entropy changes for this process are shown schematically in Fig. 27.

The quantities $\Delta H_1'$ and $\Delta H_2'$ present no problem. Consider $\Delta H_1'$. This is the case of hydrogen chemisorbing on palladium as atoms. The heat of chemisorption of H_2 on Pd is given as about 30 kcal/mole, at low coverage[6]. Since this value represents chemisorption of two moles of atoms, the heat of chemisorption per mole can be taken as half of this.

The heat of adsorption of molecular hydrogen should be of the same order as heats of physical adsorption. Using the heat of vaporization as the heat of adsorption[59], $\Delta H_2' = 0.215$ kcal/mole.

Next consider the quantity $\Delta S_1' - \Delta S_2'$. This can be written as $2S_{1a} - S_g - S_{2a} + S_g$, where the factor of 2 in the $2S_{1a}$ term accounts for the fact that a molecule adsorbs as two atoms. Consequently,

$$\Delta S_1 - \Delta S_2 = 2S_{1a} - S_{2a}$$

The entropy term in Eq. 1 is seen to depend only upon the adsorbed states.

The quantities S_{1a} and S_{2a} can be calculated by considering the degrees of freedom of the adsorbate, and then computing the entropy associated with each degree of freedom. The adsorbed hydrogen will be considered as a two dimensional gas in both cases. This is justified by the discussion in Section 2.1.C.

The adsorbed atomic hydrogen will have three degrees of freedom; two translations since it is considered as a two dimensional gas, and one vibration perpendicular to the surface due to the adsorption

bond. Adsorbed molecular hydrogen will have five degrees of freedom. There will be two translations as in the atomic case, one vibration perpendicular to the surface due to bonding, one internal vibration due to bonding between the two atoms, and one rotation parallel to the surface. The entropy calculations are shown in Appendix B. The result is

$$2S_{1a} - S_{2a} = 3.93 \text{ cal/}^{o}\text{K mole}$$

Substituting values into the residence time ratio,

$$\tau_H/\tau_{H_2} = \exp \frac{1}{RT} \left[(15{,}000-215)-1273(3.93)\right] = 710$$

Therefore, fraction of H_2 on the surface = 1/711 or 0.14%.

The above calculation shows that the entropy term is significant in this case, although it does not dominate the equation.

These calculations were performed using the assumption that no H_2 was desorbed at step 3' of the reaction equation (Section 3.2). Now the effect of this desorption must be considered. In order to do this, consider a hypothetical situation in which 100 hydrogen particles are chemisorbed on a palladium surface. If no desorption occurs at step 3', the above calculations show that there will be 99.86 atoms and 0.14 molecules on the surface. Now assume that 50% of the H_2 desorbs at step 3'. This will reduce the H concentration to half its previous value, with the H_2 concentration remaining the same. For this case, the chemisorbed hydrogen will be 99.72% atomic and 0.28% molecular. Thus,

the desorption at step 3' can be fairly large, but the adsorbed hydrogen will still be almost all atomic.

If an H_2 concentration of 5% is arbitrarily selected as being a level at which data comparisons will be sufficiently accurate, then the desorption at step 3' can amount to about 95%. Experimental results show that H_2 concentrations as high as 5% are doubtful, as discussed below.

The most direct evidence comes from the infra-red absorption work of Pliskin and Eischens[50]. Their results were discussed in Section 2.4.B. No molecular adsorption was found when hydrogen and deuterium were chemisorbed on platinum. Due to the high surface temperature used in the present experiment, we would expect to find even fewer molecules. There is also some less convincing evidence available in the literature. When hydrogen is chemisorbed on most transition metals, the total amount of gas in a monolayer, counted in atoms, is generally comparable to the total number of atom sites available[75].

Appendix B

ENTROPY OF ADSORPTION

The entropy of atomic and molecular hydrogen adsorbed on palladium will be calculated in this appendix. The entropy contributions of the various degrees of freedom will be calculated separately and then added together to give the total entropy. Subscript 2 refers to molecular hydrogen, while subscript 1 refers to the atomic species.

Entropy of Adsorption of Molecular Hydrogen

H_2 translational entropy

An expression for the molar translational entropy of a two dimensional perfect gas has been derived by Kemball[76].

$$S_{2\ trans} = R\ \ln(MTa) + 65.80$$

where R is the gas constant, M is the molecular weight, and a is the area available to each molecule.

To evaluate a, Rideal and Swett[77] used a value of 1.54×10^{15} sites/cm^2 for nickel. A "site" is defined as the surface area required by an adsorbed particle when a monolayer of gas has been adsorbed by the surface. Thus, the number of sites per cm^2 is equal to the number of adsorbed particles per cm^2 at monolayer coverage. The value used by Rideal and Swett can be corrected for palladium by using the ratio of the lattice parameters of Pd (3.88 Å) and nickel (3.52 Å)[23].

$$\text{Pd sites/cm}^2 = (3.88/3.52)(1.54\text{x}10^{15}) = 1.7\text{x}10^{15}\ \text{sites/cm}^2$$

$$\text{Area per particle} = \frac{1}{(1.7 \times 10^{15})\theta} = \frac{0.589\text{x}10^{-15}}{\theta}$$

where θ is the fraction of sites that is occupied. Substituting values,

$$S_{2\ trans} = (1.99)\ \ln \frac{(2)(1273)(.589)(10^{-15})}{\theta} = 11.6 - 4.58 \log \theta$$

In order to get numerical entropy results, the value of θ must be estimated. Due to the high filament temperature and moderate pressures used in the present experiments, it can be assumed that the fraction of adsorption sites occupied will be small. A surface coverage of 0.1 appears to be a reasonable estimate; therefore, this value will be used. Then,

$$S_{2\ trans} = \underline{16.18\ cal/mole\ ^{o}K}$$

$\underline{H_2\ rotational\ entropy}$

The rotational entropy of a diatomic gas can be found from an expression given by Hill[18]. Since a diatomic gas has two degrees of rotational freedom (rotation about the longitudinal axis is neglected) while the adsorbed H_2 has only one degree, the rotational entropy of an adsorbed molecule will be half that of a gaseous molecule, assuming that both are at the same temperature.

$$S_{2\ rot} = \frac{R}{2} \ln \left[\frac{T\ e}{\alpha\theta_r}\right] \qquad \text{Ref. 18}$$

where θ_r is a "characteristic rotation temperature", and is defined by $\theta_r = \frac{h^2}{8\pi^2 Ik}$, where I is the moment of inertia, α is the symmetry number which is 2 for hydrogen molecules, and e is the base of natural logarithms. According to Hill[18], $\theta_r = 85.4^{o}K$ for H_2. Substituting numerical values,

$$S_{2\ rot} = \frac{1.99}{2} \ln \left[\frac{(1273)(2.72)}{(2)(85.4)}\right] = \underline{\underline{2.99\ cal/mole\ ^oK}}$$

$\underline{H_2}$ vibrational entropy

The expression for vibrational entropy is also given by Hill[18].

$$S_{2\ vib} = R \left\{\frac{\theta_v/T}{\exp\ (\theta_v/T) - 1} - \ln \left[1 - \exp\ (-\theta_v/T)\right]\right\}$$

where θ_v is the "characteristic temperature for vibration", and $\theta_v = \frac{h\nu}{k}$, and ν is the vibrational frequency.

H_2 has two modes of vibration, one between the atoms and one between the molecule and the chemisorbing surface. Consider the internal vibration first. For this degree of freedom, Hill[18] gives $\theta_v = 6210^oK$, which corresponds to a frequency of 1.3×10^{14} cycles per second. Substituting values,

$$S_{2\ internal\ vib} = 1.99 \left\{\frac{6210/1273}{\exp\ (6210/1273) - 1} - \ln \left[1 - \exp(-6210/1273)\right]\right\}$$

$$= \underline{\underline{0.233\ cal/mole\ ^oK}}$$

The second vibrational mode is due to bonding with the surface (physical adsorption). Hill[78] states that ν for the case of physical adsorption is in the neighborhood of 10^{12} cycles per second. Using this value,

$$\frac{h\nu}{kT} = \frac{(6.63)(10^{-27})(10^{12})}{(1.38)(10^{-16})(1273)} = 0.0378$$

Substituting into the vibrational entropy equation,

$$S_2 \text{ adsorption vib} = 1.99 \left\{ \frac{.0378}{\exp(.0378) - 1} - \ln \left[1 - \exp(-.0378)\right] \right\}$$

$$= \underline{8.55 \text{ cal/mole } ^\circ K}$$

Total entropy of adsorbed H_2

The total entropy of adsorbed hydrogen is found by summing the entropies due to the various degrees of freedom. Thus,

$$S_{2a} = S_2 \text{ trans} + S_2 \text{ rot} + S_2 \text{ internal vib} + S_2 \text{ adsorption vib}$$

$$= \underline{27.95 \text{ cal/mole } ^\circ K}$$

Entropy of Adsorption of Atomic Hydrogen

H translational entropy

Kemball's expression for the translational entropy of a two dimensional perfect gas will be used again. Substituting,

$$S_1 \text{ trans} = 10.2 - 4.58 \log \theta$$

The S_2 trans calculation was based on $\theta = 0.1$. Since we are now considering atomic adsorption, the equivalent condition is $\theta = 0.2$.

$$S_1 \text{ trans} = \underline{13.41 \text{ cal/mole } ^\circ K}$$

H vibrational entropy

The calculation of this quantity will require assumptions. This vibration is due to the chemisorption bond between hydrogen atoms and the palladium surface. The strength of the bond lies between the bond strengths of the two molecular vibrations discussed on the previous pages. It would therefore be reasonable to expect that the vibrational frequency of the atomic chemisorption bond should be somewhere between the two

vibrational frequencies calculated for molecular hydrogen. The following method satisfies this.

The infra-red absorption spectrum for atomic hydrogen chemisorbed on platinum has been determined by Pliskin and Eischens[50]. Absorption at a wavelength of 4.86 microns was attributed to the vibration of atomic hydrogen. For lack of better data, it is assumed that this wavelength can be used for the vibrational absorption of the hydrogen-palladium system. The similarities between platinum and palladium for hydrogen chemisorption have been discussed in Section 2.4.B.

It is also assumed that the vibrational motion of the hydrogen atom is the same as that of a harmonic oscillator. For this situation, the frequency of the absorbed photons is the same as the classical frequency of the oscillator[65]. Thus,

$$\nu = \frac{c}{\lambda}$$

where ν is the frequency of the absorbed photons, c is the speed of light, and λ is the wavelength of the absorbed energy.

$$\nu = \frac{2.998 \times 10^{8}}{4.86 \times 10^{-6}} = 6.16 \times 10^{13} \text{ cycles per second, and}$$

$$\frac{h\nu}{kT} = \frac{(6.63)(10^{-27})(6.16)(10^{13})}{(1.38)(10^{-16})(1273)} = 2.32$$

Substituting this value into the vibrational entropy equation,

$$S_{1\ vib} = 1.99 \left\{ \frac{2.32}{\exp(2.32)-1} - \ln \left[1 - \exp(-2.32) \right] \right\} = \underline{2.53 \text{ cal/mole } ^{o}K}$$

Total entropy of adsorbed H

The entropy of adsorbed atomic hydrogen is found by adding the contributions of the various degrees of freedom. Thus,

$$S_{1a} = S_{1\ trans} + S_{1\ vib} = 13.41 + 2.53 = \underline{15.94\ cal/mole\ ^{o}K}$$

Difference Between the Entropies of Adsorption of H and H_2

The quantity required in Appendix A is the difference between the entropies of adsorption of H and H_2. This quantity is

$$2S_{1a} - S_{2a} = 31.88 - 27.95 = \underline{3.93\ cal/mole\ ^{o}K}$$

Appendix C

DISSOCIATION OF HYDROGEN

This calculation was performed to determine the beam source temperature necessary for an atomic hydrogen beam. The degree of dissociation of H_2 will be found as a function of temperature and beam pressure.

For a general chemical reaction in the gas phase,

$$\nu_1 A_1 + \nu_2 A_2 \rightleftharpoons \nu_3 A_3 + \nu_4 A_4$$

The equilibrium constant is defined as

$$K(T) = \frac{X_3^{\nu_3} X_4^{\nu_4}}{X_1^{\nu_1} X_2^{\nu_2}} P^{\nu_3+\nu_4-\nu_1-\nu_2} \qquad \text{(Reference 79)}$$

where X_i is the mole fraction and P is the total pressure.

For the reaction $H_2 \rightleftharpoons 2H$,

$$K(T) = \frac{X_H^2}{X_{H_2}} P \qquad \text{(C-1)}$$

It is now necessary to express the mole fractions in terms of the degree of dissociation (α). Assume that we have n_o moles of H_2 at the start of a reaction. When the reaction has reached equilibrium,

$$X_{H_2} = \frac{n_o(1-\alpha)}{n_o(1-\alpha) + 2n_o\alpha} = \frac{1-\alpha}{1+\alpha} \qquad \text{and} \qquad X_H = \frac{2\alpha}{1+\alpha}$$

Substituting these values into Eq. C-1 and rearranging,

$$\alpha = \sqrt{\frac{K}{K + 4P}}$$

Values of K are given in Ref. 60. Substituting appropriate values of K and P, the curves in Fig. 28 are obtained. These curves show that almost complete dissociation will occur at a temperature of 2400°K, provided the source pressure does not exceed about 10^{-1} torr. This temperature was therefore selected as the operating temperature for the atomic beam.

Appendix D

OPERATING PRESSURES AND ORIFICE DIAMETER OF THE BEAM SOURCE

This appendix is a design calculation to determine the size of the beam orifice and the required beam source pressures. A sketch of the beam source and filament is shown below.

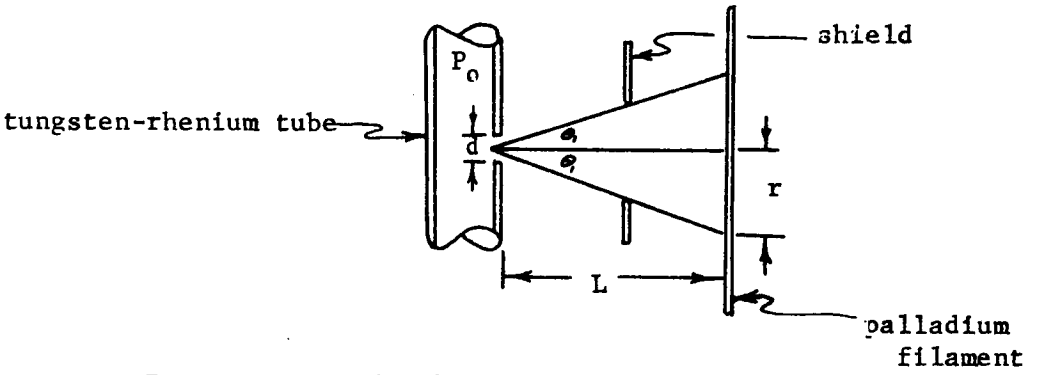

P_o = pressure in the beam source

d = diameter of the beam orifice

L = distance from the orifice to the filament

r = length of filament subtended by angle θ

The results obtained from Ref. 17 show that an ambient hydrogen pressure in the range of 10^{-8} to 10^{-5} torr is necessary to achieve the desired response. The beam must produce this equivalent pressure.

The procedure used in these calculations is as follows:

1. Determine the number of molecules per square centimeter per second which strike the filament in the required pressure range.

2. Equate this quantity to the beam flux density. This will yield an expression relating P_o, d, and the required pressure (P_e).

3. Determine numerical values of P_o and d which will provide the required equivalent pressure. This portion of the calculation is

subject to the condition that free molecular flow exists in the region of the orifice. The condition can be taken as $\lambda \geq 10d$, where λ is the mean free path of a molecule.

4. Select a beam orifice size which can be machined and will give the required flow densities. A small diameter is desirable since it is necessary to maintain low pressure conditions downstream from the orifice.

The following equation given by Ramsey[13] applies to the equilibrium system.

$$N = \frac{n_e \bar{v}_e}{4}$$

where N = no. of particles striking a unit area per unit time

n_e = number density of molecules in a system at pressure P_e and temperature T_e

$\bar{v}_e$ = mean particle speed

Subscript e refers to "equivalent", i.e., these are the equivalent conditions which the beam must produce.

Substituting the perfect gas equation, $P_e = n_e k T_e$,

$$N = \frac{P_e \bar{v}_e}{4kT_e}$$

Ramsey[13] gives the beam flux as

$$dQ = \frac{d\omega}{4\pi} n_o \bar{v}_o \cos\theta \, A_o$$

where dQ = molecular flow rate out of an aperture of area A_o within solid angle $d\omega$, in direction θ

Subscript o refers to conditions in the beam source. Since A_o is the orifice area, it can be replaced by $\pi d^2/4$. Also letting $d\omega = 2\pi \sin\theta \, d\theta$,

and substituting these values

$$Q = \frac{n_o \bar{v}_o A_o}{2} \int_o^{\theta_1} \sin\theta \cos\theta \, d\theta = \frac{n_o \bar{v}_o A_o}{4} \sin^2\theta_1$$

where the integration limit θ_1 is shown on the sketch on the previous page.

Thus, there are Q molecules per second impinging on an area of πr^2. This area is at a distance L from the beam source, as shown in the sketch. The average flux density at the plane of the filament is therefore $Q/\pi r^2$.

From the sketch, $r = L \tan \theta_1$

Equating this flux density to the number N previously used, and making appropriate substitutions,

$$\frac{P_e \bar{v}_e}{4k T_e} = \frac{n_o \bar{v}_o d^2}{16 L^2} \frac{\sin^2 \theta_1}{\tan^2 \theta_1}$$

Next substitute $n_o = \frac{P_o}{kT_o}$ and $\bar{v} = \left(\frac{8kT}{\pi m}\right)^{1/2}$, yielding

$$\frac{P_o}{P_e} = \frac{4L^2 \tan^2 \theta_1}{d^2 \sin^2 \theta_1} \left(\frac{m_o T_o}{m_e T_e}\right)^{1/2}$$

Figure 13 shows that L = 1.27 cm. The value of θ_1 can also be found from this figure. The hole through the shield is 0.24 cm in diameter, while the distance from the beam orifice to the shield is 0.49 cm. Therefore,

$$\theta_1 = \text{arc tan } 1/4 = 14^o$$

Substituting numerical values of L and θ_1

$$\frac{P_o}{P_e} = \frac{6.9}{d^2} \left(\frac{m_o\ T_o}{m_e\ T_e}\right)^{1/2}$$

Two cases must be considered; one for which the tungsten-rhenium beam source is not heated (case 1), and one for which it is (case 2).

Case 1: $T_o = T_e = 300^oK$ $\quad m_o = m_e = H_2$ mass

$$\frac{P_o}{P_e} = \frac{6.9}{d^2}$$

Case 2: $T_e = 300^oK \quad T_o = 2400^oK \quad m_o = 1/2m_e = H$ mass

$$\frac{P_o}{P_e} = \frac{13.8}{d^2}$$

Next the condition for free molecule flow will be applied.

$$\lambda \geq 10\ d$$

Dushman and Lafferty[80] give the following expression for the mean free path

$$\lambda = \frac{k\ T_o}{\sqrt{2}\ \pi\ P_o\ \delta^2}$$

where δ is the molecular diameter. This diameter can be taken as 2.5×10^{-8} cm for H_2[80]. Substituting this, and recalling that one torr equals 1,333 dynes per cm^2,

$$\lambda = 3.72 \times 10^{-5} \frac{T_o}{P_o} \qquad P_o \text{ expressed in torr}$$

The condition for molecular flow thus becomes

$$10d \leq 3.72 \times 10^{-5} \frac{T_o}{P_o}$$

Figure 29 shows a plot of P_o vs P_e for three different orifice diameters. The limit of molecular flow is also shown.

Selection of an orifice diameter depends upon several factors. First, of course, the required environments must be created. Second, it is desirable to keep the orifice size small since a large orifice will increase the pressure in the portion of the system downstream of the beam source. Third, one must be able to drill the selected hole size. Based upon these considerations, an orifice diameter of .015 cm was selected.

Appendix E

PRESSURE RELATIONSHIPS IN THE BEAM SOURCE

Comparisons between the effects of atomic and molecular hydrogen on palladium must be made at equivalent beam intensities if such comparisons are to be valid. The beam intensity depends upon the pressure at the beam source. Hydrogen pressure is measured at a point upstream of the beam source. Consequently, beam source pressure must be determined as a function of measured pressure.

The system to be analyzed is shown below. Dimensions are in centimeters.

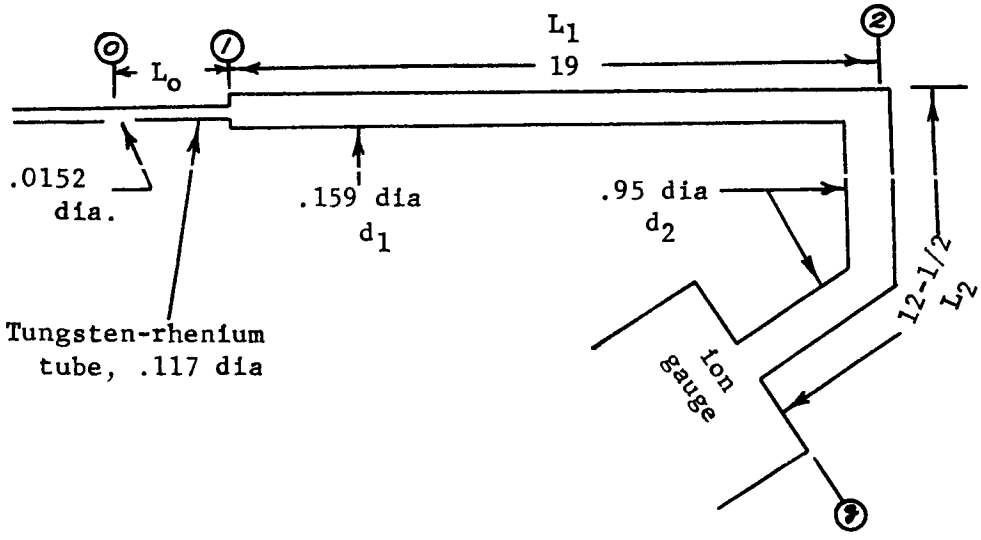

1. Flow Regime

The first problem is to find which flow regime prevails, i.e., Knudsen flow, transition (slip) flow, or Poisueille flow. We will start by determining the maximum value of the beam source (P_o) for which

usable data can be acquired. This is determined by the diameter of the source orifice. We must have molecular effusion, consequently the condition $\lambda \geq 10d$ is imposed, where λ is the mean free path of a gas particle at the source and d is the orifice diameter.

$$\text{From Ref. 80,} \quad \lambda = \frac{1}{\sqrt{2}\ \pi n\ \delta^2} = \frac{kT}{\sqrt{2}\ \pi P_o \delta^2}$$

where δ is the molecular diameter. Dushman and Lafferty[80] give this value as 2.5×10^{-8} cm. for H_2. Substituting appropriate values, and recalling that 1 torr equals 1,333 dynes per cm^2,

$$\lambda = 3.72 \times 10^{-5}\ \frac{T}{P_o} \qquad P_o \text{ expressed in torr}$$

The beam source will operate in two modes, hot and cold. The lower value of λ will correspond to low T. Since this represents the more stringent condition, let T equal 300°K. Then

$$\lambda = \frac{1.116 \times 10^{-2}}{P_o} \qquad P_o \text{ expressed in torr}$$

Substituting the value of 10 d for λ, the usable pressure range is

$$P_o \leq 7.333 \times 10^{-2} \text{ torr or } 73 \text{ microns}$$

The condition for Knudsen flow in a tube is usually taken as $\lambda \geq 20a$, where a is the tube radius. Transition flow then exists until $\lambda \leq 20a$, after which Poiseuille flow prevails.

Transition flow problems are usually solved from empirical data. One such data set is found on Page 107 of Dushman and Lafferty[80] in

which they tabulate values of a/λ and F/F_t, where F is the conductance of a tube for Knudsen flow and F_t is the conductance for transition flow. This data shows that the Knudsen flow range can be extended to $a/\lambda \leq 1$ with about a 5% error. Taking advantage of this, the condition for Knudsen flow in the tubes becomes

$$P \leq 1.116 \times 10^{-2}/a \qquad P \text{ expressed in torr}$$

This equation shows that the limiting value of P is determined by the tubing of largest radius. The sketch on the previous page shows that this is d_2. However, the pressure drop through this tube will be shown to be negligible and will not be included in the overall pressure drop. Using d_1 to determine the pressure limit,

$$P \leq 0.141 \text{ torr or } 141 \text{ microns}$$

It appears that Knudsen flow can be used for the entire range. The only restriction is that P_2 must be less than 141 microns when P_o is equal to 73 microns. It turns out that this condition is met. Therefore Knudsen flow equations will be used for the entire pressure range.

2. Knudsen Flow

The flow in the tungsten-rhenium tube is subject to variations of temperature, pressure, and particle mass when the tube is heated. It is assumed that this is the only region which has temperature and mass gradients. The mass gradient is due to dissociation of molecular hydrogen.

Following the method outlined by Kennard[81] for Knudsen flow in long tubes, we arrive at

$$N = \frac{4}{3}\sqrt{\frac{2\pi}{k}}\, a^3 \frac{d}{dx}\frac{p}{\sqrt{mT}}$$

where N is the flow rate in particles per second, k is Boltzmann's constant, a is the tube radius, p is the pressure, T is the absolute temperature, and m is the mass of a gas particle.

This is equal to the flow through the beam orifice. According to Ramsey[13], the orifice flow is

$N = \frac{1}{4} n_o v_o A_o$ where subscript $_o$ refers to source conditions.

n_o = gas particle density = p_o/kT_o

v_o = mean velocity = $\left(\frac{8kT_o}{m_o}\right)^{1/2}$

A_o = hole area = $\frac{\pi d^2}{4}$

Equating the two values of N, making appropriate substitutions, and rearranging the resultant equation,

$$\frac{d}{dx}\frac{P}{\sqrt{mT}} = \frac{3}{32}\frac{d^2}{a^3}\frac{P_o}{\sqrt{m_o T_o}}$$

By taking the location of the beam source orifice as x = 0, we have the boundary condition that

when x = 0, P, m, T = P_o, m_o, T_o

Integrating,

$$\frac{P}{\sqrt{mT}} = \frac{3\ d^2\ x\ P_o}{32\ a^3\sqrt{m_o T_o}} + A$$

Applying the boundary condition, $A = \frac{P_o}{\sqrt{m_o T_o}}$

Thus,

$$\frac{\frac{P}{\sqrt{mT}}}{\frac{P_o}{\sqrt{m_o T_o}}} = \frac{3\ d^2\ x}{32\ a^3} + 1 \qquad \text{Equation E-1}$$

The system sketch shows that three pressure drops must be found, i.e., P_o to P_1, P_1 to P_2, and P_2 to P_g.

P_o to P_1

First consider the situation with the tube heated. For this case, $T_o = 2400^oK$ and $T_1 = 300^oK$. Appendix C shows that almost all of the hydrogen is atomic at 2400^oK while at 300^oK it is almost all molecular. Therefore, let $2m_o = m_1$. Substituting into Eq. E-1,

$$\frac{2\ P_1}{P_o} = \frac{3\ d^2\ L_o}{32\ a^3} + 1 \text{ where } L_o \text{ is the tube length}$$

Substituting appropriate values from the system sketch,

$$\frac{P_1}{P_o} = 0.568 \qquad \text{hot tube}$$

For the cool tube, $m_o = m_1$ and $T_o = T_1$

Thus,

$$\frac{P_1}{P_o} = 1.136 \qquad \text{cold tube}$$

P_1 to P_g

The two remaining pressure drops occur at constant temperature and mass. The equations will be rewritten in terms of ΔP, the pressure drop between two points. Two cases must be considered. For a cold beam source, the flow through the inlet tubes equals the particle flow through the orifice. For the heated beam source, however, the tube flow is one half the orifice flow because of molecular dissociation.

The flow in the tube, according to Kennard[81], is

$$N = \frac{2\pi\, a^3\, \bar{v}\, \Delta P}{3\, k\, T\, L}$$

For the cold beam source, this is equal to the orifice flow given on page 120. Substituting and rearranging,

$$\Delta P = \frac{3\, d^2}{32\, a^3} \left(\frac{mT}{m_o T_o}\right)^{1/2} P_o L \quad \text{but } m = m_o \text{ and } T = T_o$$

Thus

$$\Delta P = \frac{3\, d^2\, P_o\, L}{32\, a^3} \qquad \text{cold source} \qquad \text{(E-2)}$$

For the hot beam source, $m = 2\, m_o$ and $T = T_o/8$

Thus

$$\Delta P = \frac{3\, d^2\, P_o\, L}{128\, a^3} \qquad \text{hot source} \qquad \text{(E-3)}$$

To find the pressure drop from P_1 to P_2, cold source, substitute into Eq. E-2. The result is

$$P_2 - P_1 = 0.82\, P_o \quad \text{but} \quad P_o = 0.88\, P_1$$

Therefore

$$\frac{P_2}{P_1} = 1.72 \text{ cold source}$$

Following the same procedure with appropriate equations for the hot source case (Equation E-3)

$$\frac{P_2}{P_1} = 1.35 \quad \text{hot source}$$

The above procedure can be carried out once more to find the pressure ratio between P_2 and P_g. These results are

$$\frac{P_g}{P_2} = 1.0013 \quad \text{cold source} \quad \text{and} \quad \frac{P_g}{P_2} = 1.0016$$

The pressure drop from P_2 to P_g may be neglected for the present experiment.

Pressure Ratio

Combining the various pressure ratios,

$$\left(\frac{P_g}{P_o}\right)_{cold} = \frac{P_1}{P_o}\ \frac{P_2}{P_1} = 1.96 \qquad \left(\frac{P_g}{P_o}\right)_{hot} = \frac{P_1}{P_o}\ \frac{P_2}{P_1} = 0.771$$

Appendix F

CURRENT FLOW DUE TO HYDROGEN IONIZED BY THERMIONICALLY EMITTED ELECTRONS

The electrons emitted by the filament will arrive at the collector with an energy in the neighborhood of 190 electron volts per electron. For the purposes of this calculation, it is assumed that any of the thermionic electrons which collide with a hydrogen particle will cause the hydrogen to ionize, and the electron released by the ionization process will travel to the collector. Thus, ionization of hydrogen will cause an increase in the measured thermionic emission current. The effect of this additional current will be calculated in this appendix.

The mean free path of an electron traveling through hydrogen can be found by using the formula given by Dushman and Lafferty[80].

$$\lambda = \frac{kT}{\sqrt{2}\,\pi\,\delta^2}$$

where T is the hydrogen temperature, P is the hydrogen pressure, and δ is the collision diameter for a hydrogen-electron collision.

In order to keep this calculation on the conservative side, the operating conditions which yield a minimum value of λ will be used. This corresponds to low temperature, high pressure, and a high value of the collision diameter. For molecular beam operation, the temperature is $300^{\circ}K$. Hydrogen pressure will be taken as $P_{equivalent}$ (see Section 4.3.B). A pressure of 10^{-5} torr or $1{,}333 \times 10^{-5}$ dynes/cm^2 will be used for the calculation. Dushman and Lafferty[80] state that δ equals

2.2×10^{-8} cm. for an H_2-electron collision. Fite and Brackmann[82] show that δ is larger for H_2 than for H. Therefore, the value of 2.2×10^{-8} will be used.

Substituting values,

$$\lambda = \frac{(1.38)(10^{-16})(300)}{\sqrt{2}\ \pi(1333)(10^{-5})(2.2\times10^{-8})^2} = 1440 \text{ cm.}$$

The actual distance which a thermionic electron travels in the experimental apparatus is 0.315 cm (see Fig. 13). Therefore, the fraction of thermionic electrons which collide with hydrogen while traveling from the filament to the collector can be estimated as the fraction 0.315/1440 or 2.19×10^{-4}. Thus, the current due to ionization will be $(2.19\times10^{-6})\%$ of the thermionic emission current; a negligible quantity.

REFERENCES

1. I. Langmuir, "Chemical Reactions at Low Pressures," J. Amer. Chem. Soc., 37, 1139, (1915)

2. O. Beeck, A. E. Smith, and A. Wheeler, "Catalytic Activity, Crystal Structure, and Adsorptive Properties of Evaporated Metal Films," Proc. of the Roy. Soc., A177, 62, (1940)

3. A. Sherman and H. Eyring, "Quantum Mechanics of Activated Adsorption," J. Amer. Chem. Soc., 54, 2661, (1932)

4. P. W. Reynolds, "Heterogeneous Catalysis II," J. Chem. Soc., 242, (1950)

5. B. M. W. Trapnell, "The Activities of Evaporated Metal Films in Gas Chemisorption," Proc. of the Roy. Soc., A218, 566, (1953)

6. D. O. Hayward and B. M. W. Trapnell, Chemisorption, 2nd Edition, Butterworths Scientific Publications, London, (1964)

7. I. Langmuir, "Monolayers on Solids," J. Chem. Soc., 511, (1940)

8. J. A. Allen, "Evaporated Metal Films," Revs. of Pure and Applied Science (Australia), 4, 133, (1954)

9. H. E. Farnsworth, "Clean Surfaces," The Surface Chemistry of Metals and Semiconductors, Edited by H. Gatos, John Wiley and Sons, Inc., New York, 21, (1960)

10. G. A. Rozgonyi, "Investigations into the Mechanics of the Surface Reactions of Copper," Ph.D. dissertation, Dept. of Aerospace and Mechanical Engineering, University of Arizona, Tucson, Arizona, 8, (1963)

11. J. Halpern, "The Catalytic Activation of Hydrogen in Homogeneous, Heterogeneous, and Biological Systems," Advances in Catalysis, 11, 301, (1959)

12. T. W. Hickmott, "Interaction of Hydrogen with Tungsten," J. Chem. Phys., 32, 810, (1960)

13. N. Ramsey, Molecular Beams, Oxford Univ. Press, (1956)

14. O. Beeck, "Heterogeneous Catalysis," Disc. of the Faraday Soc., 8, 118, (1950)

15. D. Hayward, P. Herley, and F. Tompkins, "The Interaction of Hydrogen Atoms and Molecules with Nickel Films," Surface Science, 2, 156, (1964)

16. D. S. Collins and S. A. Hoenig, "Chemisorption Detector for Oxygen," Rev. Sci. Inst., 35, 15, (1964)

17. M. M. Eisenstadt and S. A. Hoenig, "Chemisorption Detector for Hydrogen," Rev. Sci. Inst., 36, 66, (1965)

18. T. L. Hill, Introduction to Statistical Thermodynamics, Addison-Wesley Publishing Co., Inc., Reading, Mass., (1960)

19. D. M. Young and A. D. Crowell, Physical Adsorption of Gases, Butterworths Scientific Publications, London, (1962)

20. H. P. Leftin and M. C. Hobson, Jr., "Application of Spectrophotometry to the Study of Catalytic Systems," Advances in Catalysis, 14, 115, (1963)

21. M. M. Eisenstadt, "Chemisorption of O_2 on Tungsten in the Presence of CO_2," Bull. of the Amer. Phys. Soc., Series II, Vol. 9, No. 2, 151, (1964)

22. I. Langmuir, "Surface Chemistry," Chem. Revs., 13, 147, (1933)

23. C. Kittel, Introduction to Solid State Physics, 2nd Edition, John Wiley and Sons, Inc., New York, (1956)

24. R. V. Culver and F. C. Tompkins, "Surface Potentials and the Adsorption Process on Metals," Advances in Catalysis, 11, 68, (1959)

25. A. J. Dekker, Solid State Physics, Prentice-Hall Publishing Co., Inc., Englewood Cliffs, New Jersey, (1961)

26. J. C. P. Mignolet, "Nonstoichiometric Chemisorption of Hydrogen on Tungsten and Nickel," J. Chem. Phys., 20, 341, (1952)

27. W. J. M. Rootsaert, L. L. van Reijen, and W. M. Sachtler, "Field Emission Study of Composite Adsorption Layers on Tungsten and Platinum," J. of Catalysis, 1, 416, (1962)

28. R. Gomer, R. Wortman, and R. Lundy, "Mobility and Adsorption of Hydrogen on Tungsten," J. Chem. Phys., 26, 1147, (1957)

29. R. Wortman, R. Gomer, and R. Lundy, "Adsorption and Diffusion of Hydrogen on Nickel," J. Chem. Phys., 27, 1099, (1957)

30. J. H. de Boer, The Dynamical Character of Adsorption, Clarendon Press, Oxford, (1953)

31. C. Herring and M. H. Nichols, "Thermionic Emission," Revs. Mod. Phys., 21, 185, (1949)

32. E. Wigner and J. Bardeen, "Theory of the Work Function of Monovalent Metals," Phys. Rev., 48, 84, (1935)

33. N. K. Adam, The Physics and Chemistry of Surfaces, Oxford Univ. Press, London, (1941)

34. T. J. Lewis, "The Work Function of Irregular Metal Surfaces," Proc. of the Phys. Soc. (London), B67, 187, (1954)

35. E. W. Muller, "Work Function of Tungsten Single Crystal Planes Measured by the Field Emission Microscope," J. Appl. Phys., 26, 732, (1955)

36. D. A. Dowden, "Heterogeneous Catalysis, Part I," J. Chem. Soc., 242, (1950)

37. L. Pauling, "A Resonating Valence Bond Theory of Metals and Intermetallic Compounds," Proc. of the Roy. Soc., A196, 343, (1949)

38. L. Pauling, The Nature of the Chemical Bond, 3rd Edition, Cornell Univ. Press, New York, (1960)

39. M. H. Dilke, D. D. Eley, and E. B. Maxted, "Catalytic Poisons and Magnetic Susceptibility," Nature, 161, 804, (1948)

40. A. Couper and D. D. Eley, "Parahydrogen Conversion on Gold Alloys," Disc. of the Faraday Soc., 8, 183, (1950)

41. M. McD. Baker and G. I. Jenkens, "Electronic Factors in Heterogeneous Catalysis," Advances in Catalysis, 7, 1, (1955)

42. Handbook of Chemistry and Physics, 41st Edition, Chemical Rubber Publishing Co., Cleveland, Ohio, (1960)

43. W. A. Zisman, "A New Method of Measuring Contact Potential Differences in Metals," Rev. Sci. Inst., 3, 367, (1932)

44. R. Suhrmann, "Beziehungen Zwischen dem Normalen Licktelektrischen Effekt und Elektrischen Oberflacheneigenschaften Verschuidiner Metalle," Physik Z., 939, (1929)

45. W. M. H. Sachtler, "Work Function and Electrical Conductivity of Hydrogen Covered Nickel Films. The Effect of Contamination," J. Chem. Phys., 25, 751, (1956)

46. R. Culver, J. Pritchard, and F. Tompkins, "The Change of Surface Potential of Metallic Films by Chemisorption," Second Int. Congress on Surface Activity, Vol. II, Academic Press, New York, (1957)

47. J. C. P. Mignolet, "Studies in Contact Potential," Disc. of the Faraday Soc., 8, 105, (1950)

48. J. C. P. Mignolet, "Studies in Contact Potential," Recueil des Travaus Chemiques, 74, 685, (1955)

49. W. Crossland and J. Pritchard, "Negative and Positive Surface Potentials of Hydrogen on Metal Films," Surface Science, 2, 217, (1964)

50. W. A. Pliskin and R. P. Eischens, "Infra-Red Spectra of Hydrogen and Deuterium Chemisorbed on Platinum," Z. Physik. Chem. (Frankfurt), 24, 11, (1960)

51. L. J. Gillespie and L. S. Galstaun, "The Palladium-Hydrogen Equilibrium and New Palladium Hydrides," J. Amer. Chem. Soc., 58, 2565, (1936)

52. D. P. Smith, Hydrogen in Metals, Univ. of Chicago Press, Chicago, (1948)

53. L. H. Reyerson and A. Solbakken, "Effect of Hydrogen Adsorption on the Magnetic Susceptibility of Palladium Dispersed on Silica Gel," Solid Surfaces and the Solid-Gas Interface, No. 33, Amer. Chem. Soc., Washington, D. C., 86, (1961)

54. B. M. W. Trapnell, "Adsorption on Evaporated Tungsten Films," Proc. of the Roy. Soc., A206, 39, (1951)

55. G. E. Moore and F. C. Unterwald, "Adsorption-Desorption of Hydrogen on Tungsten and Molybdenum," J. Chem. Phys., 40, 2626, (1964)

56. R. Suhrmann, G. Wedler, and G. Schumicki, "Influence of Hydrogen on the Electrical Resistance of Evaporated Palladium Films," Structure and Properties of Thin Films, C. Neugebauer, Editor, John Wiley and Sons., Inc., New York, 268, (1959)

57. S. Glasstone, K. J. Laidler, and H. Eyring, The Theory of Rate Processes, McGraw-Hill Book Co., Inc., New York, (1941)

58. S. W. Benson, The Foundations of Chemical Kinetics, McGraw-Hill Book Co., Inc., New York, (1960)

59. American Institute of Physics Handbook, 2nd Edition, McGraw-Hill Book Co., Inc., New York, (1963)

60. V. Huff, S. Gordon, and V. Morrell, "General Method and Thermodynamic Tables for Computation of Equilibrium Composition and Temperature of Chemical Reactions," NACA Report No. 1037, (1951)

61. G. Lockwood, H. Helbig, and E. Everhart, "Measurement of Thermal Dissociation of Hydrogen Using Fast Protons," J. Chem. Phys., 41, 3820, (1964)

62. B. M. Rosenbaum and L. Levitt, "Thermodynamic Properties of Hydrogen from Room Temperature to 100,000°K," NASA TN D-1107, (1962)

63. R. T. Birge, "The Calculation of Errors by the Method of Least Squares," Phys. Rev., 40, 207, (1932)

64. S. J. Kline and F. A. McClintock, "Describing Uncertainties in Single Sample Experiments," Mech. Eng., 75, 3, (1953)

65. R. T. Weidner and R. L. Sells, Elementary Modern Physics, Allyn and Bacon, Inc., Boston, Mass., (1960)

66. G. Ehrlich, "Molecular Dissociation and Reconstitution on Solids," J. Chem. Phys., 31, 1111, (1959)

67. R. W. Zwanzig, "Collision of a Gas Atom with a Cold Surface," J. Chem. Phys., 32, 1173, (1960)

68. F. O. Goodman, "The Dynamics of Simple Cubic Lattices. I. Applications to the Theory of Thermal Accommodation Coefficients," J. Phys. Chem. Solids, 23, 1269, (1962)

69. L. G. Thomas and E. B. Schofield, "Thermal Accommodation Coefficient of Helium on a Bare Tungsten Surface," J. Chem. Phys., 23, 861, (1955)

70. B. McCarroll and G. Ehrlich, "Trapping and Energy Transfer in Atomic Collisions with a Crystal Surface," J. Chem. Phys., 38, 523, (1963)

71. R. D. Present, Kinetic Theory of Gases, McGraw-Hill Book Co., Inc., New York, 181, (1958)

72. P. Kisliuk, "The Sticking Probabilities of Gases Chemisorbed on the Surfaces of Solids-II," J. Phys. Chem. Solids, 5, 78, (1958)

73. J. N. Smith and W. L. Fite, "Reflection and Dissociation of H_2 on Tungsten," J. Chem. Phys., 37, 898, (1962)

74. J. H. McFee and P. M. Marcus, "Molecular Beam Investigation of Energy Exchange between a Gas and Solid Surface," Proceedings of the Atomic and Molecular Beams Conference, Univ. Of Denver, Colo., June, 1960

75. G. Ehrlich, "Adsorption and Surface Structure," Metal Surfaces, Amer. Soc. for Metals, Metals Park, Ohio, 221, (1963)

76. C. Kemball, "The Adsorption of Vapours on Mercury. II. The Entropy and Heat of Vaporization of Non-Polar Substances," Proc. of the Roy. Soc., A187, 73, (1946)

77. E. Rideal and F. Swett, "The Chemisorption of Hydrogen on Nickel," Proc. of the Roy. Soc., A205, 291, (1960)

78. T. L. Hill, "Theory of Physical Adsorption," Advances in Catalysis, 4, 212, (1952)

79. M. W. Zemansky, Heat and Thermodynamics, 4th Edition, McGraw-Hill Book Co., Inc., New York, (1957)

80. S. Dushman and J. M. Lafferty, Scientific Foundations of Vacuum Technique, John Wiley and Sons, Inc., New York, (1962)

81. E. H. Kennard, Kinetic Theory of Gases, McGraw-Hill Book Co., Inc., New York, (1938)

82. W. L. Fite and R. T. Brackmann, "Collisions of Electrons with Hydrogen Atoms," General Atomic Division of General Dynamics Corp., Report No. GA-399, April, 1958

Element	H															
Work Function													Fe	Co	Ni	Cu
Electronegativity	2.1												4.4	4.2	4.9	4.6
													1.8	1.8	1.8	1.9
											W				Pd	Ag
											4.5				5.0	4.3
											1.7				2.2	1.9
															Pt	Au
															5.4	4.4
															2.2	2.4

Table I. Work Function and Electronegativity of Several Elements Shown in Their Periodic Arrangement.

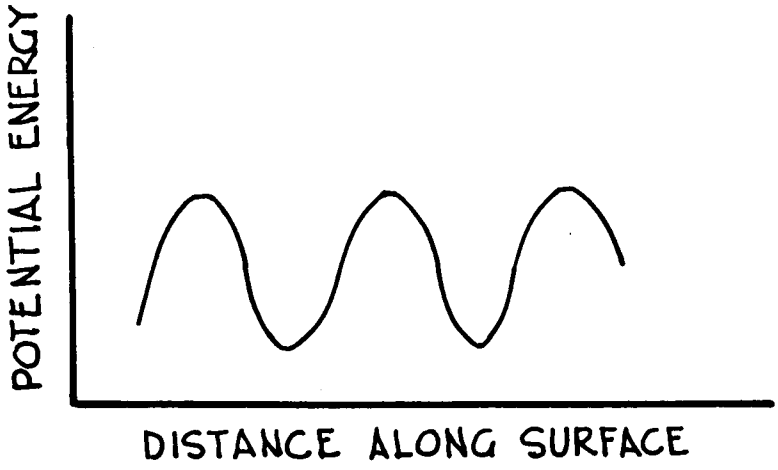

Figure 1. Schematic diagram of the variation in potential energy with surface position (one dimensional).

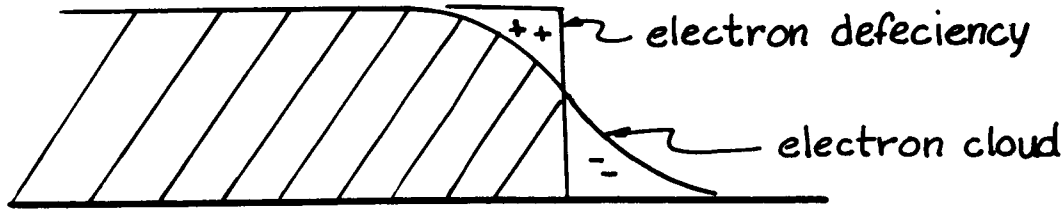

Figure 2. Schematic diagram of the charge distribution at a metal surface.

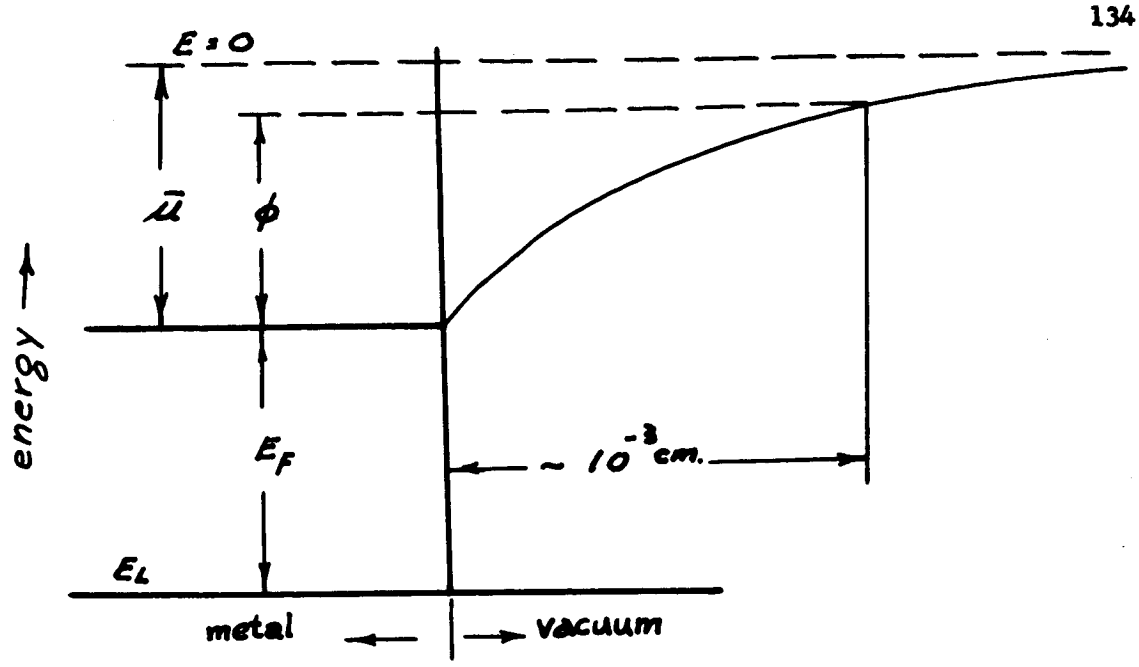

Figure 3. Schematic diagram of the energies involved in thermionic emission.

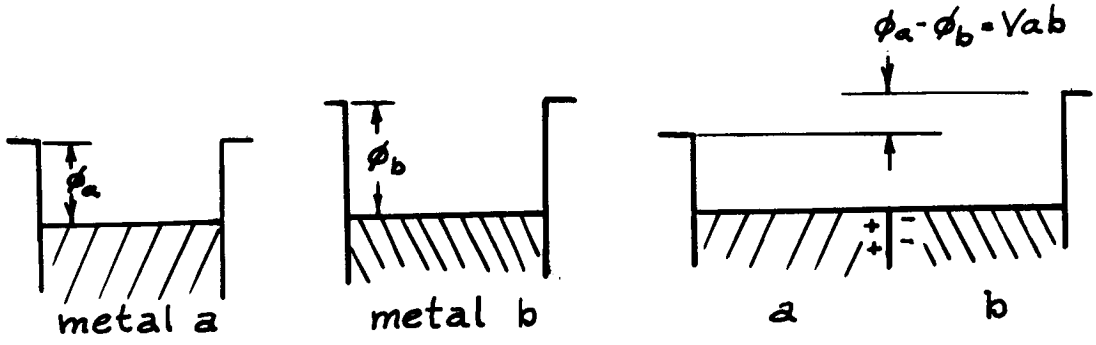

Figure 4. Schematic diagram of the contact potential difference at a metal to metal junction. Metals a and b are dissimilar.

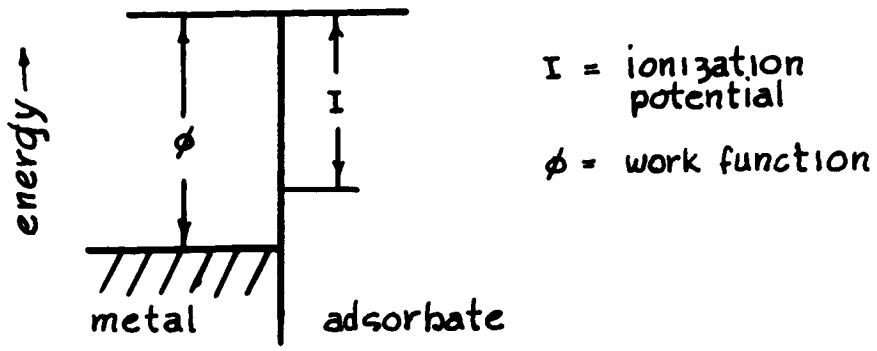

Figure 5. Relationship between ionization potential and work function which leads to a positively charged adsorbed layer.

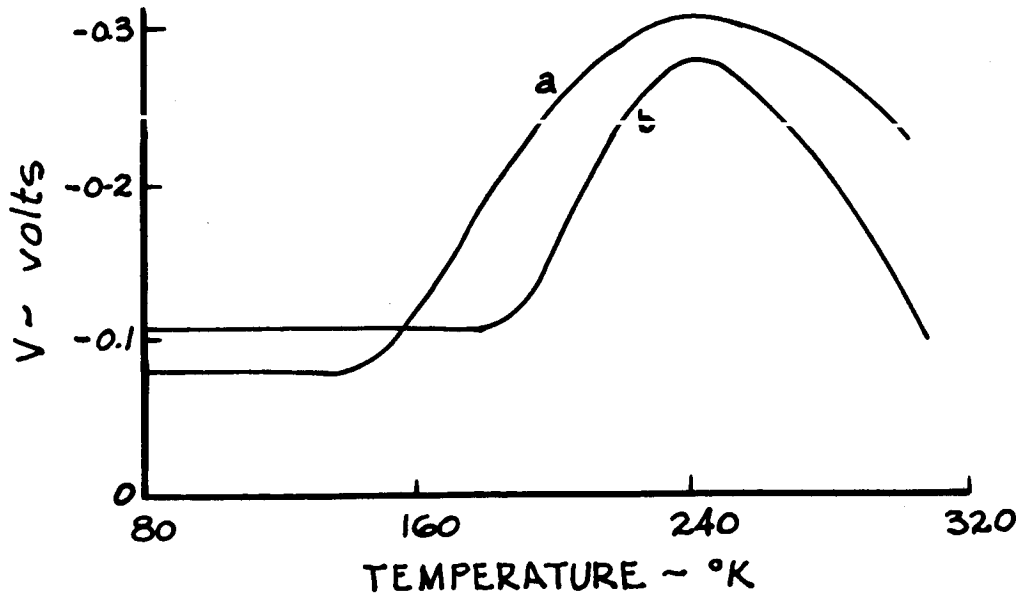

Figure 6. Surface potential of hydrogen on platinum during desorption; curve a, P = 4×10^{-6} torr; curve b, P = 10^{-9} torr. From Rootsaert and van Reijen, Ref. 27.

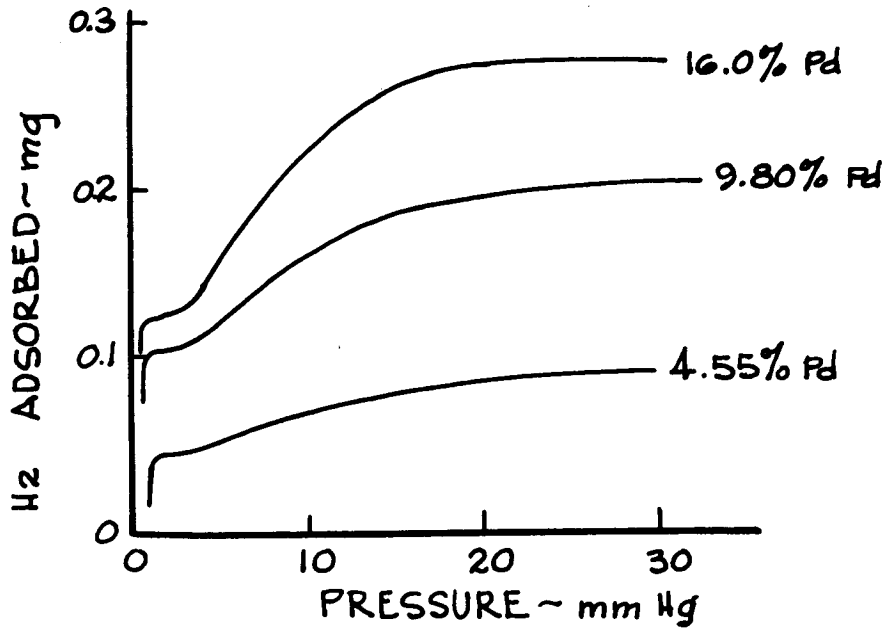

Figure 7. Hydrogen isotherms on dispersed palladium at 0°C. The percentages indicate the percent palladium by weight in the specimen studied. From Reyerson and Solbakken, Ref. 53.

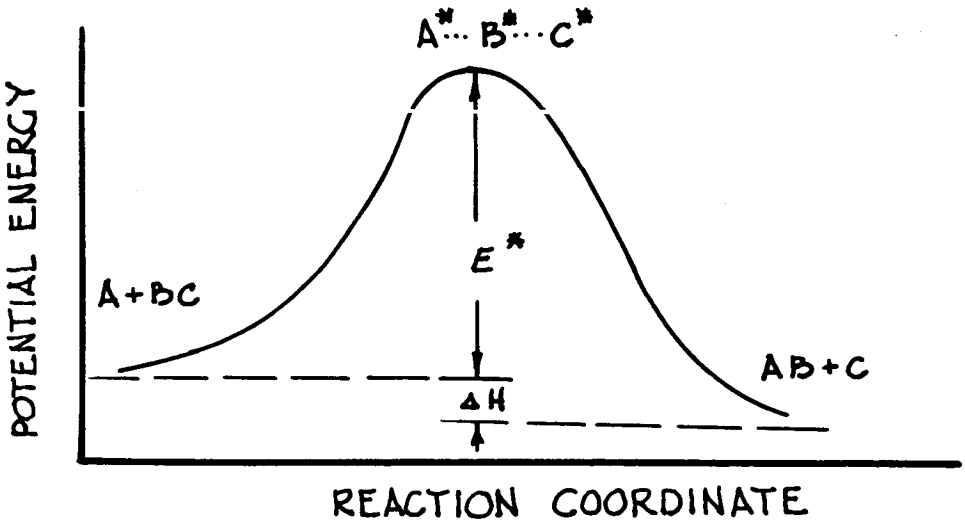

Figure 8. Variation of potential energy accompanying the reaction $A+BC \rightleftharpoons AB+C$. From Glasstone, Laidler, and Eyring, Ref. 57.

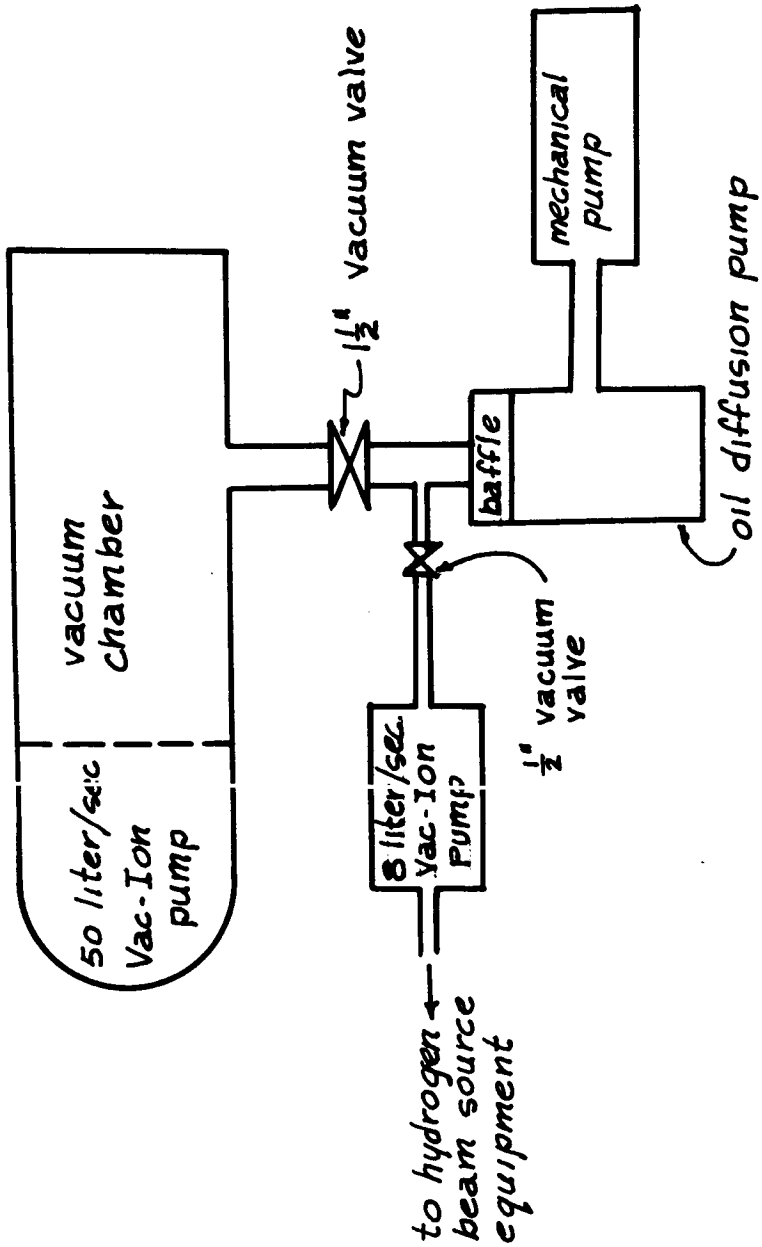

Figure 9. Arrangement of the vacuum pumps and valves.

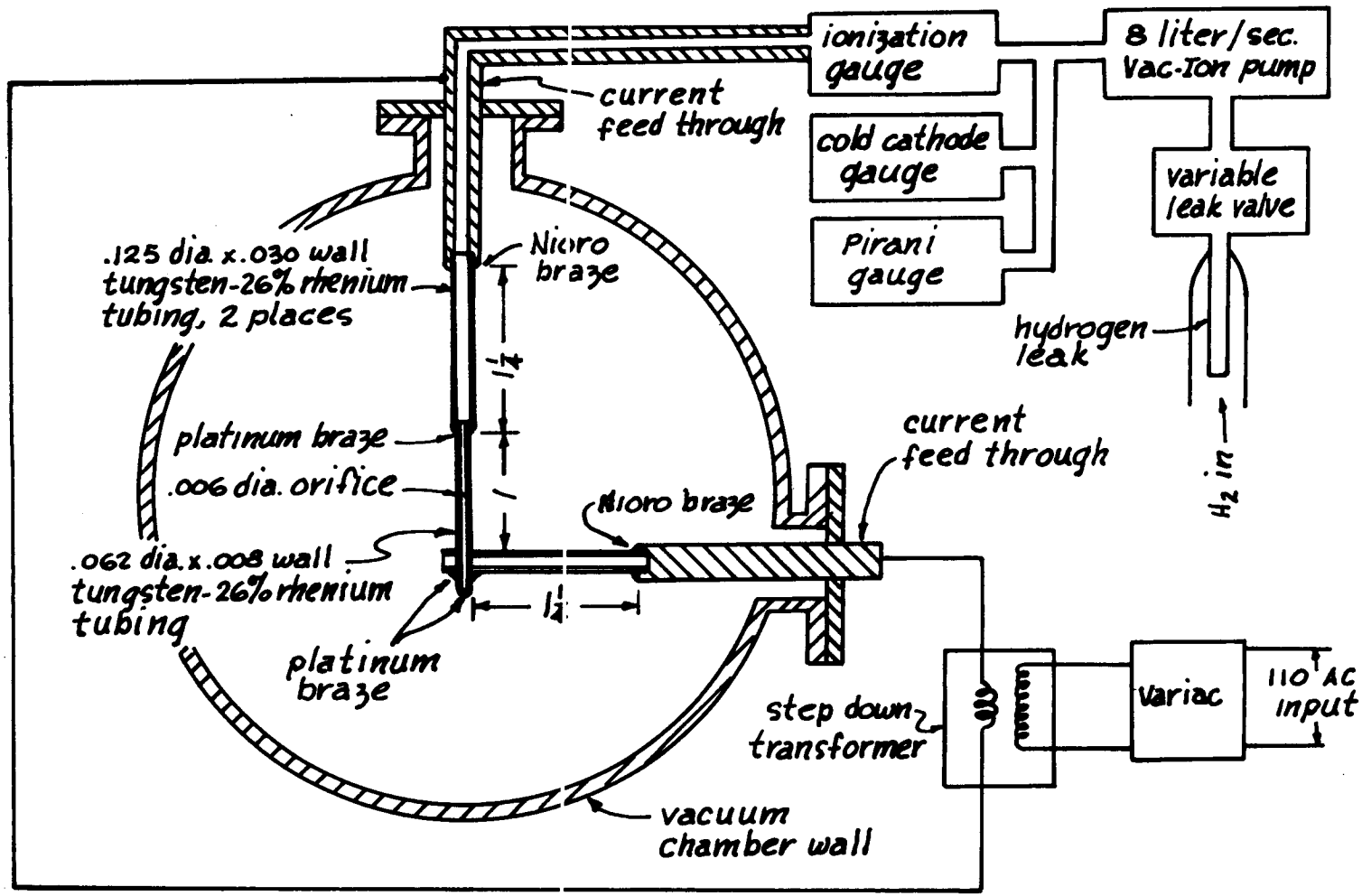

Figure 10. Schematic drawing of the leak system. The electrical arrangement for heating the oven is also shown. Parts shown are commercially available. All dimensions are in inches.

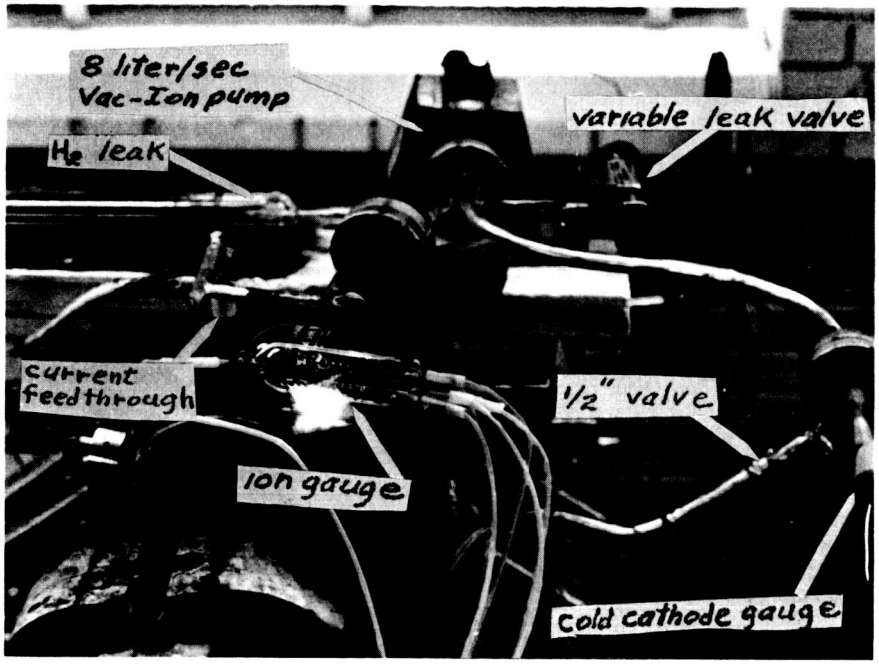

Figure 11. Photograph of the leak system components which are external to the vacuum chamber.

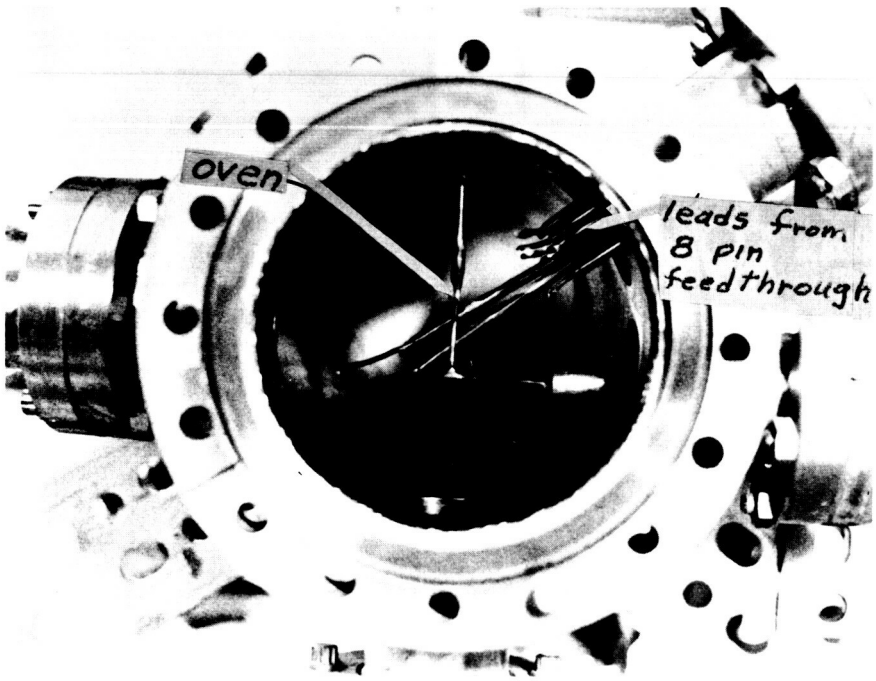

Figure 12. The oven mounted in the vacuum chamber.

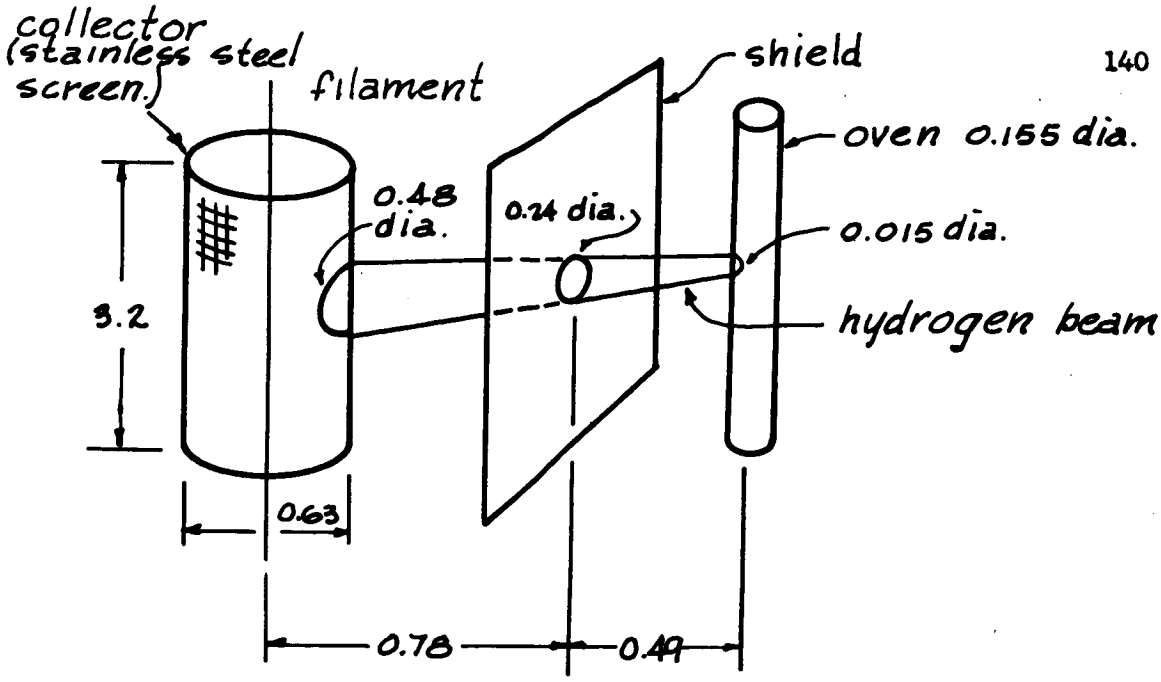

Figure 13. Physical arrangement of the oven, shield, filament, and collector. Dimensions are in centimeters.

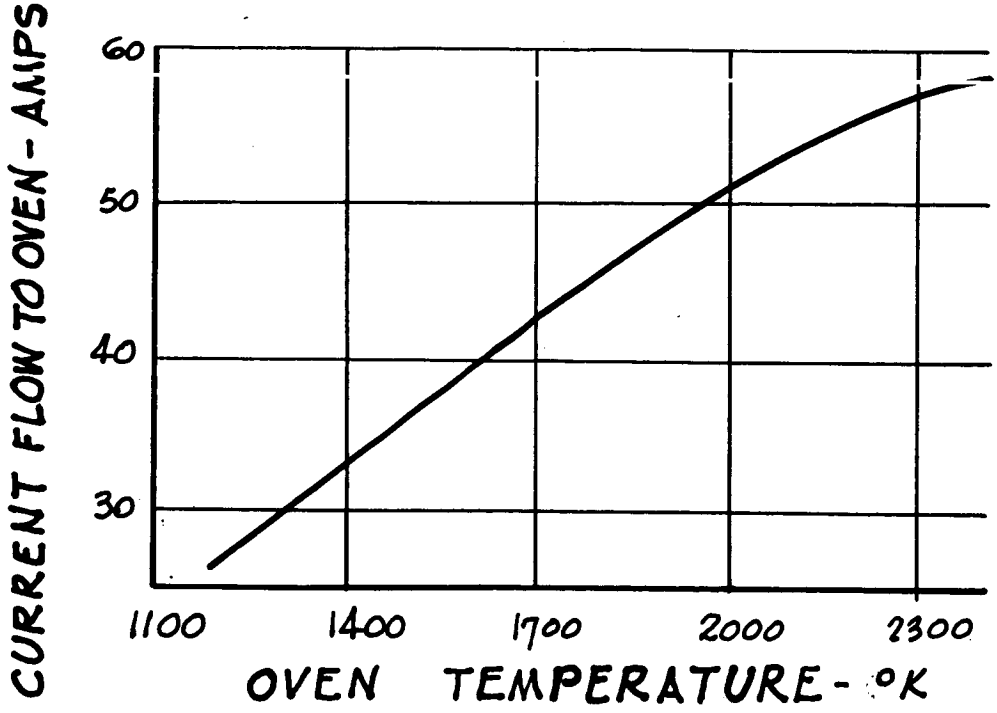

Figure 14. Oven temperature vs. current input.

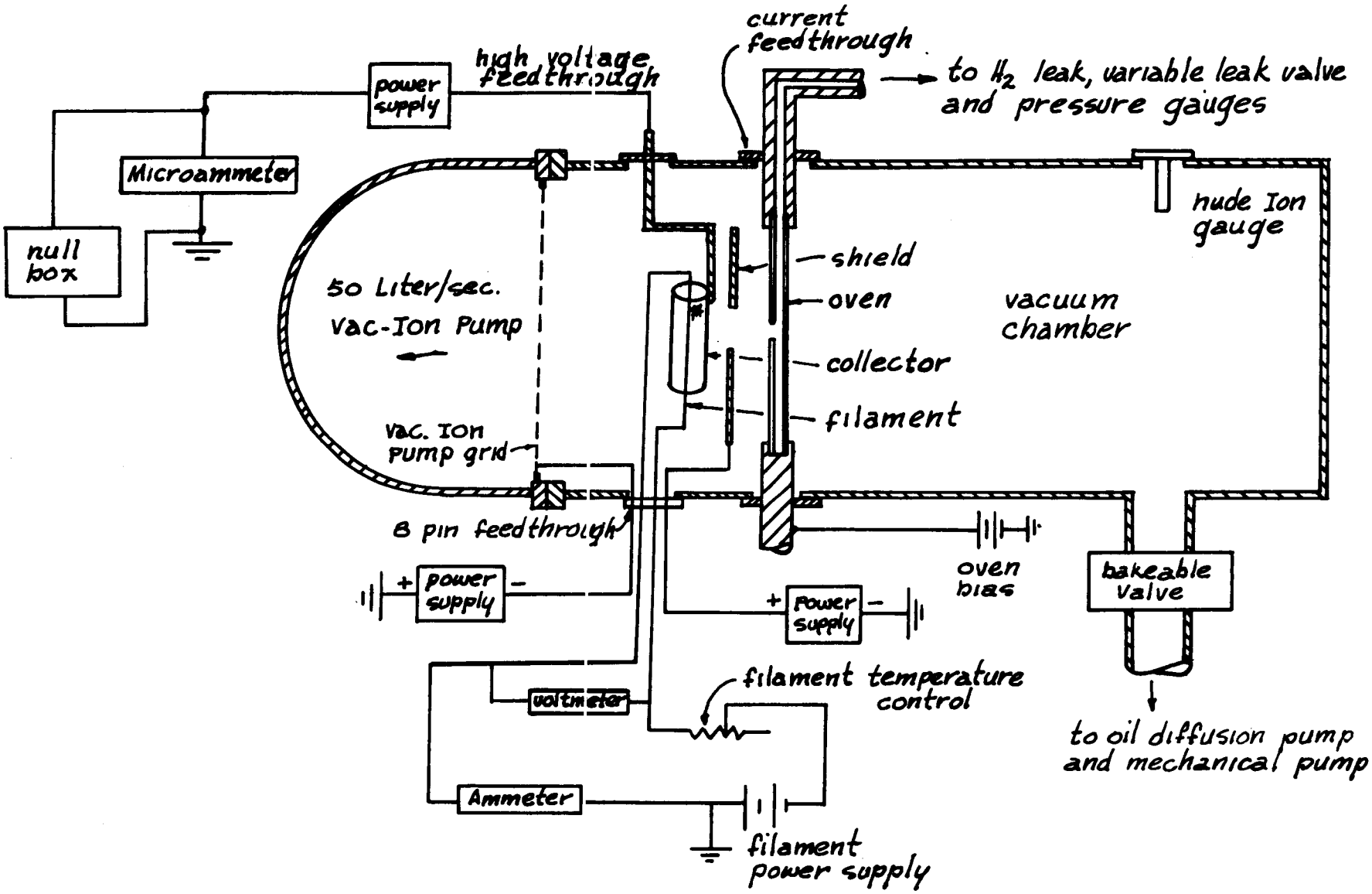

Figure 15. Schematic diagram of the beam system and associated electronic equipment.

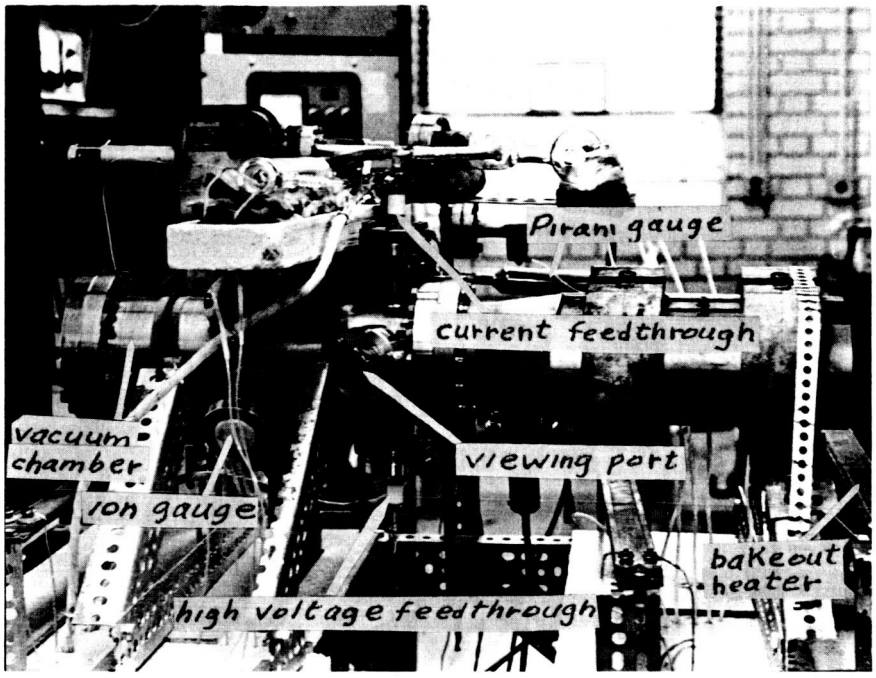

Figure 16. Photograph of the vacuum system, right side.

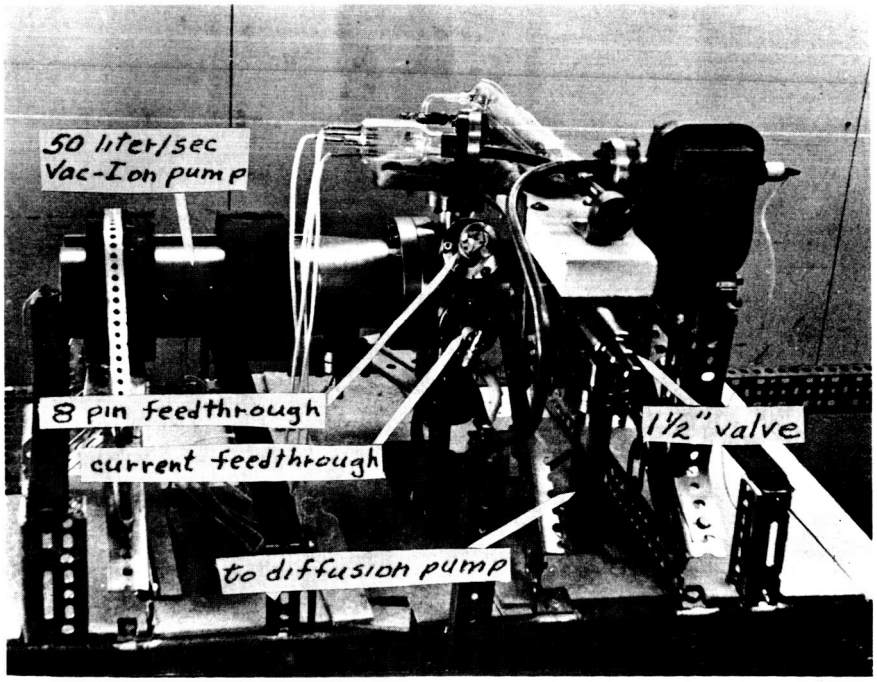

Figure 17. Photograph of the vacuum system, left side.

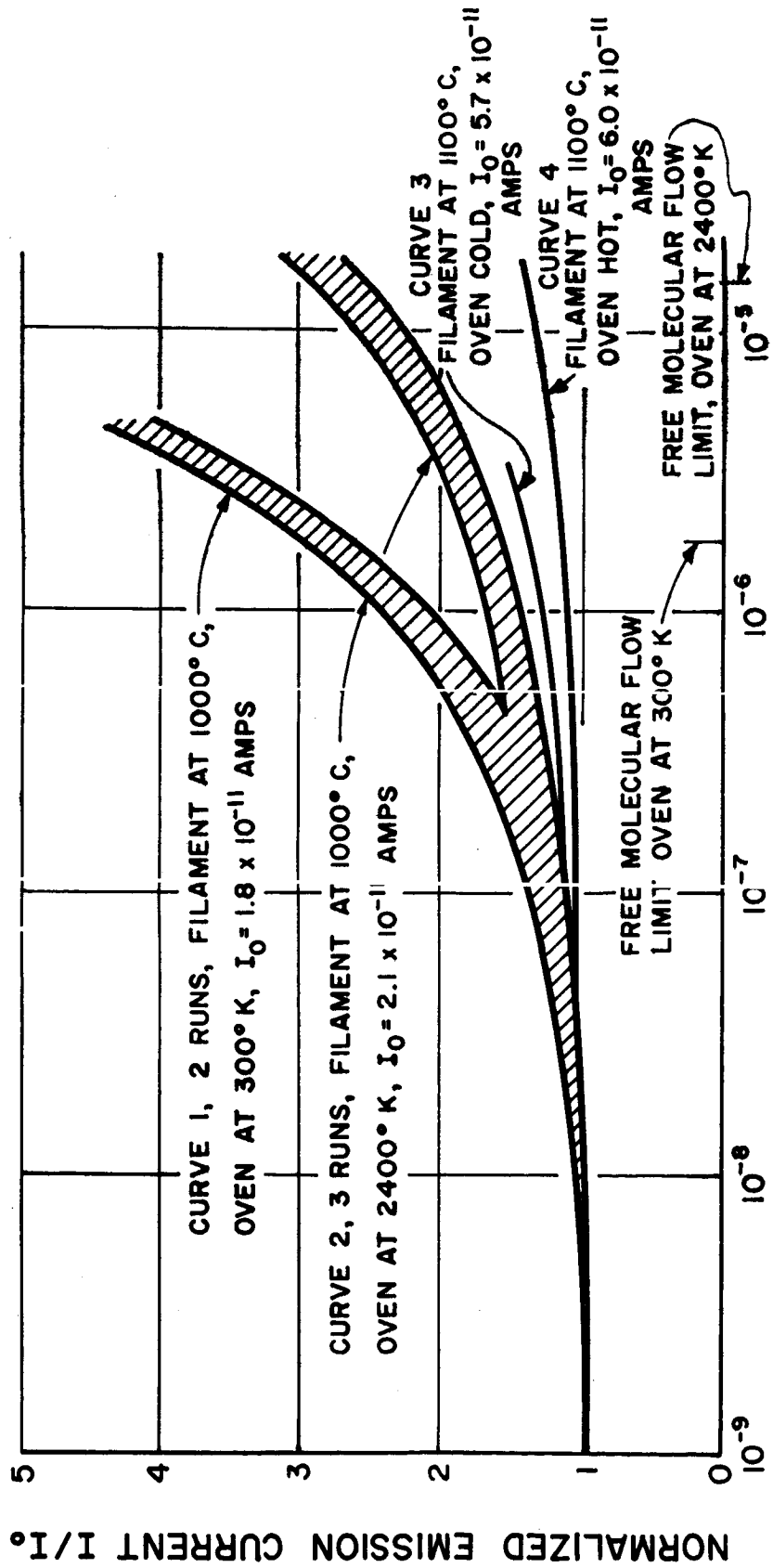

FIGURE 18. NORMALIZED EMISSION CURRENT VS. EQUIVALENT HYDROGEN PRESSURE AT FILAMENT TEMPERATURES OF 1000° C AND 1100° C, AND OVEN TEMPERATURES OF 300° K AND 2400° K (MOLECULAR AND ATOMIC BEAMS) DATA FROM FILAMENT NO. 1.

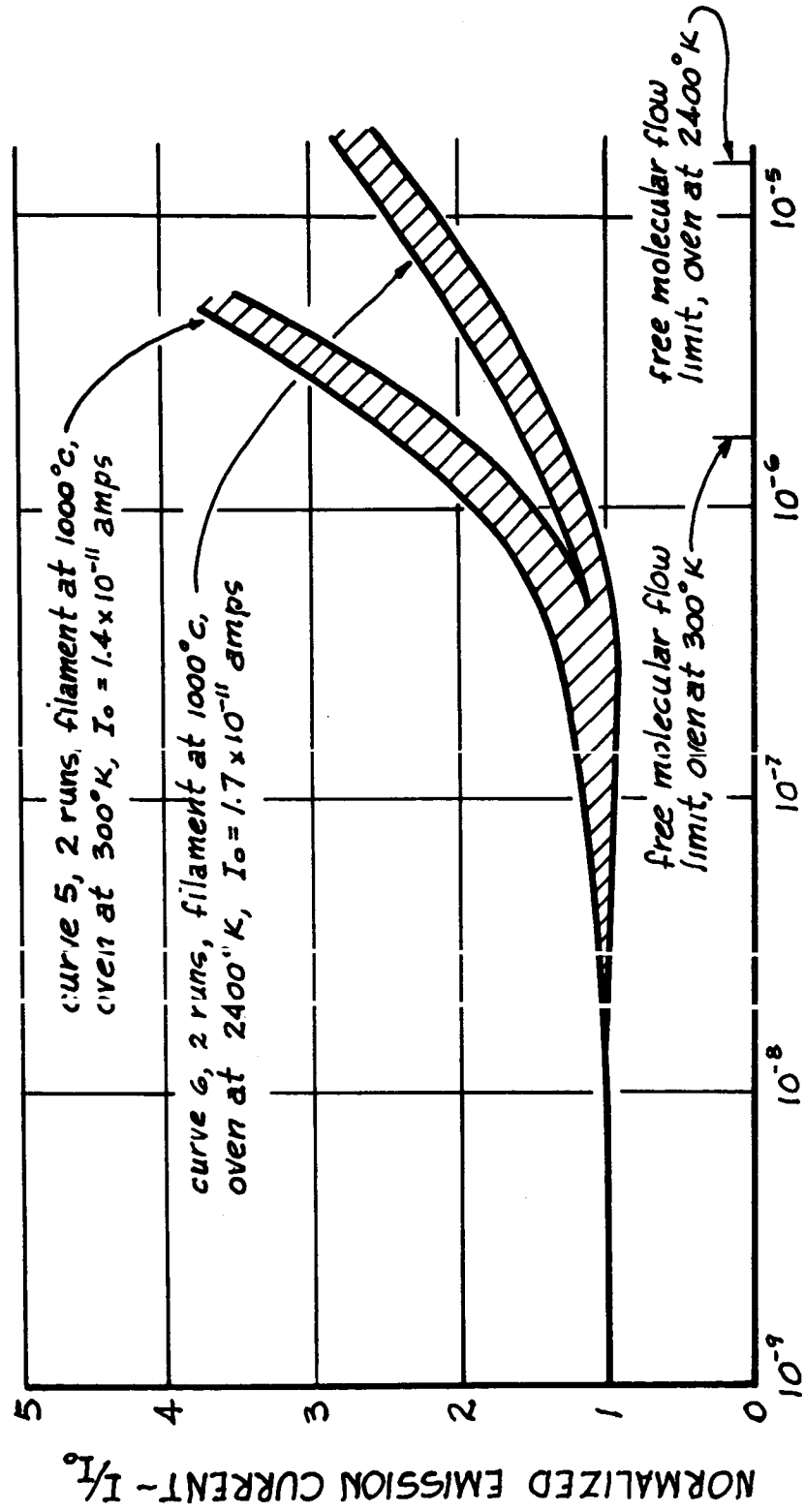

Figure 19. Normalized emission current vs. equivalent hydrogen pressure at a filament temperature of 1000°C and oven temperatures at 300°K and 2400°K. Data from filament No. 2.

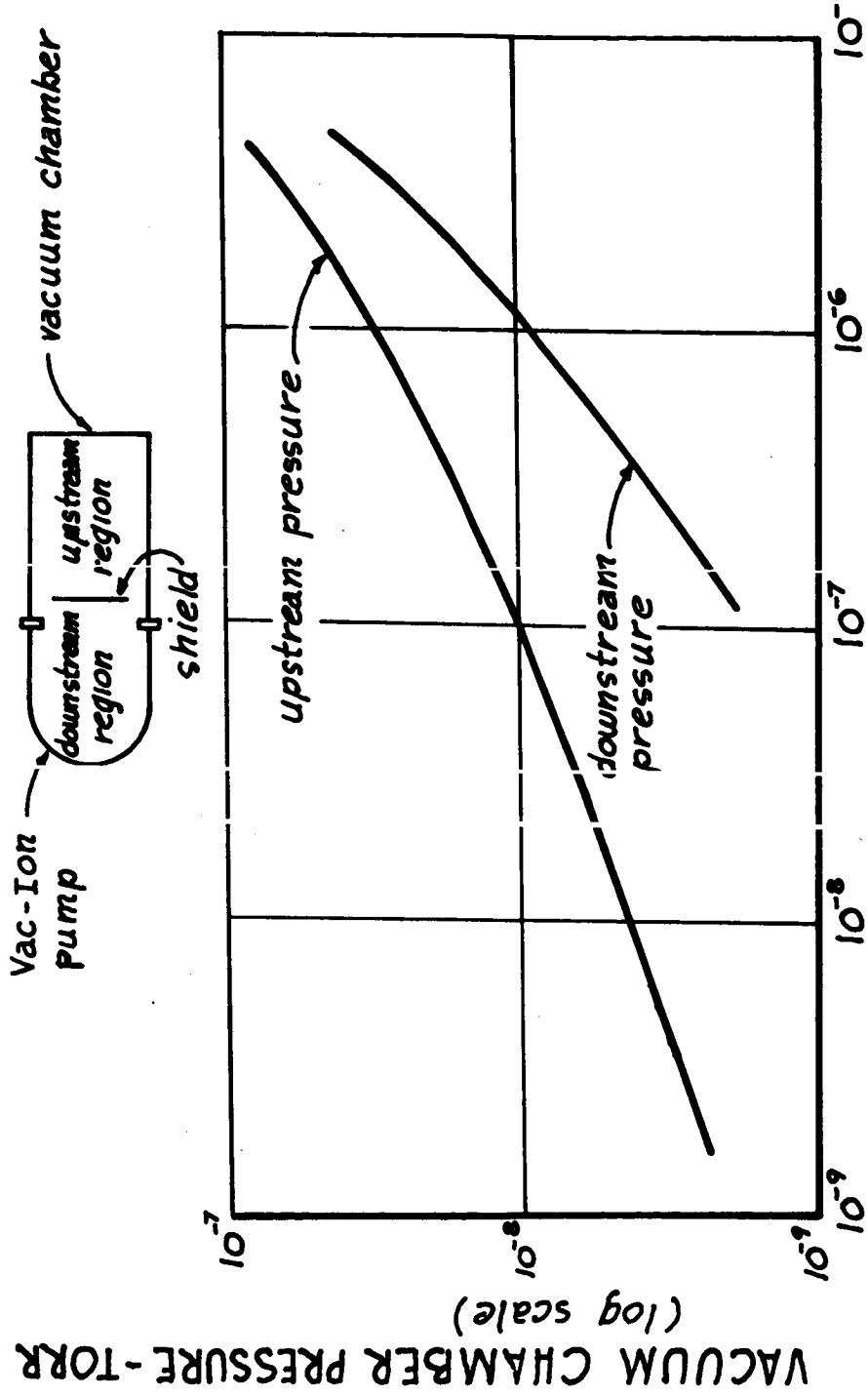

Figure 20. Vacuum chamber pressure vs. equivalent hydrogen pressure with the oven at 300°K. Pressures were measured during beam operation and are given for the upstream and downstream regions of the vacuum chamber.

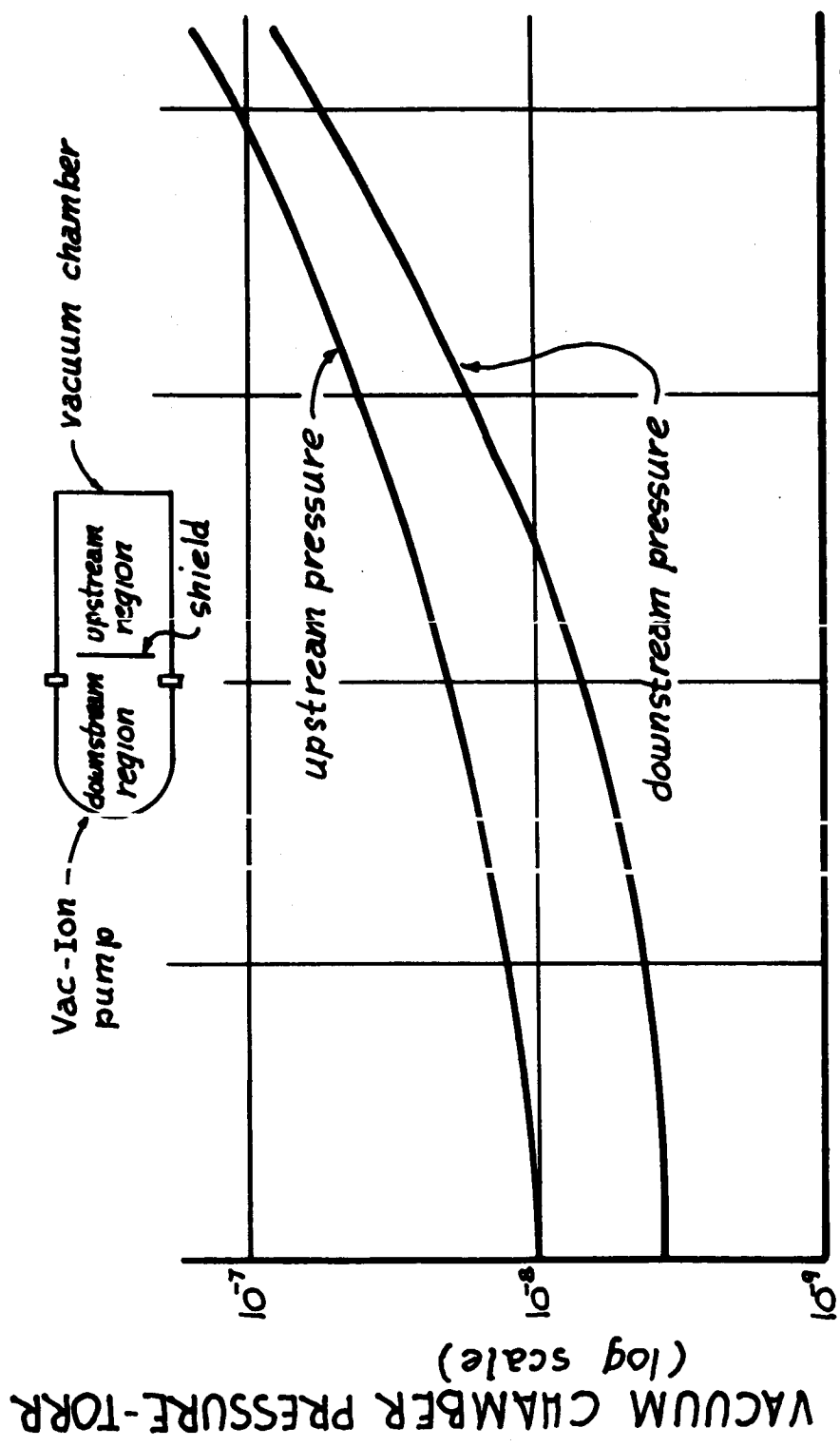

Figure 21. Vacuum chamber pressure vs. equivalent hydrogen pressure with the oven at 2400°K. Pressures were measured during operation and are given for the upstream and downstream regions of the vacuum chamber.

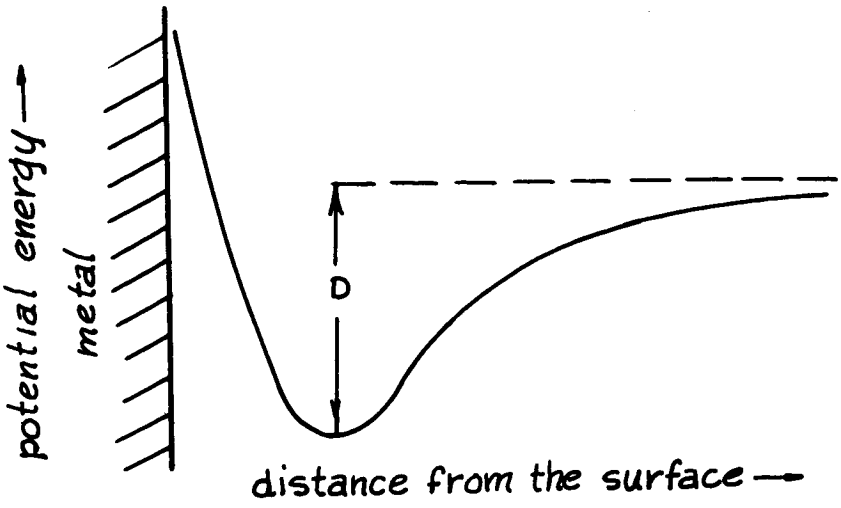

Figure 22. Schematic diagram of an adsorption potential well.

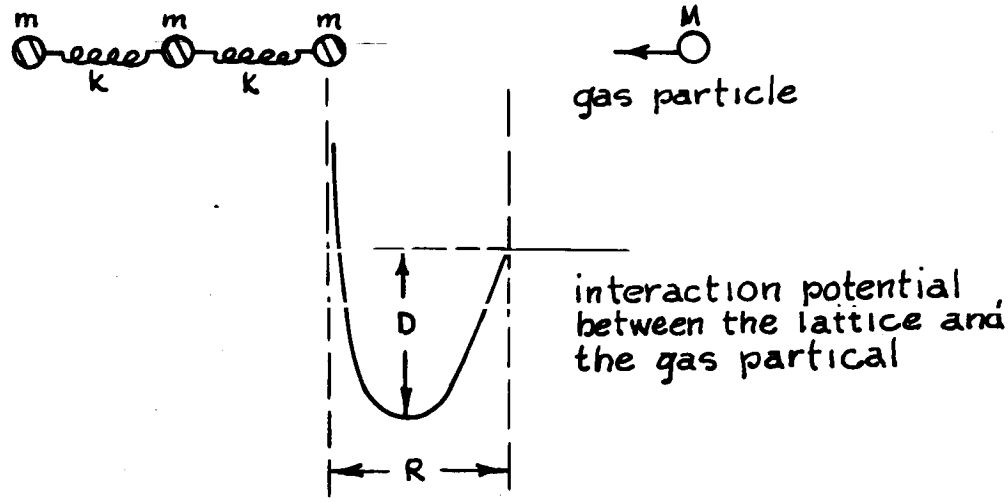

Figure 23. The one dimensional lattice and the gas atom, from Zwanzig, Ref. 67. M and m are the masses of the gas atom and the lattice atoms, while k is the lattice force constant. The interaction potential shown is a truncated harmonic oscillator potential.

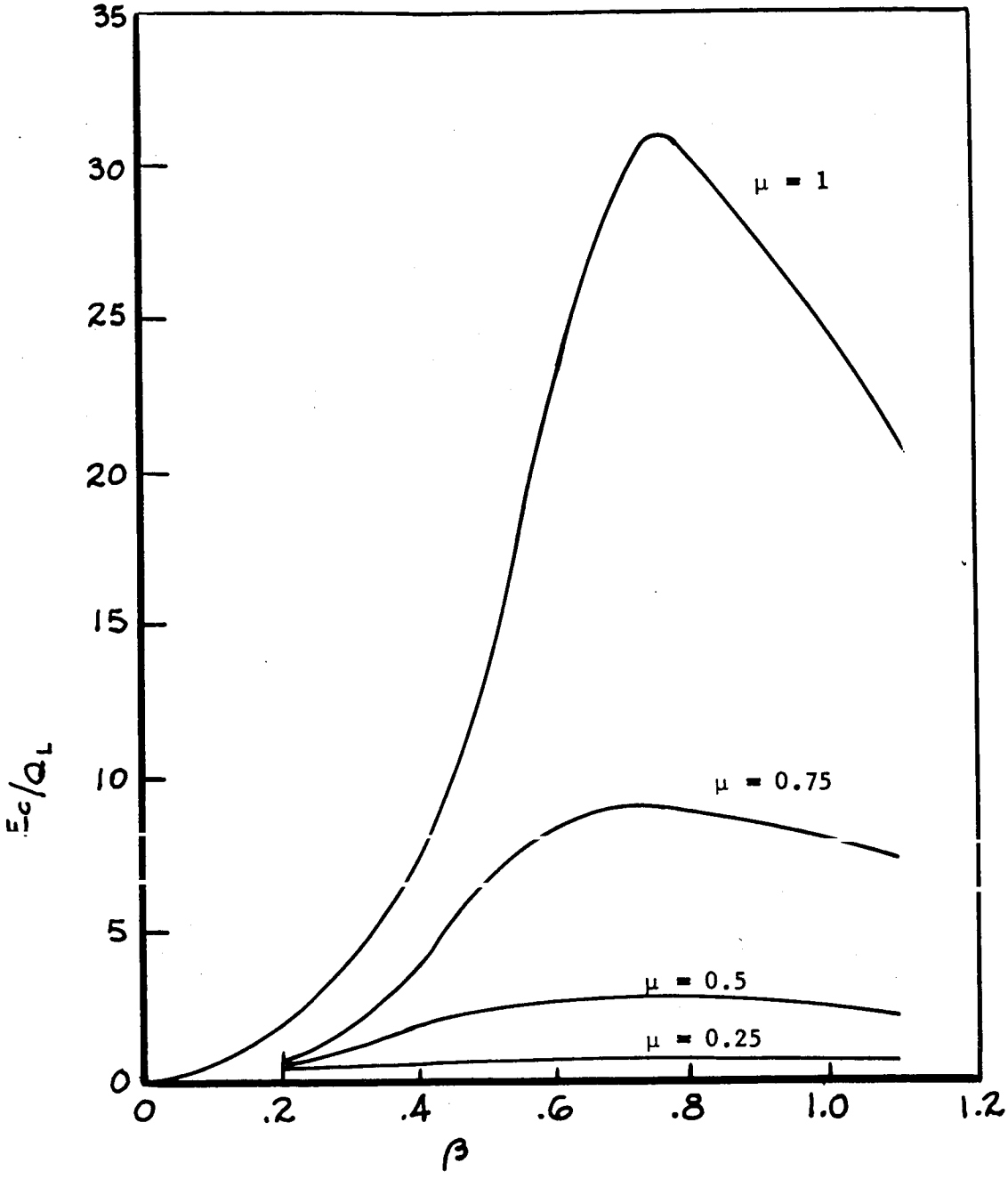

Figure 24. Critical kinetic energy for capture (E_c) as a function of the force constant ratio, $\beta = k/k_o$. Q_L is the binding energy of the homogeneous lattice. From McCarroll and Ehrlich, Ref. 70.

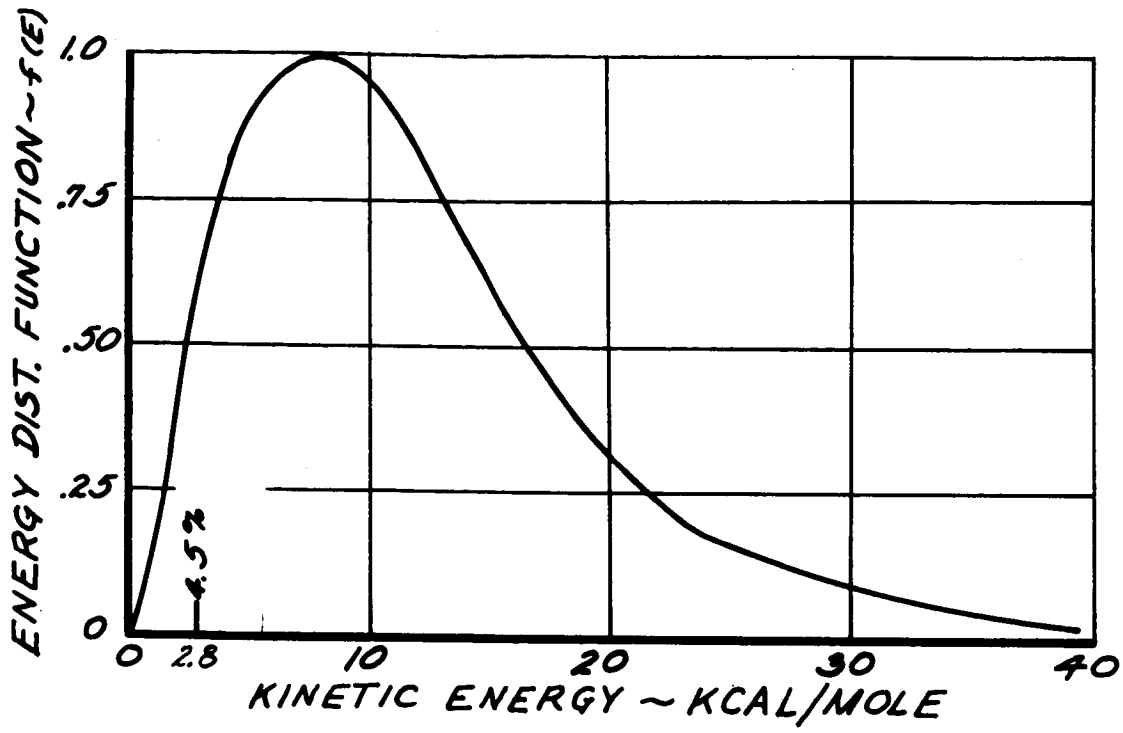

Figure 25. Kinetic energy distribution in the atomic beam (2400°).

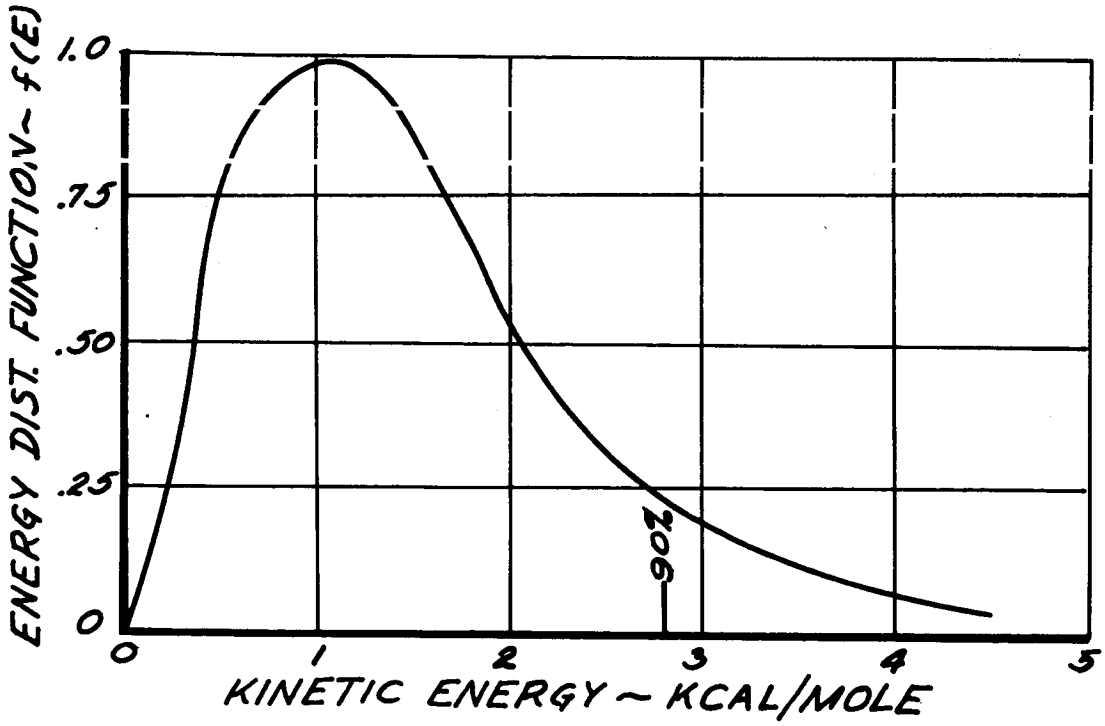

Figure 26. Kinetic energy distribution in the molecular beam (300°K).

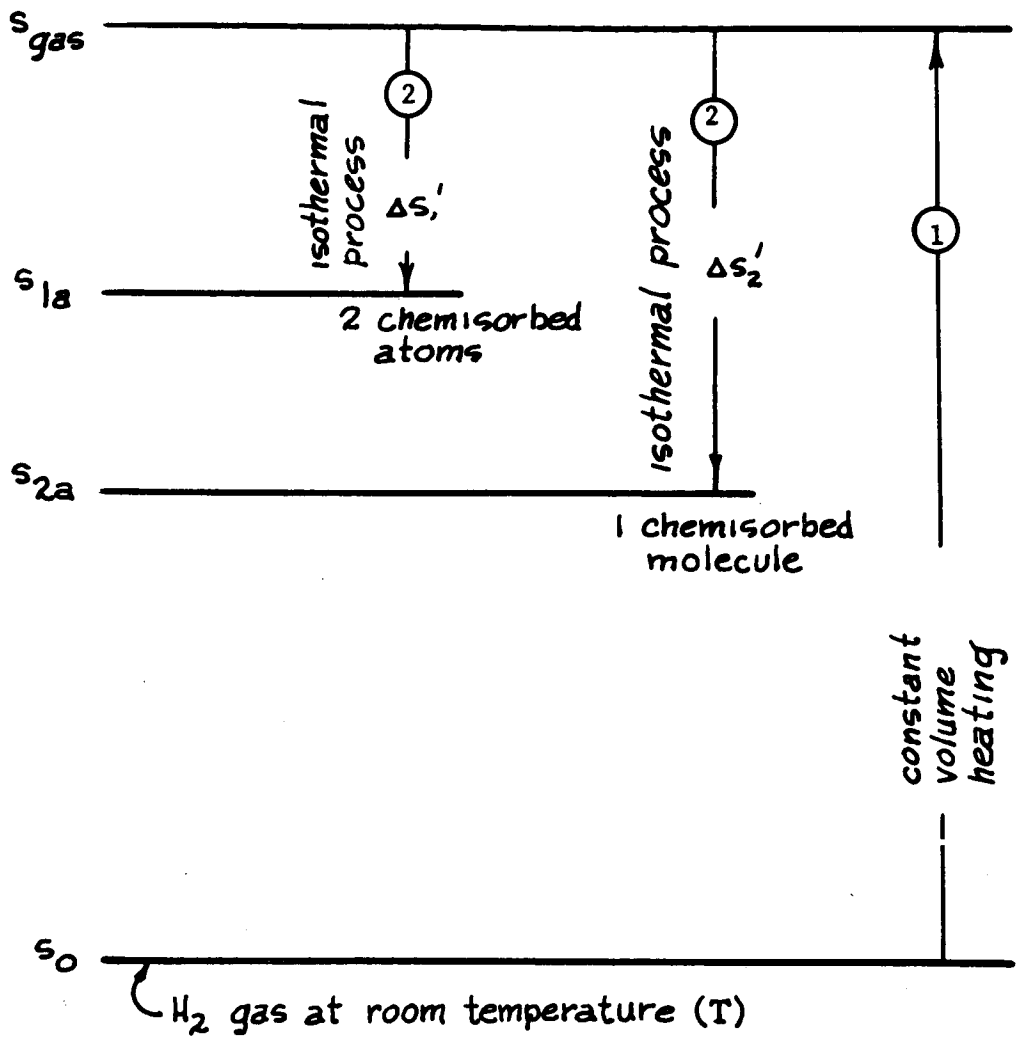

Figure 27. Entropy relationships for the chemisorption of atomic and molecular hydrogen. Step 1 represents constant volume heating, while step 2 represents isothermal chemisorption.

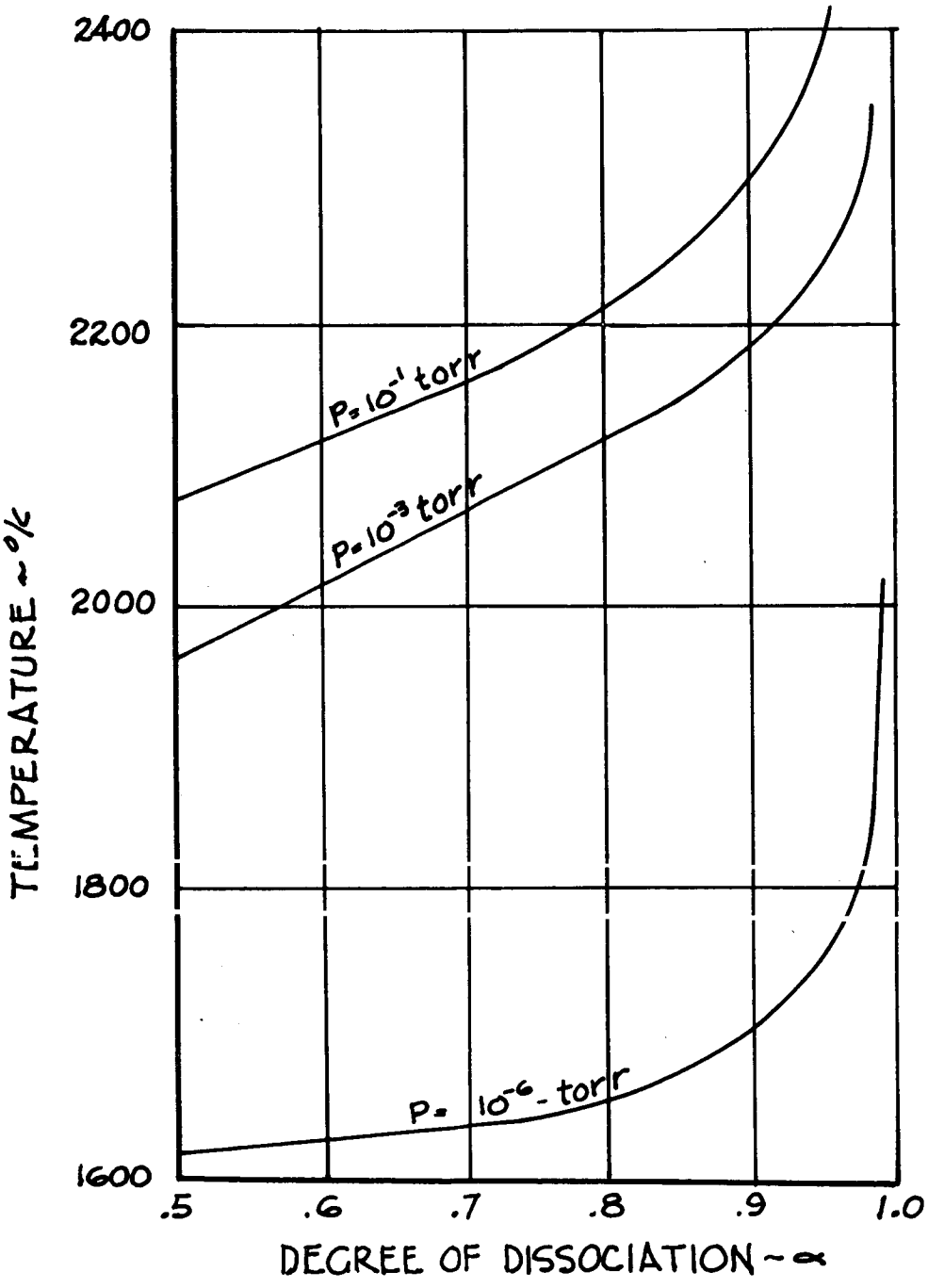

Figure 28. Degree of dissociation of hydrogen as a function of temperature, at various pressures.

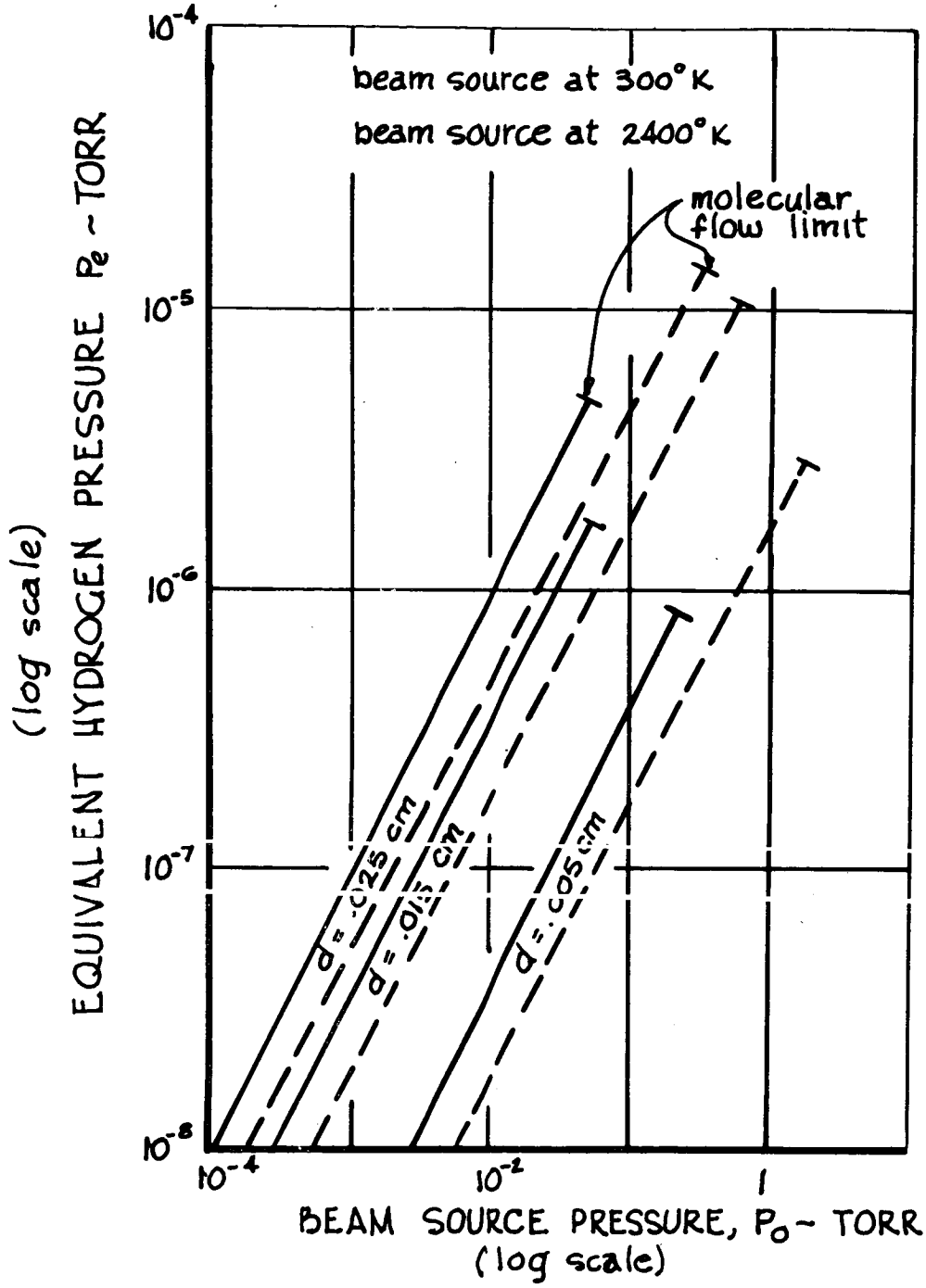

Figure 29. Equivalent beam pressure (P_e) as a function of beam source pressure (P_o) for various values of the beam source orifice diameter.